IUP Research Highlights 2015/2016

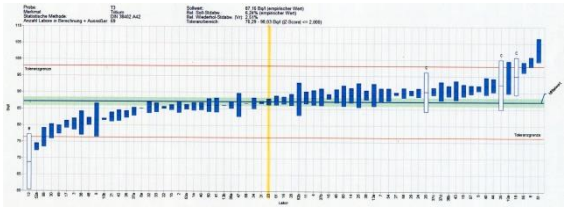

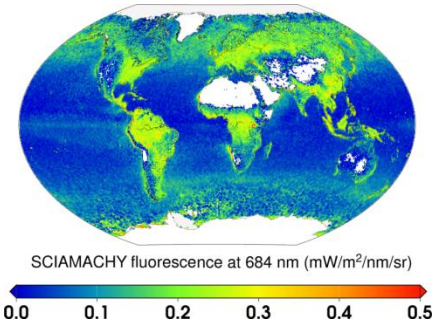

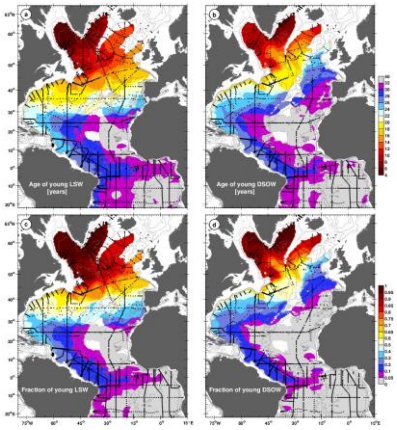

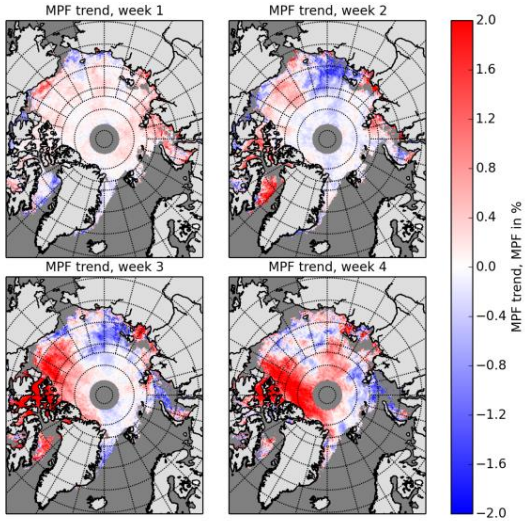

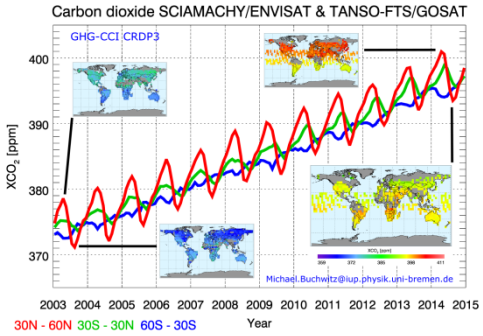

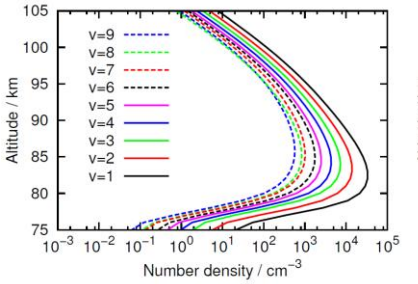

Institute of Environmental Physics (IUP)
Institute of Remote Sensing (IFE)
University of Bremen
Otto-Hahn-Allee 1, 28359 Bremen, Germany

Table of Contents

INTRODUCTION 5

REMOTE SENSING OF THE EARTH SYSTEM (PROF. DR. JUSTUS NOTHOLT) 8

Model studies on hydroxyl airglow and rotational temperatures 8
Measurements of Ammonia (NH_3) using FTIR spectroscopy 10
Year-round FTIR measurements in Paramaribo, Suriname 11
Greenhouse gas emissions from rivers 12
Multiyear sea ice area estimates from microwave satellite observations 14
Melt ponds on Arctic sea ice 16
Cooperative Junior Research Group for *Remote Sensing of Sea Ice* 18

PHYSICS AND CHEMISTRY OF THE ATMOSPHERE (PROF. DR. JOHN P. BURROWS) 20

First simultaneous detection of marine and terrestrial chlorophyll fluorescence from space 20
Carbon Dioxide and Methane from Satellites 22
Monitoring compliance with sulphur content regulations of shipping fuel by in situ measurements of ship emissions 25
Space based observation of volcanic iodine monoxide 27
Long-term ozone observations from space 29
Solar Variability 31
Trace gas and aerosol profiles in the stratosphere from limb measurements 33
Stratospheric Methane and Carbon Dioxide Profiles from SCIAMACHY Solar Occultation Measurements 35
Improved pointing information for the satellite instrument SCIAMACHY 37
Solar Induced Vegetation Fluorescence as seen from Space 39
Clouds and aerosols in the atmosphere 40
Greenhouse gas observations from aircraft: Methane Airborne Mapper (MAMAP) 42
Airborne measurement of short lived trace gases: free radicals 44
Molecular Spectroscopy Laboratory 45

LABORATORY FOR MODELING AND OBSERVATION OF THE EARTH SYSTEM (PROF. DR. MIHALIS VREKOUSSIS) 46

Introduction to LAMOS 46

OCEANOGRAPHY (PROF. DR. MONIKA RHEIN) 47

Advection of North Atlantic Deep Water from the Labrador Sea to the Southern Hemisphere 47
Coastal upwelling off Peru and Mauritania inferred from helium isotope disequilibrium 48
Recent changes in the properties of Labrador Sea Water 50
Salinity time-series in the North Atlantic 52

Long-term observations of North Atlantic Current transport at the gateway between western and eastern Atlantic 54

TERRESTRIAL ENVIRONMENTAL PHYSICS (DR. HELMUT FISCHER) 56

Routine work and emergency case support by the IUP radioactivity lab 56
Transport of anthropogenic radionuclides between the Pacific and Indian Oceans 58
Radiometric dating of recent sediment cores 60

TEACHING ACTIVITIES 62

Introduction

The IUP comprises five departments: Remote Sensing, Physics and Chemistry of the Atmosphere, Oceanography, Terrestrial Environmental Physics, and Modelling and Observation of the Earth System.

The **Department of Remote Sensing** employs passive remote sensing instrumentation such as Fourier transform interferometers and microwave radiometers taking measurements in the spectral region from the infrared to the microwave. The instruments are located at various ground based sites ranging from the high Arctic (Svalbard) to the tropics (Suriname), as well as aboard research vessels (R.V. Polarstern) and aircraft (Falcon). Furthermore, operational satellite instruments are used to monitor atmospheric and earth surface properties. Among them are sea ice coverage, water vapour and clouds. A further research focus is the investigation of stratospheric and mesospheric processes including solar effects on the terrestrial atmosphere. These activities are supported by atmospheric modelling.

The research activities carried out in the **Department of Physics and Chemistry of the Atmosphere** aim at improving the understanding of the complex physical chemical processes in the atmosphere and its interfaces to land, ocean, ice, and deep space. Emphasis is placed on the impact of climate change of either anthropogenic or natural origin on the composition of the troposphere, stratosphere, and mesosphere, including greenhouse gases, pollutants and reactive gases. A particular focus has been the scientific support and direction of the Global Ozone Monitoring Experiment (GOME) and Scanning Imaging Absorption spectroMeter for Atmospheric ChartograpHY (SCIAMACHY) missions. These satellite sensors allow characterizing the chemical composition of the atmosphere remotely by means of spectroscopy in the ultraviolet, visible and near-infrared spectral regions using grating spectrometers. Similar instruments are operated ground-based (NDACC stations, BREDOM network), on ships (R.V. Polarstern), planes and balloons. Remote sensing is complemented by in-situ experiments, laboratory work on spectroscopy and reaction kinetics, and modelling of physical and photochemical processes in the lower, middle and upper atmosphere.

IUP Mission Statement

The overarching objective of the Institute of Environmental Physics is to understand the mechanisms controlling the Earth System and its response to change. This is achieved by using physical methods and research focuses on the sub systems atmosphere, ocean, cryosphere, and their interfaces. This requires the development and use of remote sensing techniques from the ground, from ships, aircraft and satellite platforms and in-situ measurements for process studies. The data are coupled with models to interpret the observations and improve the prediction of change.

The main research topics of the **Department of Oceanography** are the climate relevant processes in the Atlantic Ocean. The global meridional overturning circulation (MOC) plays an important role in the distribution of the heat received from the sun and thus for climate and climate change. Whether and how global warming will affect the circulation and how this will feed back on the climate is one of the central issues of marine research. The department studies – mainly with experimental methods – circulation, formation, and transformation changes in key regions of the Atlantic MOC, develops methods to infer the strength of the MOC, and improves and expands the tracer analysis techniques. Other interdisciplinary research themes are the role of vertical mixing in water mass transformation and at hydrothermal vents, the calculation of upwelling velocities at the equator and at the coast, as well as the dating of groundwater. The research is part of national and international pro-

grammes such as CLIVAR (Climate Variability and Predictability) and CARBOOCEAN (EU Integrated Project).

The **Department of Terrestrial Environmental Physics** investigates transport processes in porous systems and soils and conducts research in the fields of radioecology and sediment chronology. It takes advantage of the excellent equipment available in the Bremen State Radioactivity Measurements Lab (which forms part of the state and federal nuclear emergency management networks) and of a unique Earth Field NMR apparatus.

Since 2016, the newly established **Department of Inverse Modelling of the Earth System** led by Prof. Vrekoussis hosts the joint IUP-MARUM working group called LAMOS (Laboratory for Modelling and Observation of the Earth System) . LAMOS aims at improving our understanding of the complex mechanisms controlling the emission, transport, transformation and deposition of atmospheric pollutants with the use of state-of-the-art numerical models and novel instrumentation. Special focus is given on the quantification of sources and sinks of long-lived and short-lived species using satellite observations as proxies.

The IUP is internationally well known for its participation in a number of advanced space-borne missions, like GOME and SCIAMACHY. Of particular importance is the Global Ozone Monitoring Experiment, GOME, which was the first satellite sensor to measure tropospheric trace constituents from space and has operated aboard ERS-2 for over 10 years. GOME is a smaller version of SCIAMACHY, which was launched successfully in 2002 and has provided almost a decade of successful measurements. Both sensors, GOME and SCIAMACHY, were proposed by the IUP, and the IUP acts as Principal Investigator. The GOME and SCIAMACHY data records are continued by GOME-2, OMI and the upcoming atmospheric Sentinels (5P/4/5) and IUP scientists are contributing to all those missions. The IUP is also involved in many international projects with space-borne instruments for remotely measuring the surface, such as sea ice, the Wadden sea and land use. In addition, the IUP runs instrumentation at research measurement stations worldwide. It has participated in many international and national research campaigns using ships, aircraft and ground-based instruments. Members of the IUP are actively involved in international scientific organisations like COSPAR, IGBP-IGAC, WCRP-SPARC, CACGP and WMO-IGACO.

More than 100 Ph.D. students and postdocs work at the IUP. Students in general physics have the option to specialize in environmental physics. A variety of courses, conducted in cooperation with colleagues from the Alfred-Wegener-Institut of Polar Research and Oceanography (AWI) in Bremerhaven

Department contacts

Physics and Chemistry of the Atmosphere
Prof. Dr. John P. Burrows FRS
+49-421-218 62100
burrows@iup.physik.uni-bremen.de

Remote Sensing
Prof. Dr. Justus Notholt
+49-421-218 62190
jnotholt@iup.physik.uni-bremen.de

Oceanography
Prof. Dr. Monika Rhein
+49-421 218 62160
mrhein@physik.uni-bremen.de

Terrestrial Environmental Physics
Dr. Helmut Fischer
+49-421-218 62761
hfischer@physik.uni-bremen.de

Laboratory for Modelling and Observation of the Earth System
Prof. Dr. Mihalis Vrekoussis
49 (0)421 218 – 62140
vrekoussis@iup.physik.uni-bremen.de

is offered at the IUP. The aim of the environmental physics course is to provide a basic education in the areas of the ocean, the atmosphere and the solid Earth. Whereas other German universities cover parts of environmental physics, for example physical oceanography or meteorology, as independent subjects, Bremen addresses all of them within the physics course fully integrated into the general physics. The students even have the opportunity to participate in exciting expeditions worldwide. To strengthen environmental physics as a course of study in its own right and also to motivate students from abroad to study in Bremen, a four-semester international course leading to a Master of Science (M.Sc.) in Environmental Physics and a two-semester post-graduate course for the Certificate in Environmental Physics have been offered since autumn 2000.

This document provides an overview of selected research highlights achieved by the members of the five IUP departments during the period 2015/2016.

Model studies on hydroxyl airglow and rotational temperatures

Holger Winkler and Justus Notholt

There is a layer of vibrationally-rotationally excited hydroxyl molecules in the upper mesosphere. Measurement of the infrared radiation emitted by this layer is the standard technique to retrieve temperatures in the upper mesosphere. We run computer models to investigate the hydroxyl layer and the radiation emitted by it (Winkler et al., 2016).

The main source of excited hydroxyl in the Earth's atmosphere is the reaction of atomic hydrogen with ozone:

$$H + O_3 \rightarrow OH(v,J) + O_2$$

where v is the vibrational quantum number, and J is the rotational quantum number. The exothermicity of this process leads to an excitation of OH up to $v = 9$. The chemistry of $OH(v,J)$ is controlled by reactions of oxygen and hydrogen species, as well as quenching and spontaneous emissions of photons. This leads to the formation of an emission layer which is centred at about 87 km with a full width at half maximum of about 8-10 km. While in principle, the atmospheric chemistry of excited hydroxyl seems to be understood, uncertainties concerning vibrational quenching rates of hydroxyl with atomic and molecular oxygen are a subject of ongoing research.

Emission lines due to vibrational-rotational transitions, $OH(v,J) \rightarrow OH(v',J') + h\nu$, dominate the near-infrared night-time sky spectrum. These so called hydroxyl Meinel emissions are routinely used to retrieve upper mesospheric temperatures. The underlying assumption is that the population of the rotational states is in local thermodynamic equilibrium with the ambient atmosphere, and that the rotational temperature equals the gas kinetic temperature. However, measurements have shown that the rotational temperatures of mesospheric hydroxyl are different for different vibrational states. On average there is an increase of the rotational temperatures with increasing quantum number v. There are two main possible reasons for this, 1st: Different emission altitudes of hydroxyl in different vibrational states; and 2nd: Deviations from a local thermodynamic equilibrium.

We perform computer simulations of $OH(v,J)$ in the atmosphere to investigate the reasons for the different rotational temperatures derived for different vibrational states. The aim is to understand and quantify the differences between the derived rotational temperatures on the one hand, and the atmospheric temperature on the other hand. For this purpose, a model of vibrationally excited hydroxyl (Winkler et al., 2016) is used in combination with an atmospheric chemistry model (Winkler et al., 2012). Figure 1 shows an example of a calculated height distribution of hydroxyl molecules in the upper mesosphere and lower thermosphere. It can be seen that the lower vibrational states peak at

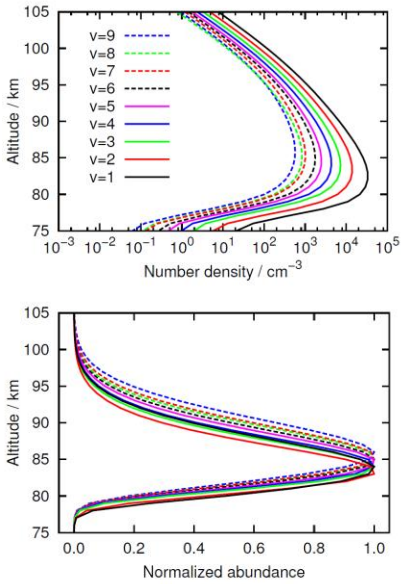

Figure 1: Hydroxyl molecules in different vibrational states simulated for local midnight at the 1st of June, 24°S, and 70°W. The top plot shows the number density profiles, and the lower plot shows the peak-normalized profiles.

lower altitudes than molecules with higher vibrational quantum numbers.

There is a shift of up to about 5 km between the profiles of the different vibrational states. As a result, there are different average gas temperatures for the different vibrational states. The actual values depend on the atmospheric temperature profile. For the date and location considered in this example there is a temperature decrease of about 2 K/km in the altitude range of interest. Figure 1 shows the mean hydroxyl emission altitude and the average temperature as a function of the vibrational quantum number. The mean altitude increases by about 3 km from low to high vibrational quantum numbers, and the rotational temperature decreases by about 4 Kelvin. Note that the calculated temperature decrease with increasing vibrational quantum number is in contrast to the generally measured temperature increase. In order to address possible deviations from a local thermodynamic equilibrium, we are currently developing a model which will allow to study the population dynamics of both vibrational and rotational states in detail. The model accounts for the chemical production of rotationally hot $OH(v,J)$, vibrational-rotational and pure rotational transitions due to collisions with air molecules as well as due to photon emissions. The preliminary model result shown in Figure 3 indicates that the rotational temperature tends to increase with vibrational quantum number. Depending on model parameters, the rotational temperature at $v = 8$ can be up to 10 K higher than the gas temperature. Note that such a temperature increase would exceed the temperature decrease due to the different emission altitudes discussed above. If these findings are confirmed by further simulations, they will have a significant impact on the interpretation of hydroxyl rotational temperature measurements.

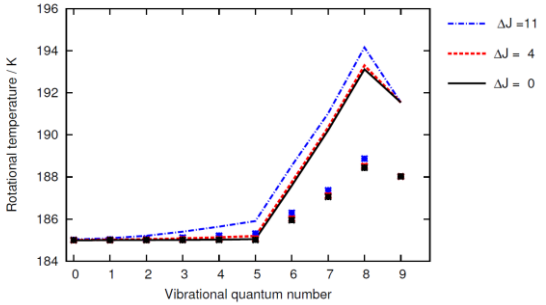

Figure 2: Modelled rotational hydroxyl temperatures at an altitude of 85 km as a function of vibrational quantum number. The gas kinetic temperature is 185 K. The results for different changes of the rotational quantum number *J* in a vibrational quenching process are shown in different colours. Lines and crosses depict the temperatures calculated with different sets of rotational quenching rate coefficients from the literature.

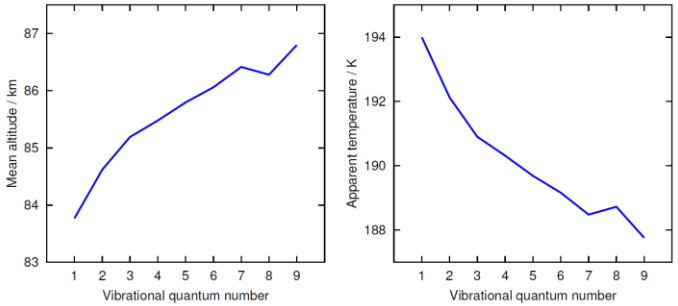

Figure 3: Left plot: Mean altitude of the hydroxyl profiles shown in Figure 1 as a function of vibrational quantum number. Right: Apparent rotational temperatures derived by a least-square fit to the weighted sum of Boltzmann populations corresponding to the different gas temperatures at the different altitudes.

References:

Winkler, H., von Savigny, C., Burrows, J. P., Wissing, J. M., Schwartz, M. J., Lambert, A., and García-Comas, M. (2012). Impacts of the January 2005 solar particle event on noctilucent clouds and water at the polar summer mesopause. *Atmos. Chem. Phys.*, 12(12):5633--5646.

Measurements of Ammonia (NH_3) using FTIR spectroscopy

Mathias Palm and Justus Notholt

Ammonia (NH_3) is a central part of the nitrogen cycle in the soil/atmosphere system. It is a highly reactive gas which is formed by excess nitrogen fertilisation, application of pig and poultry manure, but also by combustion. As can be seen in Figure 4, there are three areas in Western Europe which are "hotspots" of ammonia in the atmosphere: Northwest Germany and Netherlands, the Po-valley in the north of Italy and the Ebro valley in northern Spain. The area with the high emission in Russia has no local observatories.

All three regions in Western Europe are regions which are heavily used for agriculture. In Bremen, the routine measurements of the stationary FTIR (Fourier Transform Infrared) instrument can be used to quantify atmospheric NH_3 (compare Figure 5). The time of spring fertilization can readily be observed. A particularly high value was measured in April 2010. Although this is coincident with the outbreak of the Icelandic volcano Eyjafjallajökull which led to a standstill of air traffic in Western Europe, the high ammonia is not related to this incident.

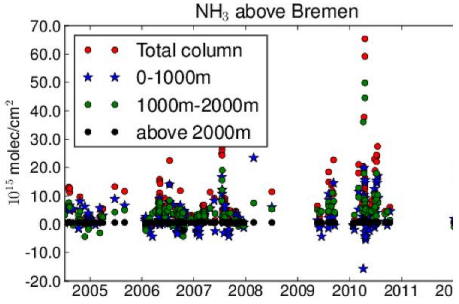

Figure 5: Time series of tropospheric NH3 above Bremen as measured by the FTIR instrument at IUP Bremen. The high values in spring and autumn are related to fertilisation.

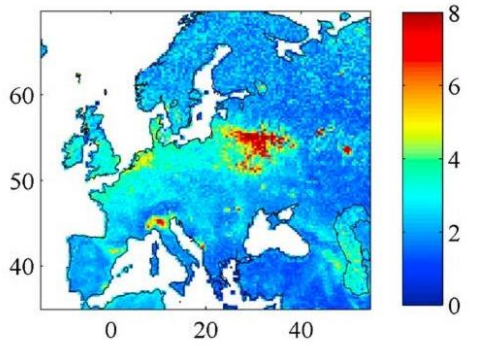

Figure 4: Yearly mean of Ammonia as measured by the IASI satellite ©Van Damme (2014)

Under certain circumstances, two atmospheric layers of ammonia may be observed. This is the case for ammonia transported from further away and lifted up above the planetary boundary layer, which is the layer between the free troposphere and the part of the troposphere influenced by the ground. Such a filament can be seen in Figure 6 which is a satellite observation from 18th of April 2010 showing a filament of ammonia reaching from the west over the location of the instrument.

In order to observe the Western European hotspots, a mobile FTIR system has been built. The first deployment was in Cabauw, Netherlands (part of the PhD work of Enrico Dammers – Vrije Universiteit Amsterdam). During a sabbatical of Prof. Notholt, a measurement campaign has been conducted in Ispra and the diurnal variation in NH3 was measured be detected. Because of the measurement principle of the FTIR (clear sight to the sun is needed), this is not always possible. To this end a car-trailer has been equipped with a small FTIR and the necessary auxiliary equipment.

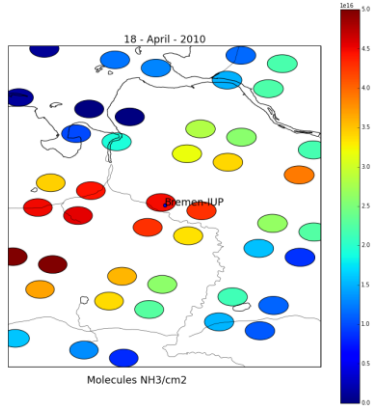

Figure 6: Measurement of ammonia by the IASI satellite on 18th April 2010 (image courtesy of Enrico Dammers). A filament coming from the west can readily be seen, which extends over the Bremen FTIR.

Year-round FTIR measurements in Paramaribo, Suriname

Mathias Palm, Thorsten Warneke and Justus Notholt

The Notholt Workgroup operates a measurement station in Paramaribo, Suriname since 2004. Until recently, the measurements were obtained only on campaign base. After 2013, the continuous operation for measurements of greenhouse gases in the near infrared portion of the spectrum was started with the help of local partners, and after 2014, continuous operation was extended to measurements in the mid-infrared region. The caveat here is the need for liquid nitrogen which is difficult to obtain locally. Figure 7 shows the development of HCl since 2004. HCl is a gas mainly found in the stratosphere and is linked to ozone depletion.

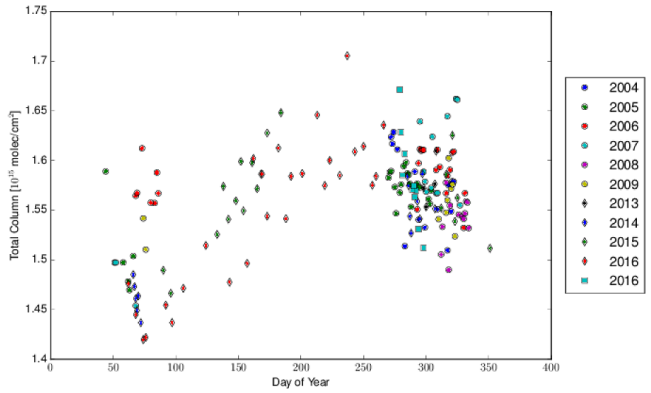

Figure 7: Measurements of HCl above Paramaribo, Suriname.

For two years, the observations extend through the whole annual cycle. Paramaribo is a special place because the ITCZ, the inner tropical convergence zone, is north of Suriname in autumn and south of it in spring. This can be seen in Figure 8 which shows measurements of SF_6 in Paramaribo. SF_6 is mainly released in the northern hemisphere. The exchange time between hemispheres is about one year, so the amount found in the southern hemisphere lags behind. Hence, from Figure 8 it can be inferred that Paramaribo is in northern hemispheric

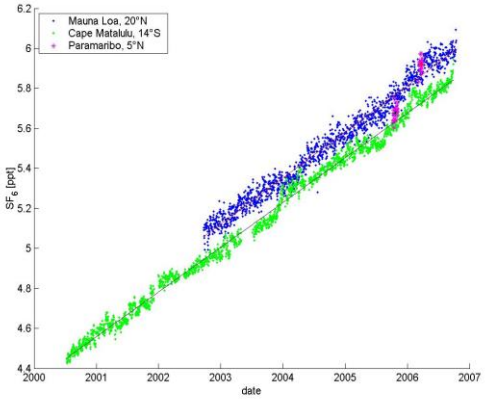

Figure 8: Measurements of SF_6, an atmospheric tracer in the northern (blue dots) and southern (green dots) hemisphere and in Surinam (pink dots).

air in spring and in southern hemispheric air in autumn. Whether this can be seen in the amount of HCl in Figure 7 is still subject to research.

Greenhouse gas emissions from rivers

Denise Müller, Thorsten Warneke, Justus Notholt

In the context of climate change, rivers and estuaries have been increasingly studied in terms of carbon and nutrient cycling. A special focus of recent research has been the production of greenhouse gas (GHG) in and emission thereof from these aquatic systems. Global estimates of riverine and estuarine evasion of GHGs usually suffer from poor data coverage in the tropics. Southeast Asia, in particular, has been considered a hotspot in the global carbon cycle, but very few data exist on aquatic GHG emissions in this region.

Southeast Asian rivers export large amounts of organic carbon to the ocean, due to both high rates of runoff and the presence of tropical peatlands. These carbon-rich soils are an important source of carbon to rivers, but the fate of this material remained unknown.

At IUP, we investigated the relevance of rivers and estuaries in western Sarawak, Malaysia as sources of GHGs to the atmosphere. During several expeditions, we measured carbon dioxide (CO_2) outgassing from an undisturbed tropical peat-draining river, the Maludam river. Furthermore, we determined dissolved CO_2, as well as methane (CH_4), carbon monoxide (CO) and nitrous oxide (N_2O), in the estuaries of the adjacent Lupar and Saribas rivers using Fourier Transform Infrared (FTIR) spectrometry.

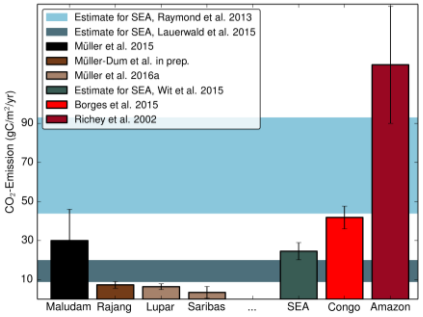

Figure 10: Annual carbon dioxide emission estimates for several tropical rivers. Estimates based on models are shown by the horizontal bars and the vertical bars indicate measurement based estimates

Figure 9: Equilibrator used for the measurement of dissolved CO_2 in the Rajang River (Sarawak, Malaysia).

Despite its high organic carbon concentrations, the Maludam river was actually a comparatively moderate source of CO_2 to the atmosphere. Only 26 ± 15 % of the carbon was evaded to the atmosphere as CO_2, and the rest was transported downstream. Probably, the rapid transit of the water does not allow sufficient time for organic carbon to be fully remineralized, so that a large fraction is conveyed to the estuary. There, the residence time is prolonged, and the tides promote oxygen supply. Therefore, aerobic respiration of organic matter is stronger in the estuaries. Measurements in the freshwater part of the Lupar and Saribas estuaries, as well as measurements in the Rajang River in northern Sarawak have confirmed that the CO_2 emissions from these rivers are relatively moderate.

Similar results were obtained by our collaboration partners from the Leibniz Centre for Tropical Marine Ecology (ZMT), who performed CO_2 measurements in Indonesian rivers. In a synthesis study, we showed that the CO_2 emissions from Southeast Asian rivers are on average lower than previously assumed. On a global perspective, riverine CO_2 emissions are far smaller in Southeast Asia than in other tropical regions like the Amazon or the Congo River.

References:

D. Müller, H. W. Bange, T. Warneke, T. Rixen, M. Müller, A. Mujahid, and J. Notholt: Nitrous oxide and methane in two tropical estuaries in a peat-

dominated region of North-western Borneo. Biogeosciences 13, 2415-2428, 2016. doi: 10.5194/bg-13-2415-2016

D. Müller, T. Warneke, T. Rixen, M. Müller, A. Mujahid, H. W. Bange and J. Notholt: Fate of terrestrial organic carbon and associated CO2 and CO emissions from two Southeast Asian estuaries. Biogeosciences 13, 691-705, 2016. doi: 10.5194/bg-13-691-2016

F. Wit, D. Müller, A. Baum, T. Warneke, W. S. Pranowo, M. Müller, and T. Rixen: The impact of disturbed peatlands on river outgassing in Southeast-Asia. Nature Communications 6, 10155, 2015. doi:10.1038/ncomms10155

D. Müller, T. Warneke, T. Rixen, M. Müller, S. Jamahari, N. Denis, A. Mujahid and J. Notholt: Lateral carbon fluxes and CO2 outgassing from a tropical peat-draining river. Biogeosciences 12, 5967-5979, 2015. doi:10.5194/bg-12-5967-2015

Multiyear sea ice area estimates from microwave satellite observations

Yufang Ye, Gunnar Spreen, and Georg Heygster

Sea ice is an important component of the global climate system and at the same time a sensitive climate indicator. Different sea ice types can be separated based on their age and stage of development: the two main classes are first-year ice (FYI) and multiyear ice (MYI). MYI is older, thicker ice that has survived at least one summer melt and FYI represents the seasonal ice cover. The sea ice area in the Arctic is rapidly decreasing with a rate of about –4% per decade. Especially pronounced is the decrease in thick MYI. Large parts of the thick MYI have been replaced by increasingly thin FYI, which impacts the weather and climate through different radiation and dynamic feedbacks and has consequences not only for the Arctic but also for mid-latitude regions. For example, MYI has more ridges, i.e. stronger surface topography, which results in a smaller surface fraction to be covered by melt ponds in summer and thereby a higher albedo and less absorption of shortwave radiation. The stronger and thicker MYI is more resistant against wind forcing, i.e., less leads can open up and less energy and gases are transferred between the ocean and atmosphere. The larger ice thickness makes it less likely to completely melt in summer, which in turn again keeps the albedo higher and avoids the ice-albedo-feedback to kick in.

Microwave satellite observations have been widely used for monitoring sea ice in Polar Regions because they are independent of sunlight and can penetrate clouds (e.g., Ye and

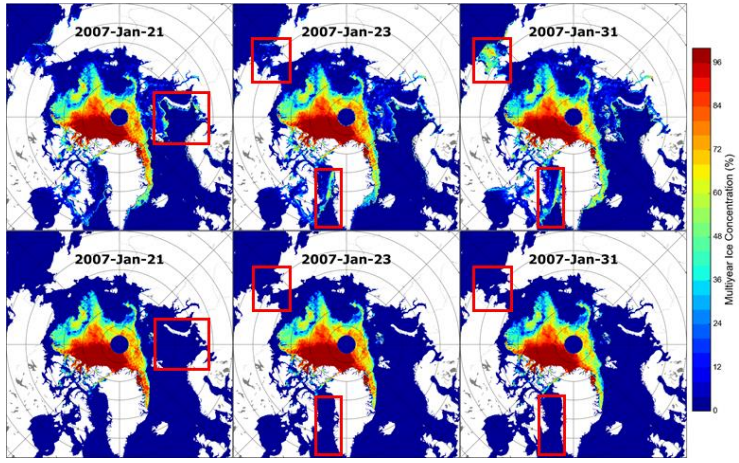

Figure 11: Multiyear sea ice concentration for selected days in January 2007 from the ECICE algorithm (top) and those after the two correction schemes have been applied (bottom). Many regions with false MYI areas, especially along the ice margins, are corrected in the bottom row (red rectangles).

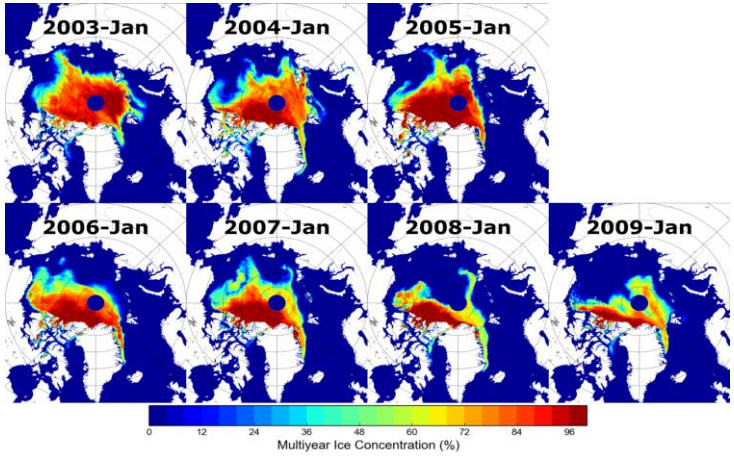

Figure 12: Monthly average multiyear sea ice concentration in the Arctic for January of the years 2003–2009, demonstrating the drastic decrease in MYI area during that time period.

Heygster, 2015). Total sea ice concentration can be derived reliably from microwave remote sensing data because of the distinct difference of microwave signatures between open water and sea ice. However, the discrimination of ice types (including MYI) can be difficult because different ice types may have similar typical microwave signatures, i.e., brightness temperatures at different polarizations, backscatter values or combination of both. Such ambiguous, radiometric signatures which can make FYI to radiometrically look like MYI can be caused by, e.g., thaw-refreeze cycles in the snow or increased surface roughness caused by sea ice deformation due to wind and waves, especially along the ice margins.

The improved Arctic MYI concentration retrieval developed at the University of Bremen is based on the Environment Canada's Ice Concentration Extractor (ECICE) using brightness temperatures from the microwave radiometer AMSR-E and radar backscatter from the Ku-band scatterometer QuikSCAT. The initial MYI ice concentrations are corrected by two correction schemes: one using temperature records from atmospheric reanalysis to identify MYI anomalies caused by warm spells and replacing them with interpolated MYI concentrations (Ye et al., 2016a), and the other utilizing mainly ice drift records from satellite observations to constrain the MYI changes within a plausible contour (Ye et al., 2016b). After the two corrections are applied, the MYI concentration estimates in the Arctic Basin, particularly along the ice margins and in the peripheral seas, are much improved and more realistic (see Figure 11).

Currently, the MYI dataset at the University of Bremen are available on a daily basis for the years 2002–2009 on a 4.45 km polar stereographic grid. From 2002 to 2009, the MYI area has decreased by about 1.5 million km^2 on average (Figure 13). The distribution of MYI for all months of January from 2003 to 2009 is shown in Figure 12. In the earlier years, the centre of the Arctic Basin was completely covered by MYI, while in recent years only a small area of MYI survives along the northern coasts of Greenland and the Canadian Arctic Archipelago. In order to better understand the mechanism of MYI changes and ascertain trends of the climate change, a long and physically consistent MYI time series is needed. The current MYI dataset ending in 2009 will be extended to the present using data from the radiometer AMSR2 and the C-band scatterometer ASCAT.

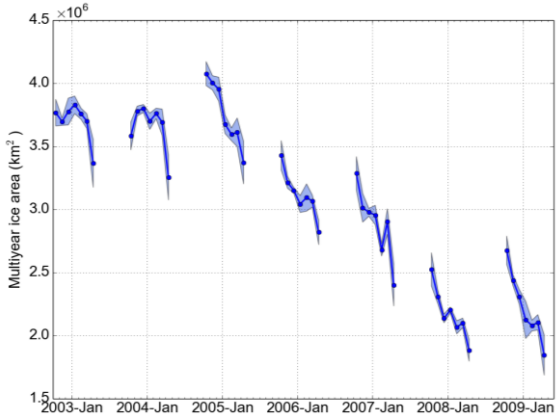

Figure 13: Monthly averaged Arctic multiyear ice area in winter months (October–April) from 2002 to 2009.

References:

Ye, Y., Heygster, G., and Shokr, M. (2016a). Improving multiyear ice concentration estimates with air temperatures. IEEE Transactions on Geoscience and Remote Sensing, 54(5), 2602- 2614, doi:10.1109/TGRS.2015.2503884.

Ye, Y., Shokr, M., Heygster, G., and Spreen, G. (2016b). Improving multiyear sea ice concentration estimates with sea ice drift. Remote Sensing, 8(5), 397, doi:10.3390/rs8050397.

Ye, Y., and Heygster, G. (2015). Arctic multiyear ice concentration retrieval from SSM/I data using the NASA Team algorithm with dynamic tie points. In Towards an Interdisciplinary Approach in Earth System Science (pp. 99-108). Springer International Publishing, doi:10.1007/978-3-319-13865-7_12.

Melt ponds on Arctic sea ice

Larysa Istomina, Georg Heygster, and Gunnar Spreen

With the onset of melt in the Arctic Ocean (depending on latitude, beginning of June to mid-July), the amount of melt ponds - puddles of fresh melt water on the Arctic sea ice - increases. The melt ponds remain present throughout the whole Arctic summer and continue to be visible as darker ice areas in autumn even after freeze up before major snowfall events cover them up (Figure 15). Melt ponds on the Arctic sea ice are the main reason for strong surface albedo decrease in summer, which in turn affects the whole Arctic climate system via climatic feedbacks. The duration of melt pond presence on the Arctic sea ice, as well as the melt pond fraction (MPF), are good indicators of the state of the local Arctic climate. In the context of Arctic warming, Arctic wide retrieval of MPF is of importance and is effectively done using satellite observations.

Melt ponds and sea ice behave differently in the visible (VIS) and near-infrared (NIR) range of the electromagnetic spectrum and thus can be resolved by their spectral properties. Therefore, optical spectroradiometers, like MERIS on the Envisat or OLCI on the Sentinel-3 satellite, are suitable for MPF retrieval. The Melt Pond Detector (MPD) retrieval developed at University of Bremen uses level 1b MERIS TOA (top of the atmosphere) reflectances and gives results for every satellite swath on an orbit by orbit base. Thereafter, the data is gridded to a 12.5 km polar stereographic grid to obtain the daily averaged MPF. The MPD retrieval uses a physical model of sea ice and melt ponds to retrieve the MPF and sea ice albedo (Zege et al., 2015; Istomina et al., 2015a,b). In addition, it utilizes over 200 spectral albedo measurements of the Arctic surface from field campaigns (Istomina et al., 2016; Malinka et al., 2016) to constrain the retrieval to realistic situations. Currently, the whole MERIS dataset (2002–2011) is processed and available at University of Bremen and can be used, e.g., as input for climate models or for specific ice morphology and melt pond studies (Istomina et al., 2015b; www.seaice.uni-bremen.de/melt-ponds).

Figure 15: Frozen melt ponds on the Arctic sea ice

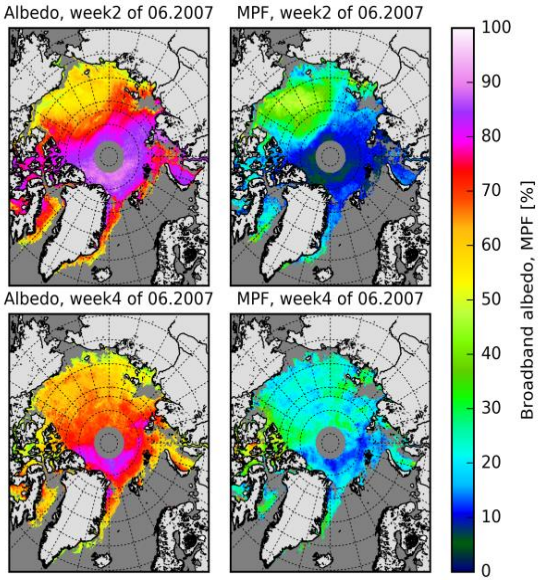

Figure 14: Example of the broadband albedo and melt pond fraction maps for week 2 and 4 of June 2007. High melt pond fraction corresponds to low sea ice albedo.

The MPF can vary in a great range of values depending on the melt stage and the underlying ice type. It can stay as low as 20% at the maximum of melt on multiyear ice - ice that has survived one or more summer melts and shows stronger surface topography. On level landfast ice, it can go up to as high as 80% during the onset of melt. Sea ice albedo is affected correspondingly. Figure 14 shows an example from

June 2007 illustrating the low MPF for the multiyear ice areas north of Greenland and the Canadian Arctic Archipelago, and higher MPF for the first-year ice in the Beaufort Sea and for the fast ice areas in the Laptev and East Siberian Sea. Satellite observations give us the possibility to watch the dynamics and variability of MPF in space and time and produce temporal trends of melt pond fraction (Figure 17). Although the spatial trends shown in Figure 17 show positive or negative values depending on location, it does not necessarily mean an increase or decrease of the maximum MPF value observed in a given region throughout the season. It mainly reflects a shift of the melt pond evolution curve in time. If the melt pond development starts earlier, i.e., is shifted towards spring (Figure 16), a positive trend in MPF will be observed early in the season. A negative MPF trend may occur if, e.g., melt pond drainage (second melt stage after melt onset) is observed in the later years of the dataset as opposed to melt onset in the earlier years (Figure 16).

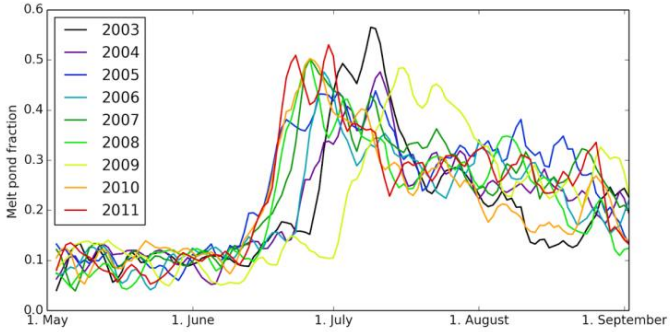

Figure 16: Time series of melt pond fraction throughout the summers 2003–2011 for the area of positive MPF trend in the Queen Elizabeth Islands (78°N, 108°W).

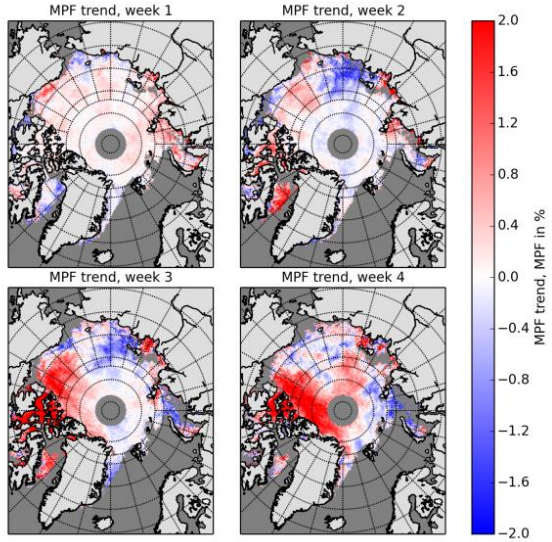

Figure 17: Weekly trend of melt pond fraction for June 2002–2011. Note the strong positive MPF trends for the 3rd and 4th weeks of June north of Greenland and the Canadian Arctic Archipelago.

References

Zege, E., Malinka, A., Katsev, I., Prikhach, A., Heygster, G., Istomina, L., Birnbaum, G., and Schwarz, P.: Algorithm to retrieve the melt pond fraction and the spectral albedo of Arctic summer ice from satellite optical data, Remote Sens. Environ., 163, 153-164, doi:10.1016/j.rse.2015.03.012, 2015.

Istomina, L., Heygster, G., Huntemann, M., Schwarz, P., Birnbaum, G., Scharien, R., Polashenski, C., Perovich, D., Zege, E., Malinka, A., Prikhach, A., and Katsev, I.: Melt pond fraction and spectral sea ice albedo retrieval from MERIS data – Part 1: Validation against in situ, aerial, and ship cruise data, The Cryosphere, 9, 1551-1566, doi:10.5194/tc-9-1551-2015, 2015a.

Istomina, L., Heygster, G., Huntemann, M., Marks, H., Melsheimer, C., Zege, E., Malinka, A., Prikhach, A., and Katsev, I.: Melt pond fraction and spectral sea ice albedo retrieval from MERIS data – Part 2: Case studies and trends of sea ice albedo and melt ponds in the Arctic for years 2002–2011, The Cryosphere, 9, 1567-1578, doi:10.5194/tc-9-1567-2015, 2015b.

Malinka, A., Zege, E., Heygster, G., Istomina, L.: Reflective properties of white sea ice and snow. The Cryosphere, 10, 2541-2557, doi:10.5194/tc-10-2541-2016, 2016.

Istomina, L., Nicolaus, M., Perovich, D. K.: Surface spectral albedo complementary to ROV transmittance measurements at 6 ice stations during POLARSTERN cruise ARK-XXVII/3 (IceArc) in 2012. doi:10.1594/PANGAEA.867292, 2016.

Cooperative Junior Research Group for *Remote Sensing of Sea Ice*

Gunnar Spreen

In August 2015, the cooperative junior research group *Remote Sensing of Sea Ice*, led by Dr. Gunnar Spreen, was established at the Institute of Environmental Physics (IUP). There is long-standing experience in sea ice remote sensing at IUP as part of Prof. Justus Notholt's research group, in particular, through work led by Dr. Georg Heygster to derive sea ice and atmospheric parameters from satellite-borne microwave radiometers.

The junior research group is supported by the Institutional Strategy of the University of Bremen, funded by the German Excellence Initiative and will last for 5 years. The performed research will not only foster but also extend the current sea ice related work at IUP. The main cooperative partner is the Alfred Wegener Institute, Helmholtz Centre for Polar and Marine Research, which provides expertise especially in the field of sea ice physics and in-situ observations needed for validation of remote sensing data.

The junior research group works on three overarching topics:

(1) Retrieving new sea ice variables, e.g., snow depth and sea ice topography, and establish reliable error estimates
(2) Merging existing observations to new products
(3) Closing the gap between sea ice monitoring and climate system understanding

Sea ice is one of the Earth's climate components exhibiting the greatest change during the last decades. Sea ice has an important role in the coupled climate system because it controls the energy and gas fluxes between ocean and atmosphere in Polar Regions. Due to its high albedo, it efficiently reflects shortwave radiation back to space, and affects the ecosystem. The sea ice area in the

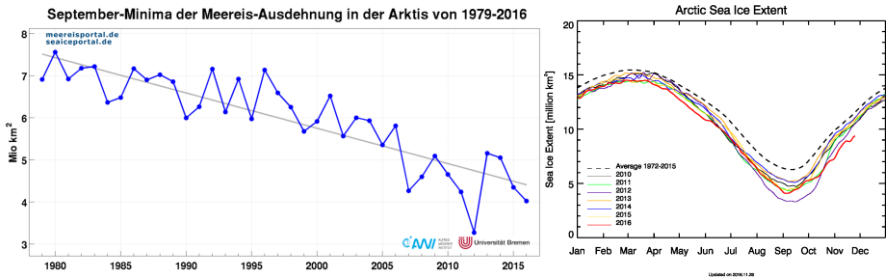

Figure 18: *Decline in Arctic summer (September) sea ice extent between 1979 and 2016 (www.meereisportal.de). (b) Seasonal development of Arctic sea ice extent in 2016 (red curve) in comparison to the last six years and the average 1972–2015 ice extent (dashed line, www.seaice.uni-bremen.de).*

Arctic is rapidly decreasing with a rate of about −4%/decade. In the Antarctic, the sea ice area is slowly increasing (about 1.5%/decade). Arctic sea ice decline is not evenly distributed throughout the year; with –13%/decade as the strongest decrease observed during summer months (Figure 18a). But sea ice declines during all seasons in the Arctic and a late freeze-up like the one observed in 2016 (Figure 18b) can precondition the ice cover for the following year because the ice stays thinner.

Such observations of sea ice area are available from satellite microwave radiometers since the 1970s and with a time series of more than 40 years, sea ice extent is one of the longest climate variables monitored from space. To improve our understanding of the polar climate system, not only sea ice area but also other parameters like ice thickness, type, snow depth, and ice drift and deformation are of importance. New methods for studying these are developed within the junior research group.

One approach is to combine measurements from different satellite sensors like active microwave scatterometers and passive microwave radiometer measurements. This was done, for example, to improve the sea ice type retrieval [Ye et al., 2016]. Current research focuses on combining microwave radiometer measurements with observations in the visual and infrared (IR) spectrum to improve

both the spatial resolution and the accuracy of today's sea ice concentration retrieval. Figure 19 shows an example of how different satellite sensors see the Arctic sea ice on one particular day, 1 April 2009. In the visual bands, shown in Figure 19a, sea ice can be clearly discriminated from the ocean and, if we zoom in, a lot of details like floes along the ice edge or cracks in the ice can be observed. But clouds cover large parts of the Arctic and reduce the area available for analysis. During the polar night, no visual data is available. If the IR channels are added (Figure 19b), clouds can be better discerned from the ice and, if thermal IR channels are used, observations are possible without daylight. Observations at microwave frequencies (Figure 19c-e) are independent of daylight and almost independent of clouds. At 89 GHz (Figure 19c), most details are visible, like cracks in the Beaufort Sea and north of Fram Strait, but cloud liquid water and water vapour can still have a significant impact on the measurement (clearly seen over the open ocean). At 19 and 13 GHz (Figure 19d,e), this influence is reduced but so is the spatial resolution. Methods are developed to combine the advantages of the different sensors to obtain a sea ice concentration product at 1 km spatial resolution and improved accuracy.

Another project focuses on the retrieval of snow depth on sea ice from microwave radiometer observations at different frequencies. Currently, it is being analysed if the snow depth retrieval can benefit from active backscatter measurements like the ones from QuikSCAT shown in Figure 19e.

Laser and radar altimeters are used to estimate the sea ice thickness based on measurements of the ice freeboard height, the part of the ice and snow sticking out of the surrounding water. But altimeter measurements are sparse and do not cover the complete Polar Oceans (Figure 19). Synthetic Aperture Measurements (SAR) have a high spatial resolution of 100 m and better. SAR data can be classified to identify different sea ice types [Ressel et al., 2016]. The sea ice type is in most cases not directly related to ice thickness but gives some indication of the ice thickness class. Methods are developed to identify leads on a basin-wide scale from Sentinel-1 SAR data and combine them with CryoSat-2 radar altimeter measurements. Another application is the retrieval of sea ice topography from the TanDEM-X interferometric SAR mission.

Results of all studies are interpreted in the context of a changing climate system to improve our understanding of underlying climate processes in Polar Regions and beyond.

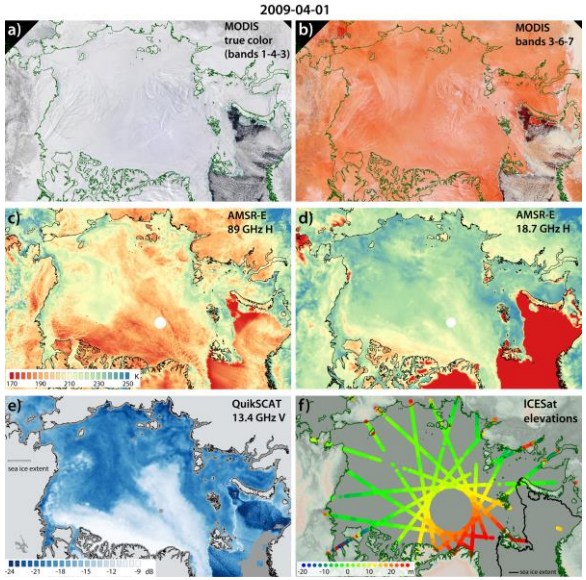

Figure 19: *The Arctic sea ice cover on 1 April 2009. (a) MODIS visible bands; (b) combined MODIS blue and short-wavelength infrared bands; (c, d) AMSR-E microwave radiometer brightness temperatures at 89 GHz H (c) and 19 GHz H (d); (e) backscatter from the QuikSCAT scatterometer at 13 GHz; (f) elevations from the ICESat GLAS laser altimeter. (From Spreen and Kern, 2017).*

References

Ressel, R., S. Singha, S. Lehner, A. Rösel, and G. Spreen (2016): Investigation into different polarimetric features for sea ice classification using X-band Synthetic Aperture Radar. *IEEE J-STARS*, 9(7), 3131-3143, doi:10.1109/JSTARS.2016.2539501.

Spreen, G. and S. Kern (2017): Chapter 9 Methods of satellite remote sensing of sea ice. In *Sea Ice*, Thomas, D. N. *(Ed.), Wiley-Blackwell*, 728pp, ISBN: 978-1-118-77838-8.

Ye, Y., M. Shokr, G. Heygster, and G. Spreen (2016): Improving Multiyear Ice Concentration Estimates with Ice Drift. *Remote Sens.*, 8(5), 397, doi:10.3390/rs8050397.

First simultaneous detection of marine and terrestrial chlorophyll fluorescence from space

Aleksandra Wolanin, Vladimir Rozanov, Stefan Noël, Tilman Dinter, Marco Vountas, John P. Burrows, and Astrid Bracher

Marine and terrestrial carbon pools are important reservoirs in the carbon cycle, and they absorb a significant part of the emitted carbon dioxide from fossil fuel combustion. It is clear that due to land-use changes worldwide, areas of pristine vegetation have been decreasing, e.g., the deforestation of the rainforest. With respect to the oceanic biosphere, there is an ongoing discussion about the changes in health, composition and abundance of phytoplankton. Observations from instrumentation on polar orbiting sun synchronous satellites have facilitated the study of changes in the phytoplankton biomass having a temporal sampling of a day and a spatial resolution on the order of a km. Information about chlorophyll fluorescence is directly linked to the physiology of phytoplankton or plants: When chlorophyll molecules absorb light, most of this energy is transformed into chemical energy in a process of photosynthesis. However, a fraction of the energy absorbed is re-emitted as fluorescence. Hence, as a result of its relationship to photosynthetic efficiency, information about chlorophyll fluorescence can be used to assess the productivity and physiological state of phytoplankton.

Inelastic processes (e.g., Raman scattering and fluorescence) lead to a redistribution of solar backscattered electromagnetic radiation and shift of the frequency towards higher or lower energy. Inelastic scattering by molecules in the air (mostly N_2 and O_2) is called rotational Raman scattering (RRS). In lakes, rivers and oceans there are two dominant inelastic processes: vibrational Raman scattering by water molecules, and fluorescence of phytoplankton pigments, mainly chlorophyll a, and coloured dissolved organic matter. Their effect on the backscattered radiation at the top of atmosphere can be identified in the filling-in of Fraunhofer lines (spectrally narrow and often saturated absorption features in the solar spectrum), the process known as the Ring effect. The filling-in of Fraunhofer lines can be observed with satellite-borne passive spectrometers, which have sufficient spectral resolution.

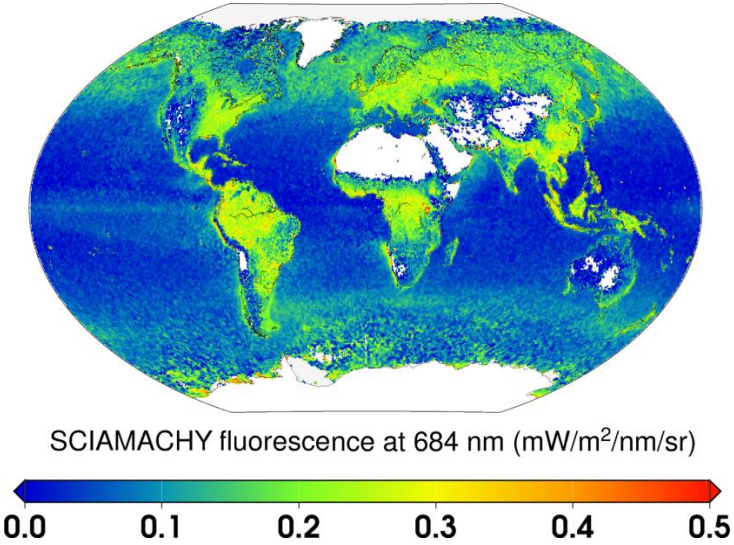

Figure 20: Global composite of red peak of chl-a fluorescence for both land and ocean retrieved from the SCIAMACHY instrument (years 2003-2011)

We have examined these effects with an approach based on the Differential Optical Absorption Spectroscopy (DOAS) technique applied to the hyperspectral data from the past and recent hyperspectral space-borne instruments: the SCIAMACHY instrument on board the ENVISAT satellite (in operation from 2002 to 2012) and GOME-2 onboard Metop satellite series and in operation since 2007. In our retrieval,

we evaluate the filling-in in SCIAMACHY and GOME-2 data of the Fraunhofer line Fe I at 684.3 nm, which is located very close to the emission peak of marine fluorescence (~685 nm) at the red peak, see Figure 20. The results on marine chlorophyll fluorescence observations from SCIAMACHY and GOME-2 were compared with the MODIS Terra normalized Fluorescence Line Height (nFLH) product for the average of the years 2003–2011 and year 2009 (only GOME-2). Our method also enables the retrieval of chlorophyll fluorescence above land vegetation scenes. The results for the fluorescence observed above terrestrial vegetation for July and December 2009 were compared to MODIS Enhanced Vegetation Index (EVI). The comparisons show good spatial agreement between different retrievals, providing evidence for the good performance of our algorithm. The method presented is generic and can be applied to other hyperspectral instruments in the future. Having established the retrieval technique, extensive studies of chlorophyll fluorescence will improve global knowledge on physiology and photosynthetic efficiency in both the marine and terrestrial realms, and its dependence on environmental factors. It is also the very first time chlorophyll fluorescence from both land and ocean was retrieved with the same approach.

Summary

This new satellite remote sensing approach enabled to retrieve chlorophyll-a fluorescence at its red peak (~685 nm)by using measurements from the hyperspectral instruments SCIAMACHY and GOME-2 from 2003 to 2011. This new retrieval enables simultaneous observations of chl-a fluorescence from both land and ocean by exploiting narrow spectral structures resulting from the filling-in of the Fraunhofer Fe I line. The red peak of chl-a fluorescence from terrestrial vegetation has never been observed from space before, and marine chl-a fluorescence was retrieved for the first time with hyperspectral satellite-borne sensors. The obtained SCIAMACHY results show good spatial agreement with other datasets, MODIS nFLH for marine chl-a fluorescence, and MODIS EVI and GOME-2 far-red chl fluorescence for land vegetation. Improved knowledge on chl-a fluorescence will improve studies on photophysiology, productivity and health of both marine and terrestrial ecosystems.

This study was performed in collaboration between IUP and the Phytooptics Group at Alfred-Wegener-Institute for Polar and Marine Research (AWI), Bremerhaven.

References

Wolanin A., Rozanov V. V., Noel S., Dinter T., Vountas M., Burrows J.P., Bracher A. (2015) Global retrieval of marine and terrestrial chlorophyll fluorescence at its red peak using hyperspectral top of atmosphere radiance measurements: Feasibility study and first results. Remote Sensing of Environment 166: 243-261 . doi: 10.1016/j.rse.2015.05.018

Carbon dioxide and methane from satellites

Michael Buchwitz, Maximilian Reuter, Oliver Schneising, Jens Heymann, Thomas Krings, Michael Hilker, Dhanyalekshmi Pillai, Vladimir Rozanov, Heinrich Bovensmann, and John P. Burrows

Carbon dioxide (CO_2) and methane (CH_4) are the two most important man-made („anthropogenic“) greenhouse gases (GHG) contributing to global warming. Despite their importance, our understanding of their variable natural and anthropogenic sources and sinks has large gaps. This limits the reliability of climate prediction, which requires an adequate understanding of their natural sources and sinks. Furthermore, reported anthropogenic GHG emissions can typically not be verified by independent observations.

A large fraction of our knowledge on CO_2 and CH_4 sources and sinks stems from accurate but sparse networks of surface observations performing local point measurements. In recent years, satellite observations of greenhouse gases are adding more and more information, thanks to their global observational coverage combined with improved data quality and analysis methods (e.g., Buchwitz et al., 2015a, 2015b).

Of particular relevance are satellite observations with high measurement sensitivity to CO_2 and CH_4 concentration changes close to the Earth's surface where the source/sink signals are largest. At present, data from three satellite instruments are available, which fulfil this requirement: SCIAMACHY on ENVISAT (2002-2012; scientifically led by IUP, Univ. Bremen), TANSO-FTS on board the Japanese GOSAT satellite (2009-today) and NASA's OCO-2 (CO_2 only; mid 2014 to today).

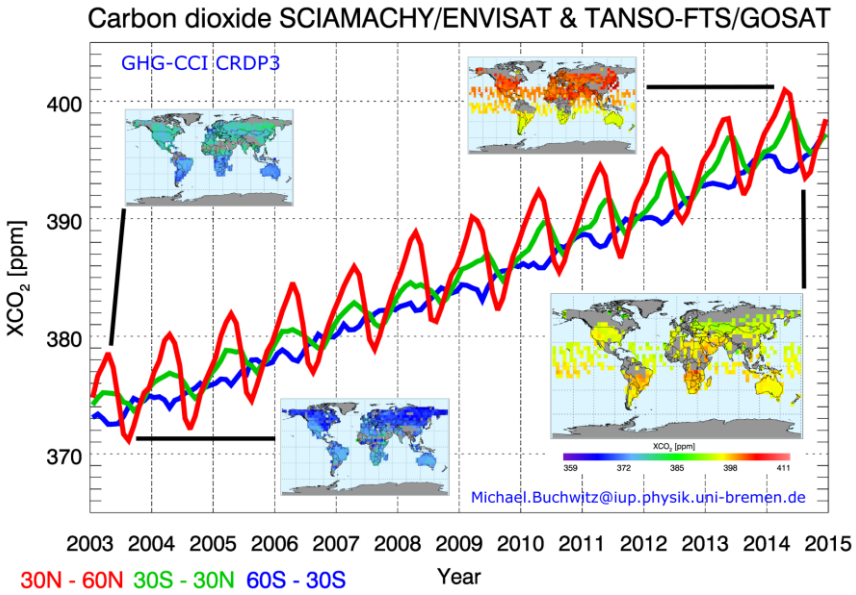

Figure 21: Time series of column-averaged CO_2 ("XCO_2") as obtained at IUP, Univ. Bremen, by merging individual SCIAMACHY and GOSAT XCO_2 satellite data products and CH_4 from Sentinel-5P from 2017 onwards.. The three curves correspond to three different latitude bands (e.g., red = 30°-60°N, i.e., northern hemispheric mid-latitudes). The maps show the spatial coverage of the satellite XCO_2 observations during selected months. As can be seen, atmospheric CO_2 increases by about 2 ppm/year (primarily due to burning of fossil fuels). The seasonal variations, which depend on latitude, are primarily due to uptake and release of CO_2 by vegetation (photosynthesis, respiration and decay of organic matter) (details: Buchwitz et al., 2015a, 2015b, and http://www.esa-ghg-cci.org/).

Activities and results from existing greenhouse gas satellites

The IUP-Bremen is among the leading institutes in the relatively new area of satellite remote sensing of the greenhouse gases (GHG) CO_2 and CH_4. Currently, IUP-Bremen is leading the GHG-CCI project of ESA's Climate Change Initiative (CCI) which delivers the "Essential Climate Variable" (ECV) Greenhouse Gases (http://www.esa-ghg-cci.org/, Buchwitz et al., 2015a, 2015b). Focus of this project is to

generate atmospheric CO_2 (see Figure 21) and CH_4 data products from satellites for climate-relevant applications. The goal is to generate consistent long-term data sets with a quality high enough for climate applications.

A complementary activity where IUP-Bremen is strongly involved is the Copernicus Atmospheric Monitoring Service (CAMS). Here, the focus is on fast data delivery. Within CAMS, IUP-Bremen generates a column-averaged CO_2 ("XCO_2") data product from radiance observations of the Japanese GOSAT satellite in quasi near-real-time and delivers this product to the European Centre for Medium-Range Weather Forecasts (ECMWF) (see Heymann et al., 2015; Massart et al. 2016).

IUP-Bremen is not only active in generating satellite-derived atmospheric data products but also in the area of data interpretation of these data products in terms of greenhouse gases sources and sinks. A focus during recent years was to use the satellite CO_2 observations in combination with modelling in order to quantify the strength of the European terrestrial (natural) carbon sink. As shown by Reuter et al., 2016, it seems clear that Europe is a carbon sink but the magnitude of this sink is very uncertain (see Figure 22). More research is needed to better quantify this potentially important carbon sink and to monitor how it changes with time.

Activities related to future greenhouse gas satellites

The IUP is also strongly involved in future greenhouse gas satellite missions. For example, IUP-Bremen has proposed a new satellite, the "Carbon Monitoring Satellite" (CarbonSat), to further improve our knowledge of the various natural and anthropogenic sources and sinks CO_2 and CH_4. End of 2015 ESA decided to implement FLEX and not CarbonSat. However, it has been recognized by an Expert Group of the European Commission that there is a strong need for CarbonSat or a CarbonSat-like satellite mission or even a constellation of these satellites in order to monitor fossil CO_2 emissions, see http://www.copernicus.eu/main/towards-european-operational-observing-system-monitor-fossil-co2-emissions. A "CO_2 Mission Task Force" has been established by ESA and the European Commission to define the requirements for such a satellite mission and IUP-Bremen is represented in this task force. IUP-Bremen is also involved in other activities related to future satellites, for example, in developing an algorithm to retrieve methane from Europe's Sentinel-5-Precursor (S5P) satellite which will be launched in 2017.

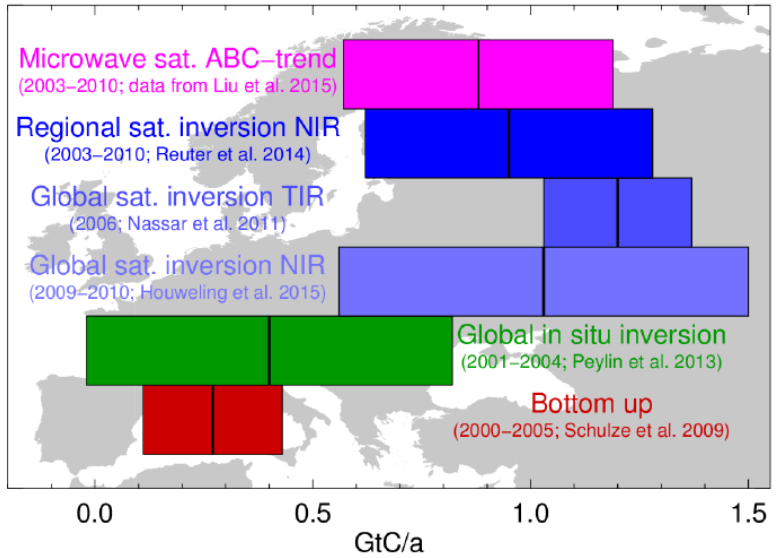

Figure 22: Range of estimates of the strength of the European terrestrial (vegetation) carbon sink (in gigatons carbon per year; based on study results published in peer-reviewed scientific publications) as derived from satellite data, in-situ observations and bottom-up methods. As can be seen, all studies agree that Europe is a carbon sink. The magnitude of this sink is however very uncertain and more research is needed to better quantify this sink (see Reuter et al., 2016, for details).

References

Buchwitz, M., M. Reuter, O. Schneising, et al., The Greenhouse Gas Climate Change Initiative (GHG-CCI): comparison and quality assessment of near-surface-sensitive satellite-derived CO2 and CH4 global data sets, Remote Sensing of Environment, 162, 344-362, doi:10.1016/j.rse.2013.04.024, 2015a.

Buchwitz, M., M. Reuter, O. Schneising, et al., The greenhouse gas project of ESA's Climate Change Initiative (GHG-CCI): Overview, achievements and future plans, The International Archives of the Photogrammetry, Remote Sensing and Spatial Information Sciences, Volume XL-7/W3, 2015 36th International Symposium on Remote Sensing of Environment, 11-15 May 2015, Berlin, Germany, 2015b.

ESA, Report for Mission Selection: CarbonSat, ESA SP-1330/1 (2 volume series), European Space Agency, Noordwijk, The Netherlands, link to CarbonSat report: http://esamultimedia.esa.int/docs/EarthObservation/SP1330-1_CarbonSat.pdf , 2015.

Heymann, J., M. Reuter, M. Hilker, et al., Consistent satellite XCO2 retrievals from SCIAMACHY and GOSAT using the BESD algorithm, Atmos. Meas. Tech., 8, 2961-2980, 2015.

Kulawik, S., D. Wunch, C. O'Dell, et al., Consistent evaluation of ACOS-GOSAT, BESD-SCIAMACHY, CarbonTracker, and MACC through comparisons to TCCON, Atmos. Meas. Tech., 9, 683-709, doi:10.5194/amt-9-683-2016, 2016.

Massart, S., A. Agusti-Panareda, J. Heymann, et al., Ability of the 4-D-Var analysis of the GOSAT BESD XCO2 retrievals to characterize atmospheric CO2 at large and synoptic scales, Atmos. Chem. Phys., 16, 1653-1671, doi:10.5194/acp-16-1653-2016, 2016.

Pillai, D., M. Buchwitz, C. Gerbig, et al., Tracking city CO2 emissions from space using a high resolution inverse modelling approach: A case study for Berlin, Germany, Atmos. Chem. Phys., 16, 9591-9610, doi:10.5194/acp-16-9591-2016, 2016.

Reuter, M., M. Buchwitz, M. Hilker, et al., How much CO2 is taken up by the European terrestrial biosphere? Bull. Amer. Meteor. Soc. doi:10.1175/BAMS-D-15-00310.1, in press, 2016.

Links

IUP CarbonGroup webite: http://www.iup.uni-bremen.de/sciamachy/NIR_NADIR_WFM_DOAS/

GHG-CCI project led by IUP, Univ. Bremen: http://www.esa-ghg-cci.org/

CAMS project: http://www.ecmwf.int/en/about/what-we-do/copernicus/copernicus-atmosphere-monitoring-service

CarbonSat: http://www.iup.uni-bremen.de/carbonsat/

Videos (in German; based on interviews with Dr. M. Reuter and Dr. M. Buchwitz, IUP, Univ. Bremen):

“Grüner Luftreiniger”: https://www.youtube.com/watch?v=DfYuXxWj73w

“Neues zu CO_2, Methan und Fracking”: https://www.youtube.com/watch?v=KIa4OD17zkw

“Warm up, cool down!” (Teil 2: Facts und Figures über das Treibhausgas Methan): http://hyperraum.tv/2016/09/30/warm-up-cool-down/

Monitoring compliance with sulphur content regulations of shipping fuel by in situ measurements of ship emissions

Lisa Kattner, Barbara Mathieu-Üffing, John P. Burrows, Andreas Richter, Stefan Schmolke, André Seyler, and Folkard Wittrock

Air pollution from shipping is a severe problem especially for coastal areas and harbour towns. In 1997, the International Maritime Organization (IMO) has addressed this problem by adopting MARPOL Annex VI. Part of this regulation is the reduction of sulphur in shipping fuels which forms sulphur dioxide (SO_2) during the combustion process, a gas that causes particle formation, health effects and acidification. The IMO regulations concerning sulphur content in shipping fuels came into force in 2005. For all oceans worldwide, the sulphur content allowed in HFOs is capped at 3.5%. In addition, Sulphur Emission Control Areas (SECA) were established; one of them comprises the Baltic Sea and the North Sea. Within these SECAs the sulphur limit was initially set to 1.5%, which was reduced to 1.0% in 2010 and has now reached its current reduction step in January 2015 with a limit of 0.1% (Figure 23). With the regulations in place, the question remains how to efficiently verify compliance by the ships. Up to now, this is done by inspection authorities who enter ships at berth, review fuel log books and, if suspicion is raised, take a fuel sample to be analysed at certified laboratories. With the results of these analyses, it is possible to take legal action, if needed. However, these controls can check just a minor number of ships and only in harbours. To increase the number of monitored ships, several studies have suggested using exhaust gas measurements of the ships to estimate the sulphur content without having to access the ships directly.

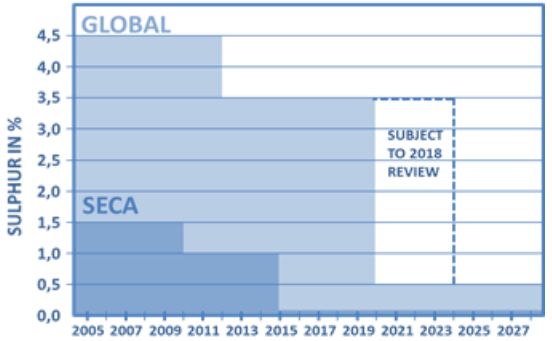

Figure 23: Sulfur reduction in shipping fuels according to IMO Marpol Annex VI

Measurements

In 2012, the project MeSmarT started as a cooperation between the University of Bremen and the German Federal Maritime and Hydrographic Agency (BSH). Part of the project was to assess and implement the method of exhaust gas measurements with in-situ instruments for sulphur fuel content monitoring. A measurement station has been set up at the northern banks of the Elbe river, in the small town Wedel near Hamburg harbour, see Figure 25. In-situ instruments for the trace gases sulphur dioxide (SO_2), carbon dioxide (CO_2), nitrogen oxides (NO_x) and ozone (O_3) in a weatherproof, temperature stabilized box were set up at the station, with a line of sight distance of around 400 m to the passing ships. In addition, a weather station provides information about wind speed and direction, and anAIS (automatic identification system) receiver collects information transmitted by passing ships about their identification, position, course and speed. To obtain the sulphur content of the fuel the passing ship was using, it is possible to use a formula with the ratio of the SO_2 to CO_2 concentrations of a plume. This gives a good estimation of the sulphur fuel content with an uncertainty between 15 to 30%.

In a second step, the peaks and thus the sulphur fuel contents can be associated with the respective ships by combining wind information and positions of the ships obtained by the AIS data.

Results

In autumn 2014, it was possible to analyse the sulphur fuel content of 824 ship plumes of 474 individual ships. During that time, the allowed sulphur content was 1% and 99.6% of all ships complied with this regulation according to our measurements and within the limits of our uncertainty. In January 2015, we analysed 589 plumes of 374 individual ships. With the new sulphur limit of 0.1% in force, we could show that still 95.4% of all ships measured complied and that it is possible to identify those ships that do not comply (Figure 24).

The lengths of the ships in 50 m size steps are color-coded. Even before the regulation change, ships smaller than 100 m (red) did not use fuel with sulphur values higher than 0.2 %, most likely because their engines cannot process such fuels, or because storage capacity for two different kinds of fuels is not available, or because they are inland water vessels

Figure 25: Measurement station in Wedel. Map source: OpenStreetMap.

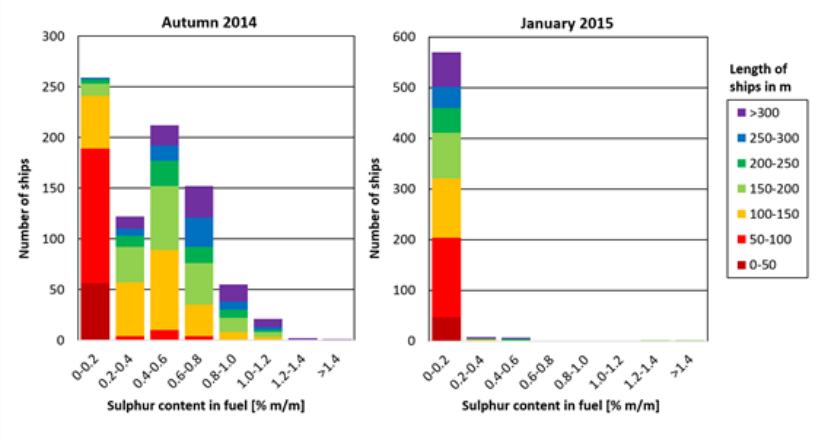

Figure 24: Sulphur fuel content in autumn 2014 before, and in January 2015, after the change of fuel regulations.

which have to follow other regulations.

The number of ships that can be detected and analysed strongly depends on wind conditions. For months with good wind conditions, it is possible to detect about 30-40% of all ships; for months with unfavourable wind conditions, this value drops to less than 10%.

Based on this work and in close cooperation with the responsible authorities BSH and the police, the measurement station has been enhanced and the analysis has been automatized, so that ships which do not comply are directly reported and checked by the police. In 2015, a total of 3500 plumes could be analysed.

Reference:

Kattner, L., Mathieu-Üffing, B., Burrows, J. P., Richter, A., Schmolke, S., Seyler, A., Wittrock, F.: Monitoring compliance with sulfur content regulations of shipping fuel by in situ measurements of ship emissions, *Atmos. Chem. Phys.*, 15, 10087 – 10092, 2015

Space based observation of volcanic iodine monoxide

Anja Schönhardt, Andreas Richter, Nicolas Theys, and John P. Burrows

Halogen oxides strongly influence atmospheric composition. Catalytic reaction cycles involving chlorine, bromine or iodine lead to ozone depletion in the troposphere., The role of chlorine and bromine released in the stratosphere predominantly as a consequence of anthropogenic emissions of chlorofluorocarbon compounds is well established, and the potential importance of iodine reactions in stratospheric ozone depletion well discussed.

Volcanic eruptions inject substantial amounts of halogens into the atmosphere. Chlorine and bromine oxides have frequently been observed in volcanic plumes from different instrumental platforms, from ground, aircraft as well as from satellite. For the first time now, we have observational evidence that iodine oxides are also emitted into the atmosphere during volcanic eruptions. Large column amounts of iodine monoxide, IO, have been observed in satellite measurements following the major eruption of the Kasatochi volcano, Alaska, in 2008.

The IO signal is detected in measurements made by two individual satellite instruments, the SCIAMACHY (SCanning Imaging Absorption spectroMeter for Atmospheric CHartography) sensor on the ENVISAT satellite, as well as GOME-2 (Global Ozone Monitoring Experiment) on the MetOp-A platform. For SCIAMACHY, an IO product has been reported before (Schönhardt et al., 2008, 2012), while IO detection in GOME-2A measurements is a recent development (Schönhardt et al., 2016). In addition to IO, column amounts of bromine monoxide, BrO, and sulphur dioxide, SO_2, are also observed by GOME-2A and compared to the detected IO column densities. The trace gas columns are retrieved by using the well-established DOAS (Differential Optical Absorption Spectroscopy) technique.

Following the eruption of Kasatochi in the afternoon of August 7, 2008, enhanced IO amounts are observed for several days starting on August 8, 2008. Maps of IO retrieved from GOME-2A data for four days after the eruption are shown in Figure 26 (left) next to the BrO column (right). The IO plume from the volcanic emission is clearly visible on all four days. The spatial shape of the IO enhancement agrees well with the area where large BrO amounts are observed. Details in the spatial distribution within the volcanic plume, however, differ between the individual compounds. A close-up of the volcanic plume on day August 09, 2008, is shown in Figure 27, comparing IO (left), BrO (centre) and SO_2 (right). While SO_2 is mostly enhanced in the plume centre, maximum BrO is located at the western side of the plume and IO maxima are observed in two areas in the North and South of the plume

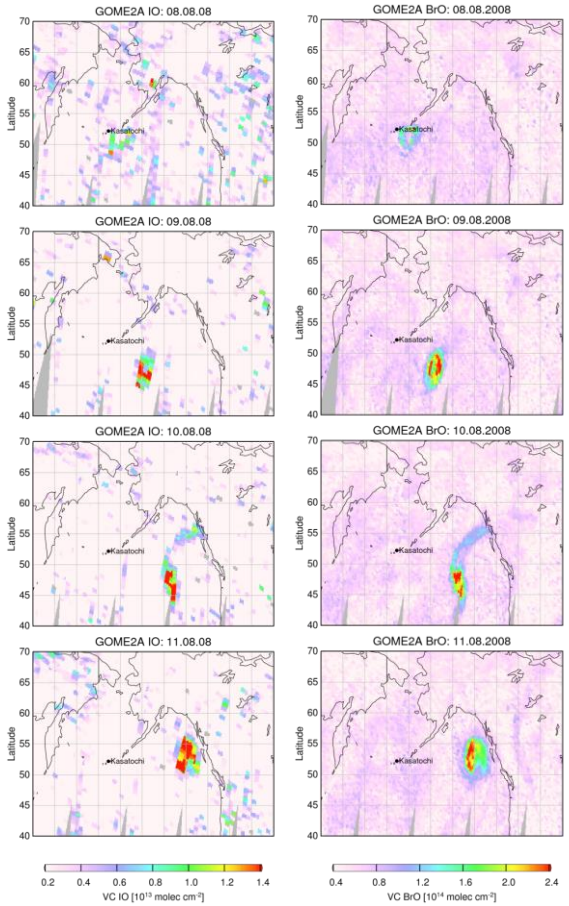

Figure 26: Observations of IO (left) and BrO (right) column amounts derived from GOME-2A satellite measurements for 4 days following the eruption of Kasatochi volcano, Alaska, on August 08, 2008.

centre. Differences in the spatial distribution argue for differences in the eruption process and chronology for the three compounds. In addition, the chemical pathways of iodine and bromine in the plume are probably not independent from each other, which may result in spatially separated maximum values for the two halogen oxides.

On day August 08, just after the start of the eruption, approximately 1.8×10^{28} molecules of IO are observed in the plume, corresponding to a mass of 4.3 metric tons, t, of IO. The amount of IO increases up to about 12.2 t on August 11. The range of IO mass between 4.3 and 12.2 t corresponds to an amount of reactive iodine between 3.9 and 10.8 t. The integrated amount of BrO within the plume increases from 26 t on August 08 to a maximum amount of 87 t on August 11. Converting this range of values to the corresponding amount of reactive Br, amounts between 22 and 73 t are derived. The observed amounts of IO and BrO are a low estimate for the amount of reactive iodine and bromine emitted to the atmosphere due to the presence of further iodine and bromine compounds not included in the IO and BrO measurements.

The Kasatochi plume altitude reached predominantly the altitude between 8 and 12 km. i.e. into the lower stratosphere. Consequently, the satellite observations of large amounts of iodine after the Kasatochi eruption indicate that volcanic eruptions may lead to a substantial input of iodine to the stratosphere, as well as to the upper troposphere lower stratosphere region. If the IO amount is homogeneously spread over the plume area and within the main 4 km thick vertical layer, a mixing ratio of 3 pptv (parts per trillion by volume) at an altitude of 10 km results. The local mixing ratio can be much higher due to inhomogeneous distribution in the volcanic plume. The inferred iodine mixing ratio

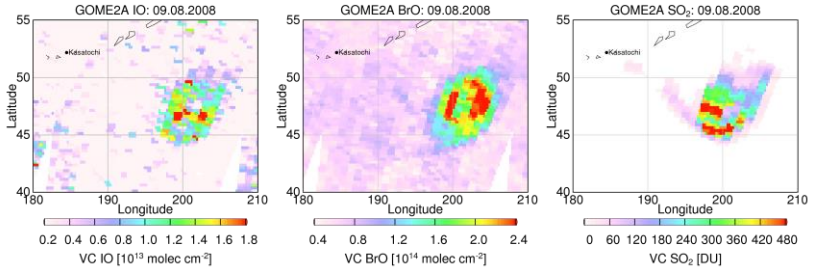

Figure 27: Close-up of the volcanic plumes of IO (left), BrO (centre) and SO_2 (right) on the day August 09, 2008. While the plume extent and shape are similar, differences in the spatial distribution patterns are visible.

has substantial impact on the atmospheric composition, e.g., through reducing the ozone levels.

IO has not yet been detected for any other eruptions investigated, at least not at the Kasatochi levels. Scaling with the observed bromine amounts, iodine levels for the other eruptions could just be below or around the detection limit of current space based instruments. Future satellite instruments with finer spatial resolution and improved signal-to-noise ratio may allow the observation and detailed investigation of iodine species in volcanic plumes more frequently.

References:

Schönhardt, A., Richter, A., Wittrock, F., Kirk, H., Oetjen, H., Roscoe, H. K., and Burrows, J. P.: Observations of iodine monoxide columns from satellite, Atmos. Chem. Phys., 8, 637–653, 2008.

Schönhardt, A., Begoin, M., Richter, A., Wittrock, F., Kaleschke, L., Gómez Martín, J. C., and Burrows, J. P.: Simultaneous satellite observations of IO and BrO over Antarctica, Atmospheric Chemistry and Physics, 12, 6565–6580, doi:10.5194/acp-12-6565-2012, 2012.

Schönhardt, A., Richter, A., Theys, N., and Burrows, J. P.: Space based observation of volcanic iodine monoxide, Atmos. Chem. Phys. Discuss., doi:10.5194/acp-2016-619, in review for Atmos. Chem. Phys., 2016.

Long-term ozone observations from space

Mark Weber, Elpida Leventidou, Kai-Uwe Eichmann, and John P. Burrows

Stratospheric ozone

From a series of European nadir viewing (downward looking) space based UV/vis spectrometers, column density ozone (also called total ozone) has been retrieved at the IUP Bremen. The combined ozone dataset now encompasses a period of twenty years and is suitable for detecting global long-term trends in connection with climate change and evolution of ozone depleting substances (ODS) that are regulated by the Montreal Protocol and its Amendments to protect the ozone layer.

At IUP Bremen, the weighting function DOAS (Differential Optical Absorption Spectroscopy) approach is applied to derive global distributions of column ozone from GOME, SCIAMACHY, and GOME-2 (1995-present). The multiple instrument datasets have been merged into a consistent long-term dataset that was recently used in the WMO Scientific Assessment of Ozone Depletion from 2014. As a result of the Montreal Protocol phasing out ozone depleting substances (ODS), ozone is expected to recover at a slow rate since the end of the 1990s. The total ozone trends observed since the late 1990s are, however, statistically not significantly different from zero due to the large year-to-year variability (Figure 28). Nevertheless, the ozone decline of several percent per decade observed in most regions of the globe before the 1990s was successfully stopped, documenting the success of the Montreal Protocol.

Tropospheric ozone

About 90% of the total column ozone resides in the stratosphere (atmospheric region above the tropopause at about 8-15 km), thus the total column is a good measure of the thickness of the ozone layer in the lower stratosphere. Human and plant health is, however, also affected by tropospheric ozone. Enhanced levels of surface ozone can lead to severe respiratory problems and ultimately to cardiovascular attacks, as well as the poisoning of plants. Measuring tropospheric ozone is, therefore, important when monitoring air quality. However, due to the small contribution of tropospheric ozone to the column ozone, it is difficult to measure from space directly. Tropospheric ozone can be retrieved using some methods that separate the stratospheric and tropospheric parts of the column ozone.

Among others, two different approaches have been implemented that combine cloud information and ozone column from space measure-

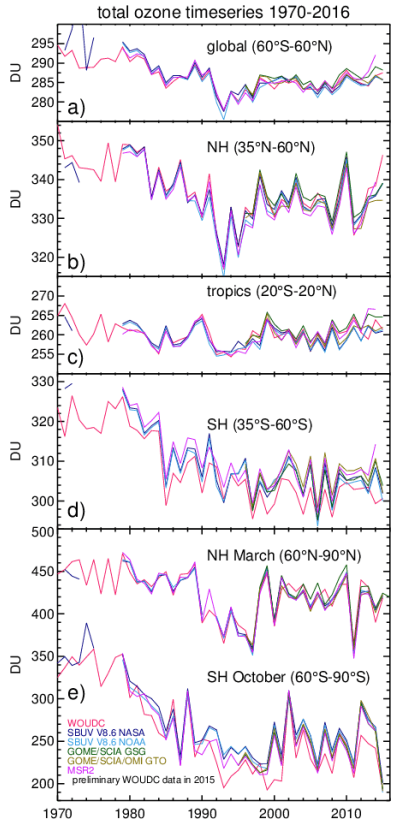

Figure 28: Zonal mean time-series of several total ozone datasets at different latitude ranges. a) near global (60°S-60°N), b) northern hemisphere (35°N-60°N), c) tropics (20°S-20°N), d) southern hemisphere (35°S-60°S), all annual means so far, and e) March Arctic values (60°N-90°N) and October Antarctic values (60°S-90°S) during ozone hole season. Colours show different datasets: red, ground-based data, green, European satellite datasets (GSG: our data, GTO: DLR Oberpfaffenhofen), blue: two different merged SBUV datasets from the US (Update from Weber et al., 2016).

ments. The so-called Convective Cloud Differential (CCD) method subtracts the above-cloud column retrieved in a region of high convective clouds, typically in the tropical region of the Pacific, from total columns observed elsewhere to obtain tropospheric ozone column amounts. A second method called Cloud Slicing (CS) regresses above-cloud ozone columns against observed cloud-top-heights to acquire mean ozone volume mixing ratio at cloud altitudes. Both methods are statistical methods that derive mean quantities by averaging over sampled data in pre-defined grid boxes and their applicability is limited to the tropical region. Figure 29 shows an example of satellite derived CCD tropospheric column time series along with ozone sonde data above Natal in South America. At this station, the agreement between satellite and sonde data is quite good.

At the moment the various tropospheric ozone satellite data are merged into a single long-term dataset for investigating trends and variability. Both tropospheric ozone methods are also being adapted to be applied to the upcoming TROPOMI mission that will be launched into space aboard Sentinel 5P in 2017 and will allow extending the satellite time series into the near future.

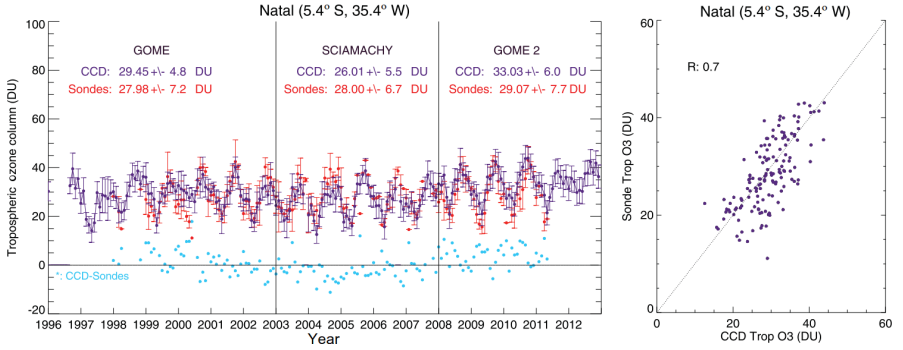

Figure 29: Time series of CCD tropospheric ozone columns up to 200 hPa (~12 km altitude) from GOME, SCIAMACHY, and GOME-2A, and ozone sondes above Natal in South America (Brazil) from 1996 to 2013. The light blue dots show the differences between monthly mean satellite and ozone sonde data. Note that the data from the three satellites have not been homogenized, meaning bias between them removed. A scatter plot is shown in the right panel. From Leventidou et al. (2016).

References

Leventidou, E., Eichmann, K.-U., Weber, M., and Burrows, J. P.: Tropical tropospheric ozone columns from nadir retrievals of GOME-1/ERS-2, SCIAMACHY/Envisat, and GOME-2/MetOp-A (1996–2012), Atmos. Meas. Tech., 9, 3407-3427, doi:10.5194/amt-9-3407-2016, 2016.

Pawson, S., W. Steinbrecht, A.J. Charlton-Perez, M. Fujiwara, A.Yu. Karpechko, I. Petropavlovskikh, J. Urban, and M. Weber, Update on Global Ozone: Past, Present, and Future, Chapter 2 in Scientific Assessment of Ozone Depletion: 2014, World Meteorological Organization, Global Ozone Research and Monitoring Project - Report No. 55, 2014.

Weber, M., W. Steinbrecht, C. Roth, M. Coldewey-Egbers, D. Degenstein, V.E. Fioletov, S. M. Frith, L. Froidevaux, J. de Laat, C. S. Long, D. Loyola, and J. D. Wild: [Global Climate] Stratospheric ozone [in "State of the Climate in 2015"], Bull. Amer. Meteor. Soc., 97, S49–S51, 2016

Solar variability

Mark Weber, Tina Hilbig, Klaus Bramstedt, and John P. Burrows

Space-borne UV spectrometers dedicated to atmospheric measurements usually observe the sun on a regular basis. The atmospheric spectra are divided by the spectral solar irradiance (SSI) to obtain sun-normalised radiances upon which atmospheric retrieval algorithms are applied to retrieve trace gases and other geophysical parameters like clouds and aerosols. The daily SSIs themselves are also of large scientific interest as they allow us to investigate irradiance variability due to solar magnetic activity on daily to decadal time scales. Daily SSI irradiance data from space are now available going back to the late 1970s from several atmospheric sounders in combination with dedicated solar missions.

A big challenge for space UV spectral measurements are the optical degradation due to harmful UV radiation and polymerisation of optical surfaces that leads to blinding of the instrument. Complex degradation corrections have to be applied to obtain reliable time-series. From the SSI, so-called solar proxies can be derived that are largely insensitive to instrument degradation. A popular solar proxy is the Mg II core-to-wing ratio (Mg II index) derived from the Mg II doublet observed at 280 nm. The narrow emission cores of the doublet varies with solar activity and highly correlates with SSI variations in the UV spectral region, thus, it is often used for SSI reconstruction in solar or climate models to investigate the atmospheric effects from the direct solar radiation.

We derive the Mg II indices from GOME, SCIAMACHY, and GOME-2 observations and combine them with other available datasets to create the Bremen Composite Mg II index as shown in Figure 30. This index nicely shows the changes with the Schwabe (11-year magnetic activity) and Carrington (27-day solar rotation) cycles and now spans nearly 36 years. The solar minimum following solar cycle 23 (in 2009) was one of the quietest periods (with virtually no solar modulation) compared to the previous ones. The most recent solar cycle 24 has a much lower activity maximum than cycles 22 and 23. The length and amplitude of the various solar cycles are very variable. Very recently we established uncertainties of the indices from the measurements, as well as from merging the various datasets. The correlation with the solar radio flux at 30cm (F30cm) is excellent.

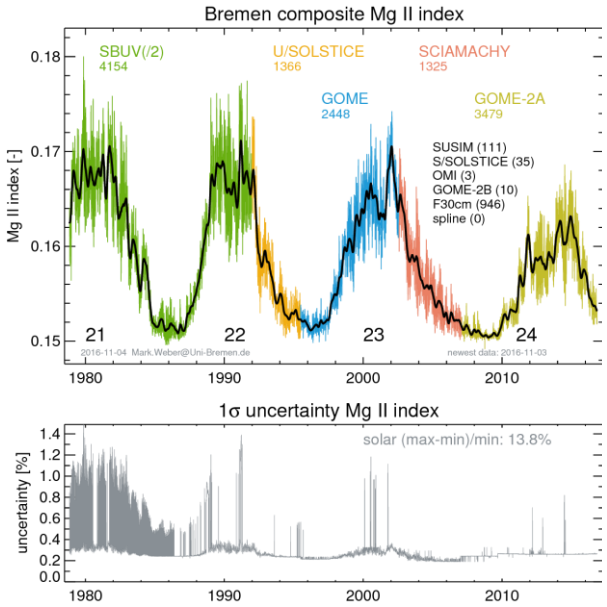

Figure 30: Top panel: Composite Mg II index ('Bremen composite') spanning the 11-year solar cycles numbered 21 to 24. Values indicate numbers of days for each satellite contributing to the composite index. Missing values were filled using scaled F30 cm radio flux data. The black curve shows the time-series smoothed twice with a 55-day boxcar removing the 27-day solar rotation signal. Bottom panel shows the estimated uncertainty of the composite Mg II index. Higher uncertainties are due to the interpolated F30cm values. The solar minimum to maximum change in this Mg II index is about 14% of the long-term mean as derived from the smoothed Mg II time series. This means that the uncertainty of the Mg II index with respect to a typical solar cycle change is about 2% and higher.

In the DFG project SCIASOL, we attempt to re-calibrate SCIAMACHY solar irradiance data using an optical bench simulator and a mirror model that accounts for contamination of the external mirror surface. The goal here is to have a degradation free 12-year time-series covering the UV to NIR that can be used to assess the

SSI variability over a solar cycle. Particularly in the visible spectral range, large uncertainties still exist. In a first step, an improved solar reference spectrum from SCIAMACHY was established and is compared to various other available solar data as shown in Figure 31. The agreement of SCIAMACHY with other data is usually within 5% or better. Larger differences are observed at the smallest wavelengths (below 270 nm) and in the NIR (above 1600 nm). The NIR is currently matter of a scientific debate as more recent solar data including SCIAMACHY show systematically lower SSI than the Atlas-3 composite that is widely considered the standard for the visible and NIR spectral range.

References:

Snow, M., M. Weber, J. Machol, R. Viereck, and E. Richard, Comparison of Magnesium II core-to-wing ratio observations during solar minimum 23/24, J. Space Weather Space Clim., 4, A04, doi:10.1051/swsc/2014001, 2014.

Weber, M.: Comment on the Article by Thuillier et al. "The Infrared Solar Spectrum Measured by the SOLSPEC Spectrometer onboard the International Space Station," Sol. Phys., 290, 1601–1605, doi:10.1007/s11207-015-0707-y, 2015.

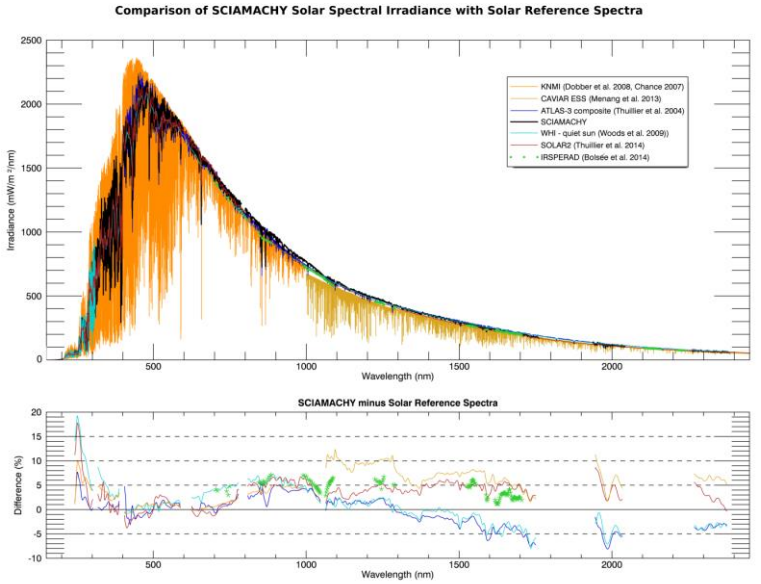

Figure 31: The upper panel shows a SCIAMACHY solar spectrum (black) in its full wavelength range from 0.24 µm (UV) to 2.4 µm (near-IR) together with several other established solar reference spectra. These reference spectra are based on different space as well as ground measurements. The lower panel presents the difference between the SCIAMACHY solar spectrum and the other data. As the data sets have different spectral resolutions, all spectra were convolved with a 10 nm Gaussian before taking the difference.

Trace gas and aerosol profiles in the stratosphere from limb measurements

Katja Weigel, Alexei Rozanov, Carlo Arosio, Elizaveta Malinina, Stefan Noël, and John P. Burrows

Among other observation geometries, SCIAMACHY on Envisat provided limb measurements of the Earth's atmosphere for almost 10 years between August 2002 and April 2012. Limb measurements from satellites look through the atmosphere tangential to the Earth's surface and can be used to retrieve height resolved information about trace gases and aerosol parameters in the upper troposphere and stratosphere.

This is a very interesting region to observe long term changes in the atmosphere because, compared to the troposphere below, it is less affected by the day to day variations due to weather. At the same time, only few long and consistent data sets exist for this altitude. In situ observations from balloon or high flying aircrafts are sparse and are often only available for measurement campaigns.

To exploit this data To the maximum, we improved the retrieval algorithms for aerosol, O_3, and H_2O.

Aerosol particle size distribution parameter retrieval

Most satellites report information about stratospheric aerosols as extinction, a measure of the attenuation of the light in the atmosphere due to the scattering and absorption by aerosols. Such a data set is also available from SCIAMACHY limb measurements; see von Savigny et al. (2015).

Due to its broad spectral range, SCIAMACHY can provide additional information about the aerosol particle size distribution, which is assumed to be a log-normal distribution dependent on the particle number density, the mode radius of the aerosol and the width of the distribution of radii. Currently, the mode radius and the distribution width can be retrieved while the influence of the number density on these measurements is estimated to be small compared to the other two parameters. So far, a representative data set of cloud free tropical measurements from SCIAMACHY has been retrieved showing promising results. The effect of volcanic eruptions on mode radius and distribution width is clearly identified in the time series (Figure 32).

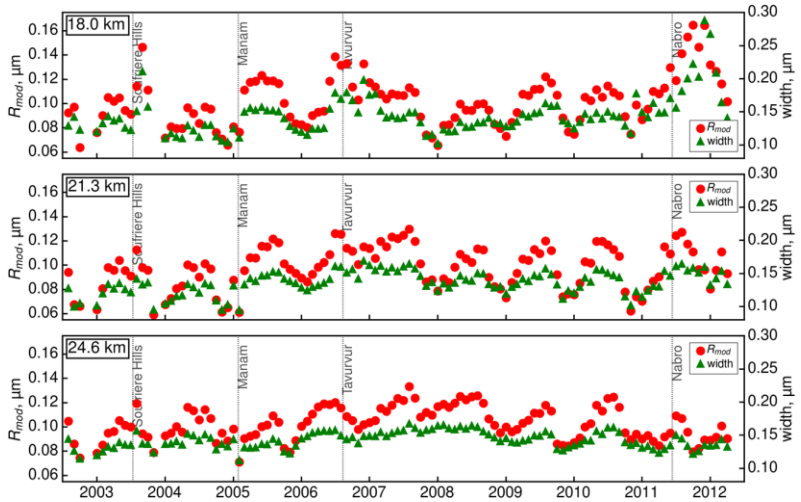

Figure 32: Aerosol mode radius and distribution width for cloud free measurements of SCIAMACHY between 20°S and 20°N (9732 cases). Important volcanic eruptions are marked.

Ozone retrieval

Published versions of the SCIAMACHY limb O3 retrieval (see e.g. Rahpoe et al., 2015) use information from the Hartley and Chappuis spectral band to retrieve O_3 in the upper and lower stratosphere.

For the most recent O_3 data version V3.5 (Figure 33), measurements from the Huggins spectral band are added to obtain more accurate data in the middle stratosphere. This and other adjustments of the algorithm clearly improved the data quality. V3.5 shows a better agreement to other satellite and in situ ozone sonde measurements. In addition to using SCIAMACHY data, there are also first results using the same algorithms developed at IUP Bremen for the O_3 limb retrieval from OMPS (Ozone Mapping Profiler Suite) data, an instrument on Suomi NPP in orbit since 2011.

Water vapour retrieval

The near infrared spectral region (1353-1410 nm) can be used to retrieve H_2O in the upper troposphere and lower stratosphere (UTLS) between about 10 and 25 km. The retrieval needs extensive calculations (Weigel et al., 2016). Currently, a new data version V4.2 is being processed with a different regularization, improved aerosol correction, and updated input data. V4.2 shows a better convergence and vertical resolution compared to V3.01 and agrees better to other data sets especially above 18 km. Using parallelization with MPI this data set can be processed more efficiently on high performance computers like the HLRN (Norddeutscher Verbund für Hoch- und Höchstleistungsrechnen).

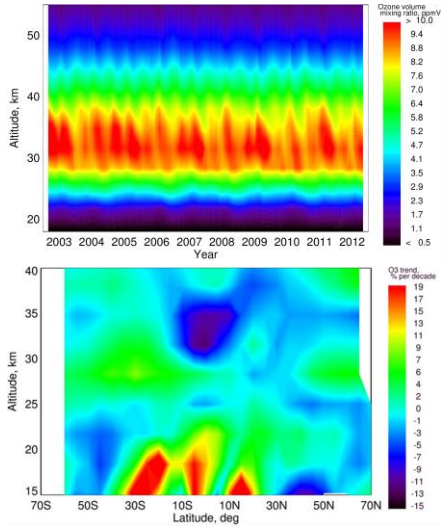

Figure 33: Time series for the tropics between 10°S and 10°N (top) and linear change for zonal mean data from a linear regression (bottom) for the new ozone data set V3.5 for 2004 to 2011.

Acknowledgements

The work on the limb data sets was performed within the framework of several projects: SADOS, the DFG research groups ROSE-ROMIC and SHARP, the ESA projects Ozone-CCI, SCILOV-15, SQWG, and SPIN. We also thank HLRN for the opportunity to use their facilities for computation.

References:

Rahpoe, N., Weber, M., Rozanov, A. V., Weigel, K., Bovensmann, H., Burrows, J. P., Laeng, A., Stiller, G., von Clarmann, T., Kyrölä, E., Sofieva, V. F., Tamminen, J., Walker, K., Degenstein, D., Bourassa, A. E., Hargreaves, R., Bernath, P., Urban, J., and Murtagh, D. P.: Relative drifts and biases between six ozone limb satellite measurements from the last decade, Atmos. Meas. Tech., 8, 4369-4381, doi:10.5194/amt-8-4369-2015, 2015.

von Savigny, C., Ernst, F., Rozanov, A., Hommel, R., Eichmann, K.-U., Rozanov, V., Burrows, J. P., and Thomason, L. W.: Improved stratospheric aerosol extinction profiles from SCIAMACHY: validation and sample results, Atmos. Meas. Tech., 8, 5223-5235, doi:10.5194/amt-8-5223-2015, 2015.

Weigel, K., Rozanov, A., Azam, F., Bramstedt, K., Damadeo, R., Eichmann, K.-U., Gebhardt, C., Hurst, D., Kraemer, M., Lossow, S., Read, W., Spelten, N., Stiller, G. P., Walker, K. A., Weber, M., Bovensmann, H., and Burrows, J. P.: UTLS water vapour from SCIAMACHY limb measurementsV3.01 (2002–2012), Atmos. Meas. Tech., 9, 133-158, doi:10.5194/amt-9-133-2016, 2016.

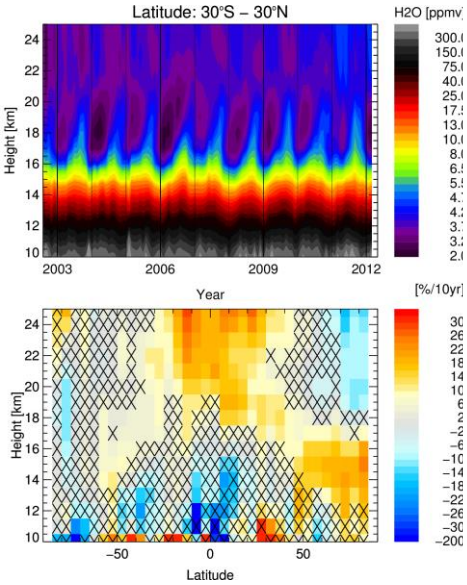

Figure 34: Time series for the tropics between 30°S and 30°N (top) and linear change for zonal mean data from a linear regression (bottom) for the new water vapour data set V4.2 for August 2002 to March 2012, data from every 8th day used.

Stratospheric Methane and Carbon Dioxide Profiles from SCIAMACHY Solar Occultation Measurements

Stefan Noël, Klaus Bramstedt, Patricia Liebing, Max Reuter, Alexei Rozanov, Heinrich Bovensmann, and John P. Burrows

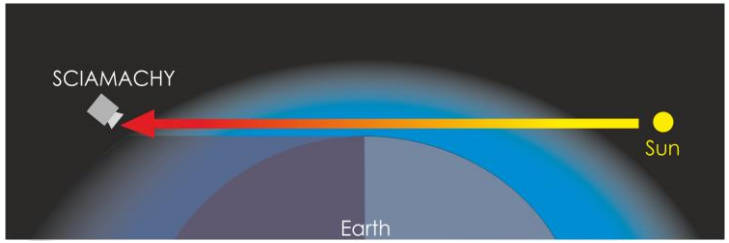

Figure 35: Solar occultation viewing geometry

Atmospheric carbon dioxide (CO_2) and methane (CH_4) are the most important man-made greenhouse gases. They are mainly produced in the troposphere, but are also transported upwards into the stratosphere where they play a significant role in atmospheric chemistry and climate.

There are various methods to measure and monitor the tropospheric concentrations or total column amounts of CH_4 and CO_2, both from the ground and from satellites. However, there are only few data sources for stratospheric information about these gases, especially for CO_2.

One of these data sources is the SCanning Imaging Absorption spectroMeter for Atmospheric CHartographY (SCIAMACHY) which operated from 2002 to 2012 as part of the atmospheric chemistry payload of the Envisat satellite. SCIAMACHY performed spectral measurements over a large wavelength range from the UV to the SWIR at various viewing geometries, including solar occultation. During solar occultation, the (appearing) rising sun is observed through the atmosphere (see Figure 35).

Already some years ago, the so-called Onion Peeling DOAS (ONPD) method has been developed at IUP to derive stratospheric water vapour and later also first methane profiles from SCIAMACHY solar occultation measurements (Noël et al., 2010, 2011). This method, which combines a weighting function DOAS (Differential Optical Absorption Spectroscopy) fit with an onion peeling approach, has been further improved. The vertical range of the retrieved profiles could be extended from 20-40 km to 17-45 km, and it is now also possible to derive reasonable CO_2 stratospheric profiles.

With this new algorithm, the complete time series of SCIAMACHY solar occultation measurements has been analysed. The method and the results for CH_4 and CO_2 are described in detail in Noël et al. (2016). The produced data set covers the latitudinal range between about 50°N and 70°N. It has been made available to the public via the ESA Greenhouse Gas Climate Change Initiative (GHG-CCI) web site (www.esa-ghg-cci.org).

Figure 36 shows the complete time series of daily averaged CH_4 and CO_2 stratospheric volume mixing ratios (VMRs) derived with the improved ONPD method. Temperature and pressure profiles provided by the European Centre for Medium Range Weather Forecasts (ECMWF) have been used as input. Especially the CH_4 data set shows a pronounced seasonal variation which is mainly caused by the specific observational geometry due to the sun-fixed Envisat orbit, which results in a similar temporal variation in latitude of the measurements and related changes of tropopause heights. The retrieved CH_4 and CO_2 profiles show some unexpected vertical oscillations with amplitudes in the order of a few percent. These are especially visible in the CO_2 data set be-

cause of its lower variability. Such oscillations are not seen in data from other instruments; they are therefore assumed to be an artefact specific to the SCIAMACHY measurements or the retrieval method. However, there are actually no other CO_2 measurements available which cover the spatial and temporal range of the SCIAMACHY data; therefore, this issue is still under investigation.

There is no obvious trend visible in the methane time series. The CO_2 data show a general increase with time. This is expected and in line with the known increase of tropospheric CO_2.

Acknowledgements

SCIAMACHY is a national contribution to the ESA Envisat project, funded by Germany, the Netherlands and Belgium. SCIAMACHY data have been provided by ESA. We thank the European Centre for Medium Range Weather Forecasts (ECMWF) for providing us with analysed meteorological fields. We thank Geoffrey Toon of the NASA Jet Propulsion Laboratory for providing the empirical solar line list used in this work. This work has been funded by DLR Space Agency (Germany), the ESA GHG-CCI and the University of Bremen.

References

Noël, S., Bramstedt, K., Rozanov, A., Bovensmann, H., and Burrows, J. P.: Water vapour profiles from SCIAMACHY solar occultation measurements derived with an onion peeling approach, Atmos. Meas. Tech., 3, 523–535, doi:10.5194/amt-3-523-2010, 2010.

Noël, S., Bramstedt, K., Rozanov, A., Bovensmann, H., and Burrows, J. P.: Stratospheric methane profiles from SCIAMACHY solar occultation measurements derived with onion peeling DOAS, Atmos. Meas. Tech., 4, 2567–2577, doi:10.5194/amt-4-2567-2011, 2011.

Noël, S., K. Bramstedt, M. Hilker, P. Liebing, J. Plieninger, M. Reuter, A. Rozanov, C. E. Sioris, H. Bovensmann and J. P. Burrows, Stratospheric CH_4 and CO_2 profiles derived from SCIAMACHY solar occultation measurements, *Atmos. Meas. Tech.*, 9(4), 1485-1503, 2016, doi: 10.5194/amt-9-1485-2016.

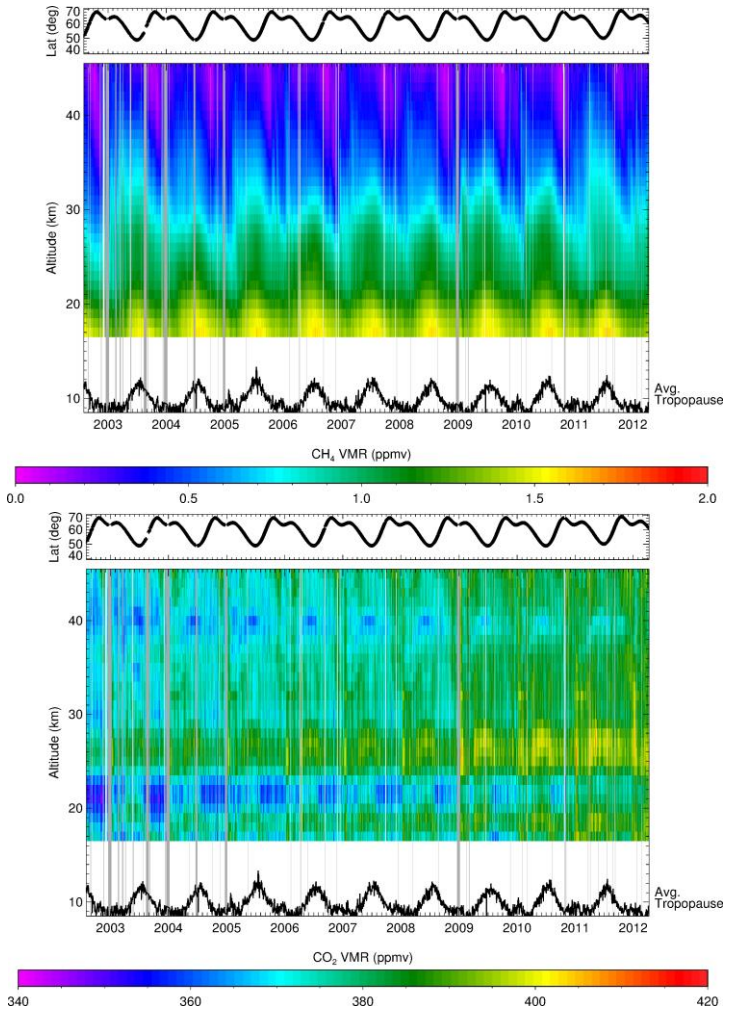

Figure 36: *Time series of daily averaged CH_4 (top) and CO_2 (bottom) profiles August 2002 – April 2012. The vertical grey bars mask out periods of reduced SCIAMACHY data quality (e.g. due to instrument switch-offs or decontamination periods). In addition, the latitude of the measurements and the average tropopause height (derived from ECMWF data) are shown. (from Noël et al., 2016)*

Improved pointing information for the satellite instrument SCIAMACHY

Klaus Bramstedt, Stefan Noël, Heinrich Bovensmann, and John P. Burrows

SCIAMACHY (SCanning Imaging Absorption spectroMeter for Atmospheric CHartographY) is a passive remote sensing moderate-resolution imaging UV-Vis-NIR spectrometer on board the European Space Agency's (ESA) Environmental Satellite (Envisat). Envisat was launched in March 2002 from Kourou, French Guiana into a sun synchronous orbit, where it accomplished 10 years of successful mission. SCIAMACHY observed Earth's atmosphere in nadir, limb and occultation geometry. A critical point in the latter two is always the pointing knowledge, i.e. the precise knowledge of the viewing direction and with that the altitude grid of the observations.

We investigated SCIAMACHYs pointing performance by using three types of in-flight measurements. In solar and lunar occultation, the atmosphere is observed by measuring the light from sun or moon transmitted through the atmosphere. Above the atmosphere, these measurements can be used to determine the viewing direction towards the sun and the moon, respectively. As the moon is a highly variable target, special care is needed to take lunar phase and libration into account (see Figure 37). Additionally, the sun is regularly observed through the so-called sub-solar port (a measurement dedicated to monitoring the degradation of the instrument). Also for these measurements the viewing towards the sun can be derived.

The measured viewing directions are compared to the expected viewing directions at the orbital position of the satellite. A mismatch between these two quantities indicates a so-called mis-pointing of the instrument. This can be caused by uncertainties in the attitude information of the platform or by offsets in the positions of the two scan mirrors of SCIAMACHY. The mis-pointing can be described (and therefore corrected) by a set of mis-pointing parameters.

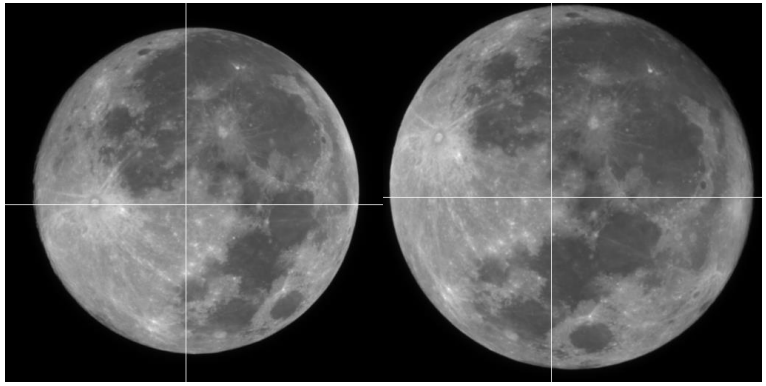

Figure 37: SCIAMACHY steers the viewing direction towards sun or moon in most cases with its *Sun Follower Device* (SFD). For the highly variable moon, we simulated the steering on lunar reference images from the Robotic Lunar Observatory (ROLO) of the U.S. Geological Survey (USGS). Shown are two examples: The white cross-hair on the lunar image indicates the intensity centroid on the moon, which is the SFD target. From a set of 15 ROLO images, a parameterisation for the location of the IC for observations close to full moon has been derived.

For each month over SCIAMACHYs lifetime, a viewing direction measurement for each type has been selected (a total of 282 measurements). An improved set of mis-pointing parameters has been fitted by simultaneously minimising the viewing direction offsets for all measurements. The viewing direction is expressed by an elevation and azimuth angle. Figure 38 shows the elevation and azimuth angle offsets with the old and the newly fitted mis-pointing parameters.

An elevation angle offset corresponds to an offset of the altitude at the tangent point (i.e. an altitude offset in retrieved atmospheric profiles). With the old mis-pointing parameters, tangent height offsets of about +270 m for solar occultation,

and about -200 m for lunar occultation are observed. With the new mis-pointing parameters, both offsets are close to zero. Additionally, the less important horizontal offset of about 5 km in the occultation measurements is removed.

The new mis-pointing parameters will be used in the next release of the SCIAMACHY data processor and will improve the geolocation for all measurements. Most important is the better knowledge of the tangent heights for SCIAMACHYs limb and occultation measurements.

References:

Bramstedt, K., Noël, S., Bovensmann, H., Gottwald, M., and Burrows, J. P.: Precise pointing knowledge for SCIAMACHY solar occultation measurements, *Atmospheric Measurement Techniques*, 5, 2867–2880, doi:10.5194/amt-5-2867-2012, 2012.

Bramstedt, K., Stone, T. C., Noël, S., Gottwald, M., Bovensmann, H., and Burrows, J. P.: Improved pointing information for SCIAMACHY from in-flight measurements of the viewing directions towards sun and moon, *submitted to Atmospheric Measurement Techniques*, 2016.

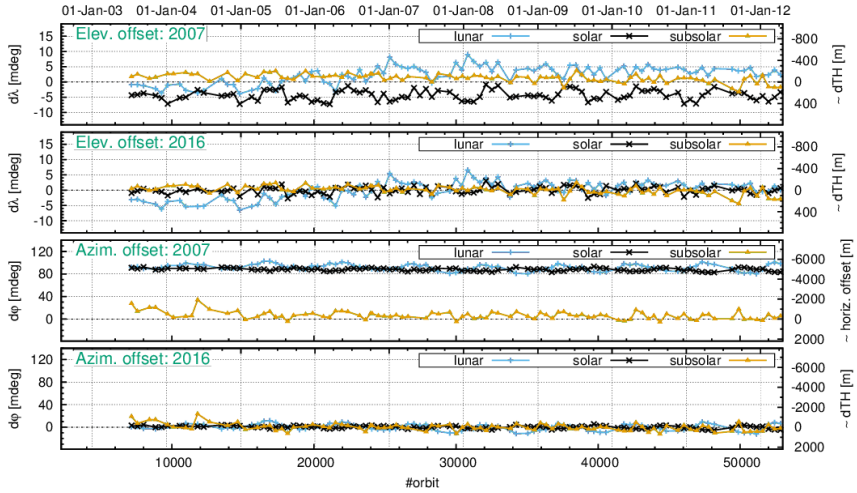

Figure 38: The elevation / azimuth angle offsets dλ /dφ for the measurements used in the fit of the new mis-pointing parameters. Top and second panel: The elevation angle offset using the mis-pointing parameters from 2007 and the newly fitted parameters (2016). Third and fourth panel show the azimuth angle offset for both cases. With the new parameters, the offsets are strongly reduced.

Solar Induced Vegetation Fluorescence as seen from Space

Narges Khosravi, Marco Vountas, Vladimir Rozanov, John P. Burrows

Sun-Induced vegetation Fluorescence (SIF) has been retrieved globally utilizing SCIAMACHY measurements. SIF as a by-product of photosynthesis has, to a large extent, a linear relationship to the Gross Primary Production (GPP) of plants which is highly affected by the absorbed solar radiation (also known as APAR). Therefore, SIF is an indicator of photosynthetic efficiency and vegetation health and stress, making it very useful in land-use management. The study focuses on land vegetation and is therefore partially related to the study done by Wolanin et al. (2015), see page 20 of this report. However, here a different spectral range and methodology is used.

SCIAMACHY provides moderate spectral resolution and very good spectral calibration and large SNR. The retrieved SIF values follow the seasonal trend of vegetation, regionally and globally as illustrated in Figure 39. The monthly averaged fluorescence retrievals from SCIAMACHY show a clear contribution to the GPP and APAR provided from field measurements of fluxes from eddy co-variance towers in the US (see Figure 40) belonging to the Ameriflux measurement network.

Reference:

Khosravi N, Vountas M, Rozanov VV, Bracher A, Wolanin A and Burrows JP (2015) Retrieval of Terrestrial Plant Fluorescence Based on the In-Filling of Far-Red Fraunhofer Lines Using SCIAMACHY Observations. *Front. Environ. Sci.* 3:78. doi: 10.3389/fenvs.2015.00078

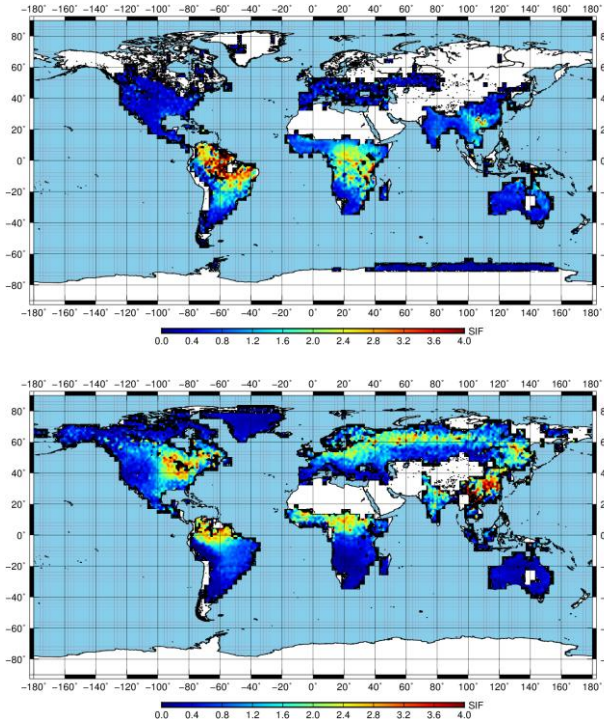

Figure 39: Global values of SIF in [mW m^{-2} sr^{-1} nm^{-1}] at top of canopy layer as seen from SCIAMACHY retrievals. Above: For boreal winter (DFJ) - high SIF values are obtained over larger parts of the southern hemisphere; Below: For boreal summer- reduced values of SIF can be seen in the southern hemisphere while a well pronounced trans-Siberian vegetation belt is observed.

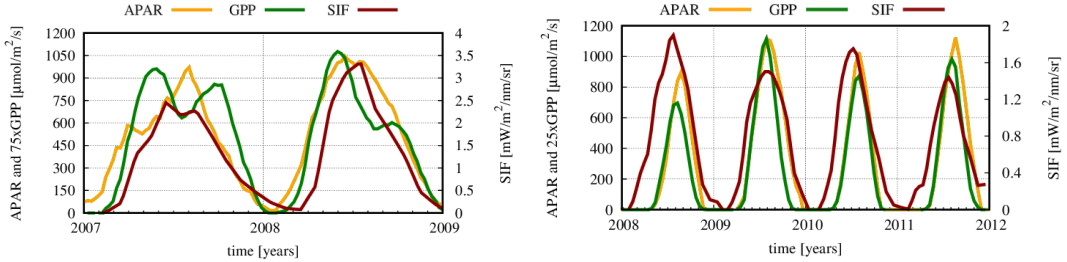

Figure 40: Satellite-based SIF retrieval results co-located with monthly averaged values of ground-based measurements of APAR (Absorbed Photosynthetic Active Radiation) and GPP (Gross Primary Product) over (Left): a suburban US-flux tower measurement station near Minneapolis-Saint Paul and (Right): over rural Ameriflux stations in Nebraska, US.

Clouds and aerosols in the atmosphere

Marco Vountas, Luca Lelli, Linlu Mei, Malte Jäger, Vladimir Rozanov, and John P. Burrows

Evaluation of SCIAMACHY cloud parameters by comparisons to ground-based and other satellite data

Satellite-based remote sensing of clouds is based upon the investigation of the interaction of reflected solar light with water droplets and ice crystals across the full electromagnetic spectrum. Clouds will look different depending on the spectral region the space borne instruments are looking at, because of the different microphysical properties of water and ice. It is also well-known that a change in thermodynamic phase of water induces a change in absorption of radiation by clouds. Therefore, when synergistically combining records of clouds properties inferred from sensors of different (and complementary) spectral specifications, bias assessments are of guidance for optimal data usage and algorithm refinement. The satellite records from the spectrometer SCIAMACHY and the radiometer AATSR (both instruments on board ENVISAT) have been cross-compared with ground-based cloud retrievals across the globe. It has been found that SCIAMACHY cloud top heights, inferred in the visible-near infrared around 760 nm, have a seasonal dependent overestimation in range 0.6 - 1.0 km when compared to the thermal infrared-derived (11 and 12 µm) AATSR cloud top heights (see Figure 42). Comparison with in-situ cloud retrievals reveals that SCIAMACHY cloud altitudes are more accurate for local values of cloud-covered sky greater than 60%. Optimally designed algorithms shall exploit co-registered measurements from both spectral windows from different sensors. This approach can be beneficial, not only for the discrimination of cloud thermodynamic phase and a more accurate vertical profiling of cloud bodies, but also of scenes contaminated by natural and anthropogenic aerosol particles.

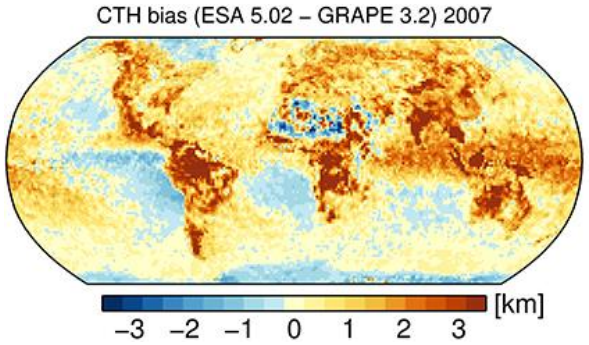

Figure 42: Map of the difference (SCIAMACHY - AATSR) in cloud top height for the year 2007.

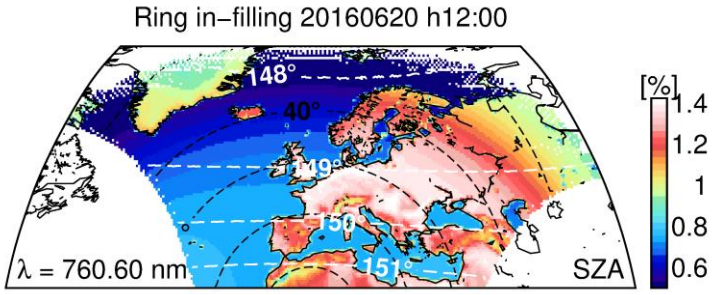

Figure 41: In-filling amount of the absorption band of molecular oxygen induced by inelastically scattered photons in a clear summer atmosphere for the UVN sensor on board the upcoming Sentinel-4 mission.

Polarized radiative transfer including inelastic scattering in presence of ice clouds and dust aerosols

In general, the wavelength of photons remains unchanged upon interaction with molecules. Depending on various conditions, such as viewing geometry, temperature and pressure of the local air column, this is true for almost 95% of the sunlight travelling through the atmosphere. However, a fraction of light has its wavelength shifted after interaction

with matter and inelastic scattering has occurred. Still, even if it is only a small fraction of the total radiation field, wavelength-shifted photons can be detected and they especially fill in solar Fraunhofer lines, as well as those spectral bands characterised by strong absorption by atmospheric gases, such as molecular oxygen (760 nm) or carbon dioxide (2.7, 4.3, or 15 µm). Therefore, satellite algorithms coded for the exploitation of these bands and the monitoring of air quality, aerosol and cloud properties from space can be affected by inelastic scattering. The impact of this scattering process, and the light polarization induced by it, can be already demonstrated for simulated measurements of the UVN sensor on board the upcoming ESA Sentinel-4 platform, whose launch is scheduled for 2020 (Figure 41).

Aerosols

A new Aerosol Optical Thickness (AOT) retrieval algorithm for MERIS over land surfaces, referred to as eXtensible Bremen AErosol Retrieval (XBAER) was successfully developed at IUP/ University of Bremen. XBAER uses a lookup table (LUT) to match to satellite-observed reflectance and derive the AOT. A set of spectral coefficients to prescribe surface properties enables XBAER to retrieve AOT over both dark surfaces (vegetation) and bright surfaces (desert, semiarid, and urban areas). Preliminary validation of the MERIS-derived AOT and the ground-based Aerosol Robotic Network (AERONET) measurements yields good agreement, the resulting regression equation being $y = (0.92x \pm 0.07) + (0.05 \pm 0.01)$ and the Pearson correlation coefficient R=0.78. Global monthly means of AOT have been compared between XBAER, MODIS and other satellite-derived datasets (see Figure 43). The current version of the XBAER algorithm focuses on the retrieval of AOT and SSR for land ground scenes. The use of XBAER for aerosol retrieval over water and snow is under development and benefits from the experience of retrieval techniques developed at IUP/University Bremen over water (von Hoyningen-Huene et al., 2003, 2011), and snow (Istomina et al., 2011; Mei et al., 2013). A global data set for aerosol properties under cloud free condition will be created.

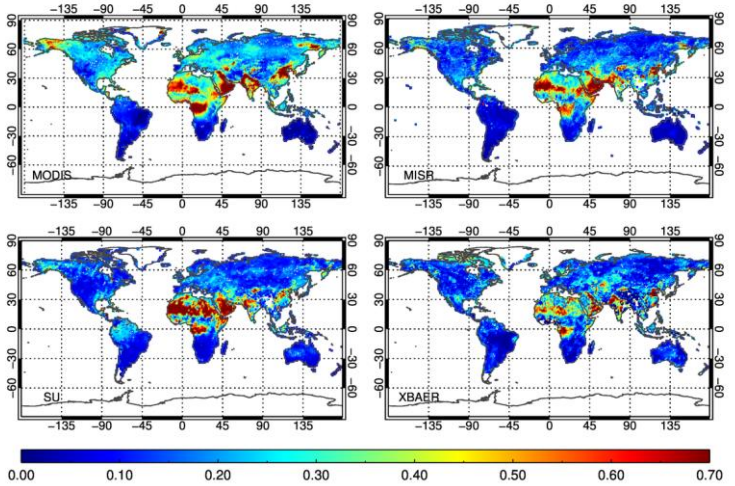

Figure 43: Comparison of retrieved global monthly mean AOT at 550 nm for July 2009. Upper row: left – MODIS, right-MISR. Lower row: left-AATSR (SU), right- MERIS (XBAER)

References:

Lelli, L., Weber, M., Burrows, J.P., Evaluation of SCIAMACHY cloud parameters by comparisons to ground-based and other satellite data, *Frontiers in Environmental Science*, 4, 43, 2016, doi:10.3389/fenvs.2016.00043.

Lelli, L., Rozanov, V.V., Vountas, M., Burrows, J. P., Polarized radiative transfer including inelastic scattering in presence of ice clouds and dust aerosols, *Journal of Quantitative Spectroscopy and Radiative Transfer*, 2016, to be submitted.

Mei, L., Rozanov, V. V., Vountas, M., Burrows, J. P., Levy, R. C., Lotz, W.A. (2016). Retrieval of aerosol optical properties using MERIS observations: algorithm and some first results. Remote sensing of Environment (accepted for publication).

Greenhouse gas observations from aircraft: Methane Airborne Mapper (MAMAP)

Heinrich Bovensmann 1), Michael Buchwitz, Thomas Krings, Konstantin Gerilowski, Sven Krautwurst, Jakob Borchardt and John P. Burrows

The two most important man-made ("anthropogenic") greenhouse gases (GHG) carbon dioxide (CO_2) and methane (CH_4) have large sources on small spatial scales (100 m to a few km). These are, for example, CO_2 from power plants, volcanoes and cities, or CH_4 from fossil fuel production (coal, gas, oil), landfills, and geological seeps. Often, the strength and/or the position of these sources are not well known and an independent verification of the emissions is needed. Remote sensing of atmospheric GHG distributions, so-called greenhouse gas imaging, could close an important information gap on small spatial scales. In cooperation with the GeoForschungsZentrum (GFZ) in Potsdam, scientists at IUP developed an airborne spectrometer system called MAMAP (Methane Airborne MAPper), which demonstrates that imaging the spatial distribution of atmospheric GHG concentrations in the vicinity of strong sources can be used to infer the emission strength of the source. The spectrometer uses solar absorption spectroscopy in the near and short-wave infrared, in a similar way as the satellite sensors SCIAMACHY and GOSAT, to derive very accurate gradients (precision better < 0.3%) in atmospheric CO_2 and CH_4 with a spatial resolution of approx. 50 m over spatial scales of several km.

During the years 2015-2016, the work at IUP focussed on data analysis of the campaigns performed in 2012 and 2014. During these campaigns, MAMAP was used to demonstrate that with passive remote sensing of greenhouse gas distributions on small spatial scales, the emission strength of selected sources can be quantified. The campaigns were co-funded by the European Space Agency in support of the development of the CarbonSat mission concept (CMAPExp and COMEX campaigns), by NASA (COMEX campaign) as well by the University of Bremen.

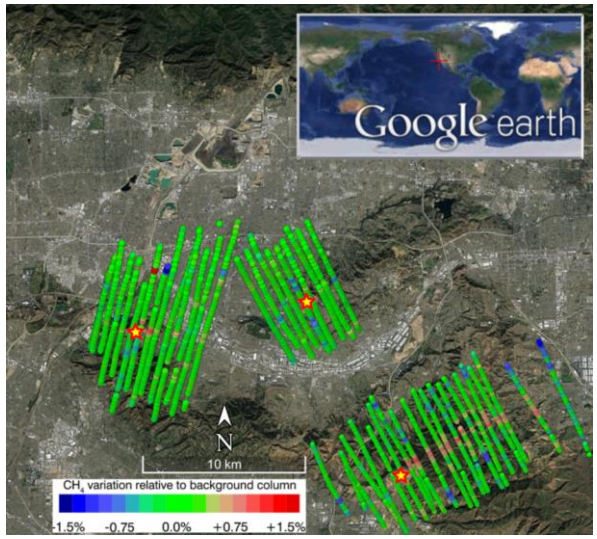

Figure 44: MAMAP remote sensing survey flights over the landfills in the Los Angeles Basin (red cross in the world map, top right). Their locations are marked by red/yellow stars. Only the Olinda Alpha Landfill (lower right) shows a clear plume in downwind direction. The wind direction was in general southwest during the measurements. The map underneath is provided by Google Earth

In summer 2014, ESA and NASA joined forces when carrying out the COMEX campaign that not only supported CarbonSat but also NASA's proposed Hyperspectral Infrared Imager, HYSPIRI, mission. The campaign exploited passive remote-sensing spectroscopy – the unique absorption signature that the gases leave in sunlight as it passes through the atmosphere. Measurements are taken from aircraft above, as would the satellite, and compared to other measurements taken by aircraft and on the ground near the source of emissions. The measurements were taken in the San Joaquin Valley and around Los Angeles in California, USA – an area that features oil refineries, farms and landfill sites, which all release methane into the atmosphere.

For the first time using this type of remote sensing data, the methane emissions from a landfill (see overview Figure 44)

were quantified in an independent way (Krautwurst et al 2016). The derived emissions of approx. 15 kT CH_4/year were consistent with the reported emissions. In addition, the campaign was also able to capture a large methane plume over one of California's oil fields as depicted in Figure 46. For that oil field (Figure 45) no emissions were reported. A huge CH_4 plume of unknown origin was detected up to several km downwind over the oil field by remote sensing. The data was of good quality and the source strength of the total field CH_4 emissions was determined to be about 30kT CH_4/year.

Beside the detailed data analysis on campaign data, the scientists at IUP prepared campaign activities for 2017 (COMET) and further developed the concept of 2-dimensional imaging of CH_4 and CO_2 distributions. Using this approach, similar measurements as with MAMAP (1D) will be possible, but on time scales of approx. 10 minutes instead to several hours (as with MAMAP (1D)). This will improve the detection limit of small sources by nearly an order of magnitude and will minimise systematic errors due to changing meteorological conditions during measurement time. The technical concept was developed in cooperation with Carl Zeiss Jena and AIM.

Figure 45: Photo of the oil field in California taken from the CIRPAS aircraft during the August/September 2014 COMEX campaign by IUP scientists. Numerous oil wells were under conventional oil production.

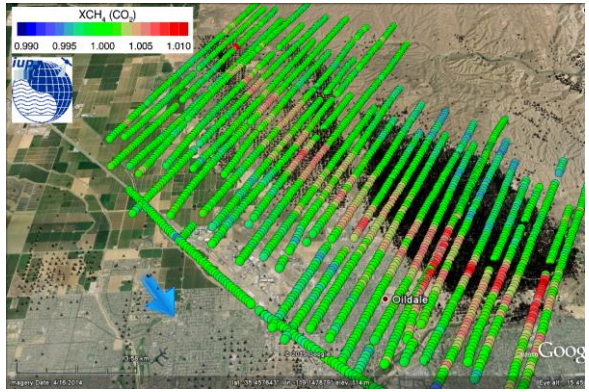

Figure 46: Large scale (several km of extent) methane plume as measured over an oil field with passive remote sensing. Measurement performed with MAMAP on 04 Sep. 2014. Oil wells are depicted in black.

References:

Gerilowski, K., Krautwurst, S., Kolyer, R., Thompson, D. R., Jonsson, H., Krings, T., Horstjann, M., Leifer, I., Eastwood, M., Green, R. O., Vigil, S., Schuettemeyer, D., Fladeland, M., Burrows, J., and Bovensman, H.: Remote sensing of large-scale methane emission sources with the Methane Airborne MAPper (MAMAP) instrument over Kern River and Kern Front oil fields and validation through airborne in-situ measurements – initial results from COMEX, in: AGU Fall Meeting, San Francisco, CA, 2014 https://agu.confex.com/agu/fm14/meetingapp.cgi#Paper/21807

Gerilowski, K., Krings, T., Hartmann, J., Buchwitz, M., Sachs, T., Erzinger, J., Burrows, J.P.; Bovensmann, H.; Methane Remote Sensing Constraints on direct Sea-Air Flux from the 22/4b North Sea Massive Blowout Bubble Plume, Journal of Marine and Petroleum Geology, doi:10.1016/j.marpetgeo.2015.07.011 (2015)

Krings, T., Neininger, B., Gerilowski, K., Krautwurst, S., Buchwitz, M., Burrows, J.P., Lindemann, C., Ruhtz, T., Schüttemeyer, D., Bovensmann, H.; Airborne remote sensing and in-situ measurements of atmospheric CO2 to quantify point source emissions, Atmos. Meas. Tech. Discuss., doi:10.5194/amt-2016-362, 2016, 2016

Krautwurst, S. at al., Methane emissions from a Californian landfill, determined from airborne remote sensing and in-situ measurements, submitted to Atmos. Meas. Tech. Discuss., 2016

Links:

NASA COMEX pages:

https://espo.nasa.gov/home/comex/content/COMEX

CarbonSat at IUP Web: http://www.iup.uni-bremen.de/carbonsat/

Airborne measurement of short lived trace gases: free radicals

Maria Dolores Andrés-Hernández, Vladyslav Nenakhov, Midhun George, and John P. Burrows

Oxidation dominates tropospheric gas phase chemistry and, more specifically, the phenomenon of summer smog. Free radicals, in particular OH and peroxy radicals, are involved in most photo-oxidation processes in the troposphere and are therefore drivers of the atmospheric chemical composition. Knowledge of their abundance and variability is consequently crucial for the determination of the oxidation capacity of the atmosphere, i.e., the rate of chemical removal of gases emitted into the atmosphere by oxidising reactions and the characterisation of air masses.

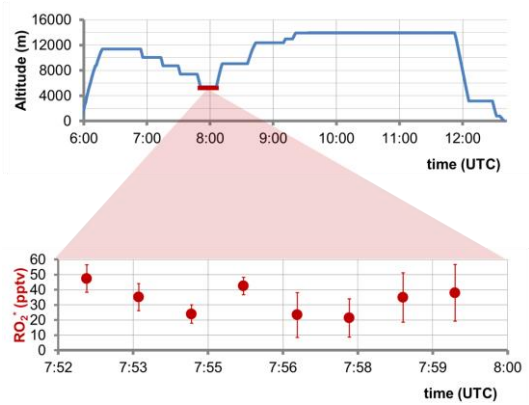

Figure 48: Peroxy radical mixing ratios measured by PeRCEAS on the 23.08.2015 on flight level FL170. The upper panel depicts the flight track in yellow and the corresponding flown area over Egypt is marked in red.

Following the long term development and optimisation of airborne instrumentation for the measurement of atmospheric peroxy radicals at IUP Bremen, the PeRCEAS (Peroxy Radical Chemical Enhancement and Absorption Spectrometer) instrument was successfully deployed on the research aircraft HALO (High altitude and long range research aircraft; see http//www.halo.dlr.de/) to take part in the OMO mission (Oxidation mechanisms observations in the extra-tropical free troposphere, see http://www.mpic.de/forschung/kooperationen/halo/omo-mission) lead by the Max Planck Institute for Chemistry in Mainz in summer 2015.

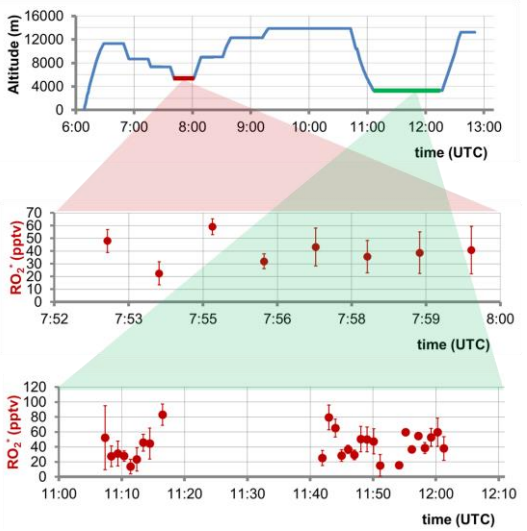

Figure 47: Peroxy radical mixing ratios measured by PeRCEAS on the 25.08.2015 on flight level FL170 over Egypt (in red) and FL100 over Etna (in green). The upper panel depicts the flight track and the corresponding flown areas.

The OMO mission focused on the characterization of oxidation processes and long range transport of Asian emissions during the summer monsoon by using a comprehensive set of HALO instrumentation for the airborne measurement of trace gases in the upper troposphere and mostly at 10-15 km altitude across the Arabian Sea up to the Bay of Bengal, the Indian Ocean and the Mediterranean Sea.

For the time being, the analysis of results indicates monsoon signatures above 12 km and photochemically active air masses at 5-6 km altitudes. Figure 47 and Figure 48 depict exemplary mixing ratios of the sum of peroxy radicals (RO_2^*) measured by PeRCEAS over Egypt and in the emission plume of Etna over the Mediterranean Sea.

Molecular Spectroscopy Laboratory

Victor Gorshelev, Mark Weber, and John P. Burrows

Algorithms that retrieve trace gas amounts from remotely sensed spectral data rely, among others, on spectroscopic data characterizing the molecular absorption. Errors and uncertainties in spectroscopic data often limit the accuracy of the retrieval results. Although numerous spectroscopic datasets based on laboratory measurements and theoretical considerations are already available, in many cases they are not of sufficient quality and there is still room for improvements that benefit the retrieval accuracy. Advances in experimental instrumentation and setups allow us to produce spectroscopic parameters with lower uncertainties. Acquisition of high-quality spectroscopic data for remote sensing applications is an essential part of the experimental activity at our Molecular Spectroscopy Laboratory.

In our laboratory, we perform spectroscopic measurements using an Echelle spectrometer covering the UV spectral region and a Fourier transform spectrometer (FTS) encompassing the near UV, visible, and near IR. Several absorption cell setups with extended cooling capacities allow us to measure molecular absorption cross-sections at atmospherically relevant temperatures ranging from -80°C to room temperature.

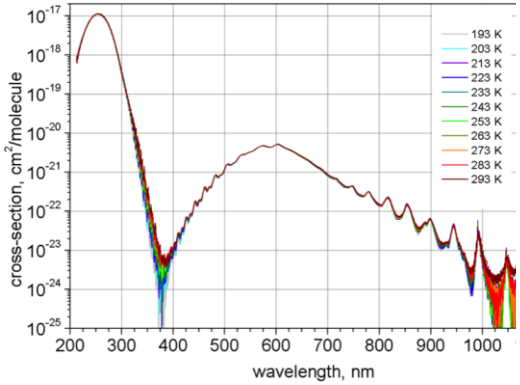

Figure 50: Ozone absorption cross-sections between 210 nm and 1100 nm at 11 temperatures.

The most recent measurement campaigns of the Molecular Spectroscopy Laboratory include the acquisition of ozone (O_3) absorption cross-sections in the UV-VIS-IR spectral range from 210 to 1100 nm at an unprecedented high number of temperatures (Figure 50) and selected methane (CH_4) absorption lines and bands in the short-wave infrared (SWIR). As part of a metrological European project we currently focus on measurements to further improve ozone cross-sections in the UV using an improved experimental set-up (Figure 49) allowing us to further reduce uncertainties in the temperature dependence of the ozone cross-section data close to the 1% level.

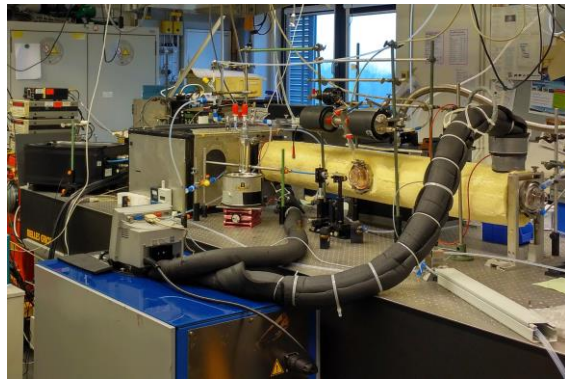

Figure 49: Echelle spectrometer setup with insulated double wall absorption cell for ozone absorption cross-section measurements at cold temperatures.

The Molecular Spectroscopy Laboratory is also involved in several educational projects, introducing the basic practical concepts of absorption spectroscopy to high school students and participating in the international postgraduate programme in environmental physics.

References

Gorshelev V., Serdyuchenko A., Weber M., and Burrows J.P.: High spectral resolution ozone absorption cross-sections: Part I. Measurements, data analysis and comparison around 293 K, *Atmos. Meas. Tech.*, 7, 609–624, 2014.

Serdyuchenko A., Gorshelev V., Weber M., Chehade W., and Burrows J.P.: New high-resolution ozone absorption cross-sections in UV, visible and near infrared: Part II. Temperature dependence, *Atmos. Meas. Tech.*, 7, 625–636, 2014.

Weber, M., Gorshelev, V., and Serdyuchenko, A.: Uncertainty budgets of major ozone absorption cross-sections used in UV remote sensing applications, *Atmos. Meas. Tech.*, 9, 4459-4470, doi:10.5194/amt-9-4459-2016, 2016.

Laboratory for Modeling and Observation of the Earth System (LAMOS)

Mihalis Vrekoussis and Andreas Hilboll

In 2016, a new working group was established at IUP, the Laboratory for Modeling and Observation of the Earth System (LAMOS) led by Prof. Vrekoussis.

The group's main focus is the interpretation of remote sensing observations of atmospheric composition using high-performance numerical models. The research questions evolve around the understanding of the complex mechanisms controlling the emission, transport, and transformation of pollutants in the atmosphere. Three different forward models will be used: (a) the Eulerian global chemical Transport Model TM5, (b) the regional Weather Forecast coupled with chemistry model WRF-Chem, and (c) the Lagrangian particle dispersion model FLEXPART.

In addition, the inverse scheme of the TM5 model (TM5-4DVAR) will be used in conjunction with satellite remote sensing measurements to provide information on emission fluxes. Overall, the main goals of the group are (i) to quantify sources and sinks of long and short-lived species (CO_2, CH_4, NOx) using satellite data as proxies, (ii) to understand the transport mechanisms of trace constituents from large agglomerations impacting on global chemistry, and (iii) to understand the processes controlling the amounts of the elements nitrogen, phosphorus, and sulphur being deposited to the oceans.

As a second pillar of its research activities, the LAMOS group conducts ground-based remote-sensing measurements of atmospheric composition. In collaboration with the DOAS group (J.P. Burrows, A. Richter, E. Peters), we developed a new prototype, the Imaging MaPper for AtmospheriC observaTions (IMPACT, see Figure 51). The instrument has already participated successfully in a semi-blind international intercomparison campaign (CINDI-2). Its broad field of view (45°) allows the acquisition of high quality atmospheric observations of trace constituents over all viewing directions at the same time. IMPACT will provide novel information on the gradient and transport of emitted species from various sources including dispersed pollution plumes from stacks and ships.

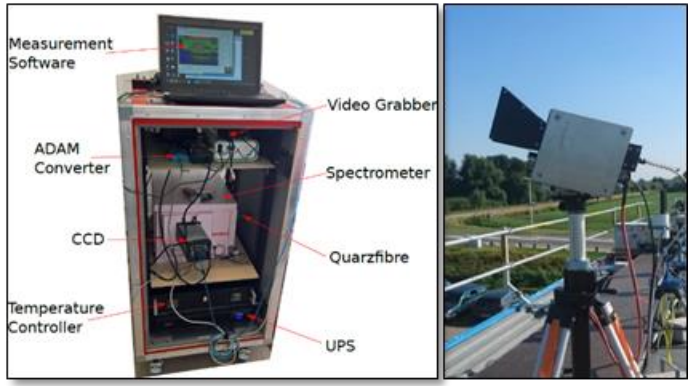

Figure 51: The Imaging MaPper for AtmospheriC observaTions (IMPACT) (left) and its telescope conducting atmospheric observations in Cabauw, the Netherlands.

In addition, the LAMOS group participated in a ship campaign on board the Maria S. Merian research vessel in October 2016 during the COPMAR Project (continental outflow of pollutants towards the marine lower troposphere) of DFG. COPMAR's scientific objective was to provide novel remote sensing-based information of the spatial gradient and the ambient marine levels of key atmospheric species (NO_2, CHOCHO, O_4) for the maritime region in between Ponta Delgada and Cape Town.

Links

TM5 model: http://tm.knmi.nl/index.php/Main_Page

WRF-Chem model: http://ruc.noaa.gov/wrf/wrf-chem /

FLEXPART model: https://www.flexpart.eu/

TM5-4DVAR model: https://sourceforge.net/projects/tm5/

CINDI-2 campaign: http://www.tropomi.eu/science/cindi-2

Advection of North Atlantic Deep Water from the Labrador Sea to the Southern Hemisphere

Monika Rhein, Dagmar Kieke, and Reiner Steinfeldt

The deep western boundary current (DWBC) is the main feature of the cold limb of the Atlantic meridional overturning circulation (AMOC). The DWBC transports North Atlantic Deep Water (NADW) components from the formation regions in the northern North Atlantic to the south, thereby transferring climate signals introduced during formation of these water masses into the southern hemisphere. Labrador Sea Water (LSW) is the lightest component of NADW and is formed by winter-time convection in the central Labrador Sea. In general, LSW covers the depth range between 500 m and 2500 m. Denmark Strait Overflow Water (DSOW) is the densest component of the NADW and found between 3500-4500 m depth. Source water masses of DSOW are mainly formed in the Norwegian Sea by cooling of surface water. Both LSW and DSOW recently had contact with the surface ocean and thus the atmosphere, and therefore carry high loads of transient trace gases like chlorofluorocarbons (CFCs) and sulphurhexafluoride (SF_6).

Recently, the role of the DWBC as a principal conduit for newly formed NADW components was under discussion. Based on model results and the trajectories of deep autonomous floats, doubts were voiced whether the DWBC is a continuous boundary current, and interior pathways were postulated to have a much larger impact than previously thought. On the other hand, the spatial distribution of the aforementioned transient trace gases in LSW and DSOW showed that the DWBC carries the highest CFC concentrations in LSW and DSOW throughout the subtropical and tropical Atlantic and clearly marks the DWBC as the most important pathway. The relatively slow spreading compared to measured DWBC velocities was explained by an exchange between the boundary current and the interior. In the early 1990s measurable CFC concentrations in LSW and DSOW were observed from 60°N to 20°S in the western Atlantic and along the equator but the highest concentrations were associated with the DWBC, followed by the recirculation offshore.

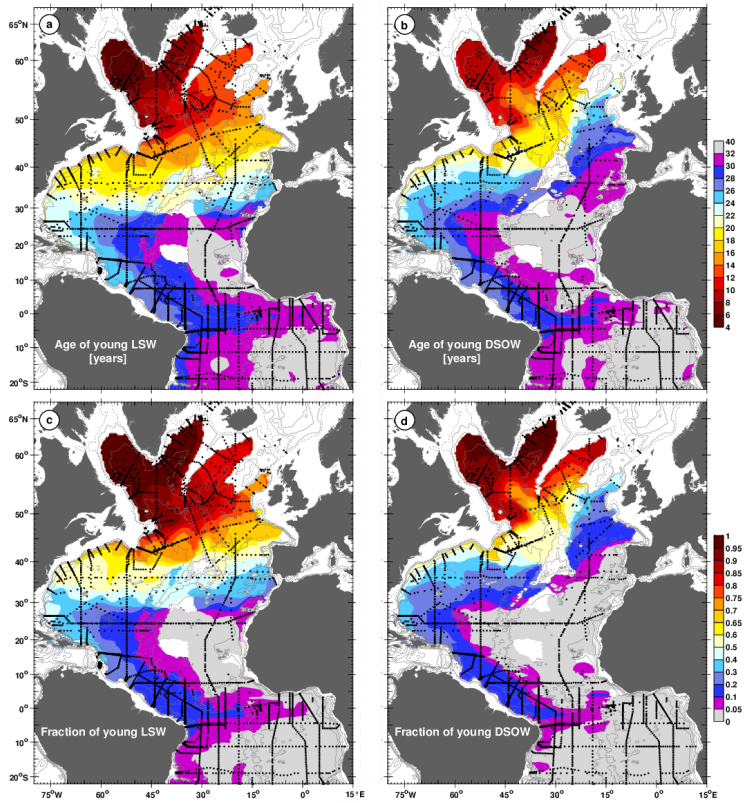

Figure 52: Maps of water mass ages (a and b) and water mass fractions (c and d) calculated for Labrador Sea Water (LSW, left column) and Denmark Strait Overflow Water (DSOW, right column) younger than 40 years. Figure from Rhein et al., 2015.

In Rhein et al., 2015 we used 25 years of CFC observations in the Atlantic to study the main features of the LSW and DSOW circulation from the Labrador Sea to the tropical South Atlantic. The CFC data show that the DWBC is the fastest conduit for recently formed LSW and DSOW from the formation region to the southern hemisphere. The presented CFC data set is extensive enough to show that the continuous export of tracer-enriched deep water in the DWBC is a robust feature. Further support comes from mooring-derived observations and, for the DSOW, from floats released in the subtropical Atlantic. South of about 45°N, the CFC data characterize the DWBC as a carrier of the youngest LSW and DSOW. The downstream decrease of the fraction of young water (Figure 52) indicates that the DWBC permanently exchanges water with the ocean interior. This exchange, however, is not spatially uniform, but dependent on the interaction between the DWBC and the local circulation. Compared to DSOW, the distributions indicate a higher tendency for LSW to follow additional interior pathways.

Reference:

Rhein, M., D. Kieke, and R. Steinfeldt (2015), Advection of North Atlantic Deep Water from the Labrador Sea to the southern hemisphere, *J. Geophys. Res.*, 20, 2471-2487, doi:10.1002/2014JC010605

Coastal upwelling off Peru and Mauritania inferred from helium isotope disequilibrium

Reiner Steinfeldt, Jürgen Sültenfuß, and Monika Rhein

Eastern boundary upwelling systems, such as the Canary, California, Humboldt, and Benguela Currents belong to the most productive marine ecosystems. Alongshore, trade winds drive an offshore Ekman flux, which leads to a horizontal flow divergence at the coast and, as a consequence, upwelling of cold and nutrient-rich subsurface water. The upwelled water also transports climate relevant trace gases such as N_2O from the ocean's interior into the mixed layer and ultimately into the atmosphere. Crucial for quantifying the role of upwelling for nutrient and tracer budgets is the vertical velocity by which substances and gases are transferred from the subsurface into the mixed layer. It is, however, much too small to be measured directly. In a recent study (Steinfeldt et al., 2015), the excess of ^{3}He in the mixed layer has been used to quantify the upwelling velocity. The oceanic source for ^{3}He is hydrothermal venting, mainly near mid-ocean ridges, where primordial ^{3}He is emitted. The ^{3}He enriched waters eventually

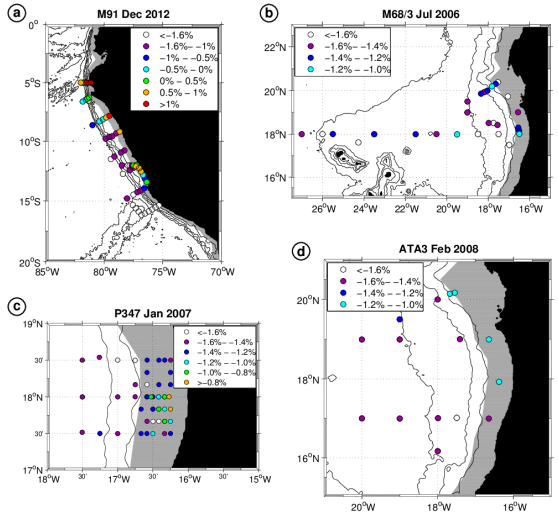

Figure 53: δ^3He [%] in the mixed layer for cruise M91 off Peru (a) and for cruises M68/3, P347 and ATA3 off Mauritania (b-d). Isobaths are drawn every 1000 m, and the area of the 'coastal region' is shaded grey. Note the different colour scale for the cruises from the Peruvian (a) and Mauritanian (b-d) region. The error of the δ^3He values in the mixed layer is 0.2 %.

reach the mixed layer, where the excess ^{3}He is outgassing from the ocean into the atmosphere.

Helium samples from the upwelling regions off Mauritania (three cruises) and off Peru (one cruise) have been analysed with the Bremen high-resolution noble gas mass spectrometer. The ^{3}He values in the mixed layer are shown in Figure 53 (given as δ^3He, the deviation of the ^{3}He/^{4}He ratio from the atmospheric value) for all cruises from both regions, with much higher values off Peru than off Mauritania. This is the result of the larger ^{3}He excess of the subsurface waters in the Pacific compared to the Atlantic, thus indicating the entrainment of water into the mixed layer from below. From the helium data, vertical velocities are computed assuming an equilibrium in the mixed layer between outgassing of ^{3}He on the one side and supply by vertical advection and mixing on the other side. Mean values of the helium derived upwelling velocity for the coastal regions (within 50 km distance from the 50 m isobath) and further offshore are shown in Figure 54. For the coastal regions, the upwelling velocities are of the order of 10^{-5} m s^{-1}, whereas for the offshore regions they vary between 10^{-5} m s^{-1} and only 10^{-6} m s^{-1}.

Vertical velocities can also be inferred from the wind field based on the Ekman theory. These wind derived values are compared with the results from the helium method (Figure 54). The coastal values for w_{Helium} and w_{Wind} off Mauritania agree for all three cruises within their error bars. For the Peruvian area, the differences between w_{Helium} and w_{Wind} show an opposite behaviour: they are relatively small for the offshore region, but large for the coastal area. One reason for the high value of w_{Helium} might be an overestimation of the gas exchange velocity due to the presence of organic surface films (surfactants). These films have been observed on cruise M91 off Peru. They have a damping effect on surface waves and also drastically reduce the transport of gases across the water surface. The helium derived vertical velocity for a reduced gas exchange due to surfactants is included in Figure 54 for the Peruvian area (cruise M91) and shows a better agreement with the wind driven upwelling.

The good agreement between wind and helium derived vertical velocities over the coastal areas indicate that the upwelling there is mainly wind driven. For the offshore regions, the helium method suggests the existence of additional upwelling mechanisms. Considering the sea level anomalies (SLA) at the locations of enhanced upwelling indicates that strong upwelling occurs at small values of SLA, i.e. at the boundary of eddies, where they might become instable. Both, the wind driven upwelling in coastal areas and the eddy driven upwelling further offshore, play important roles in the nutrient supply of the euphotic zone.

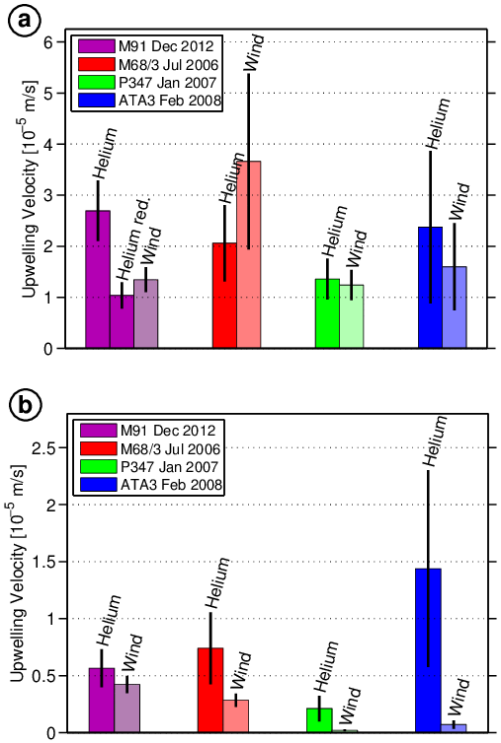

Figure 54: Mean values of helium and wind derived upwelling velocities for the coastal (a) and offshore (b) areas of cruises M91, M68/3, P347 and ATA3. The vertical black line indicates the standard deviation of the mean. 'Helium red.' in (a) means that the helium derived upwelling is calculated with reduced gas exchange velocity due to the presence of surface organic films.

Reference:

Steinfeldt, R., J. Sültenfuß, M. Dengler, T. Fischer and M. Rhein (2015), Coastal upwelling off Peru and Mauritania inferred from helium isotope disequilibrium, *Biogeosci.*, 12, 7519-7533, doi:10.194/bg-12-719-201.

Recent changes in the properties of Labrador Sea Water

Dagmar Kieke, Linn Schneider, Reiner Steinfeldt, and Monika Rhein

Labrador Sea Water (LSW) is the lightest contribution to North Atlantic Deep Water (NADW). It is one of the most prominent water masses of the subpolar North Atlantic and contributes to the deep southward return flow of the climate-modulating Atlantic meridional overturning circulation (AMOC). Many model studies have revealed links between changes in the strength of the AMOC and long-term variations in LSW formation in times of global climate change. Therefore, investigating and monitoring changes in the formation, hydrographic properties, and export rates of LSW is important and requires sustained physical and chemical observations from the deep ocean, making it one of the main areas of research at the Department of Oceanography at IUP.

Originating in the Labrador Sea, LSW is formed through wintertime ocean convection of varying intensity and vertical and spatial extent. This formation, followed by the respective injection of LSW into the mid-depth circulation system, is mandatory for ventilating and renewing water layers of the interior ocean. As a direct result of varying intensity of convection, at different times a lighter upper mode or a deeper denser mode of LSW is formed, termed ULSW or DLSW. Both LSW modes are exported out of the formation region along different pathways. A substantial part of LSW is injected into the Deep Western Boundary Current (DWBC), the major and fastest of several spreading pathways, and propagates southward along the western rim of the North Atlantic (Rhein et al., 2015). Other LSW pathways follow eastward directions, one into the Irminger Sea and another one toward the Mid-Atlantic Ridge and the eastern subpolar North Atlantic.

At about 49°N/47°W the DWBC encounters the Flemish Cap, a topographic obstacle with water depths at the top of the cap of less than 200 m. The presence of the obstacle divides the DWBC into two branches. The major so-called DWBC branch carries all upper layer and deep water components including both LSW modes east around Flemish Cap. A minor so-called Flemish Pass branch enables the upper layers and the shallow components of the DWBC and thus ULSW to enter Flemish Pass, a shallow passage located to the west of Flemish Cap (sill depth ~1200 m). South of Flemish Cap, both branches presumably merge again, though loss of deep water into the interior ocean and thus a weakening of the strength of the DWBC is known to occur between 47°N and 43°N (Mertens et al., 2014).

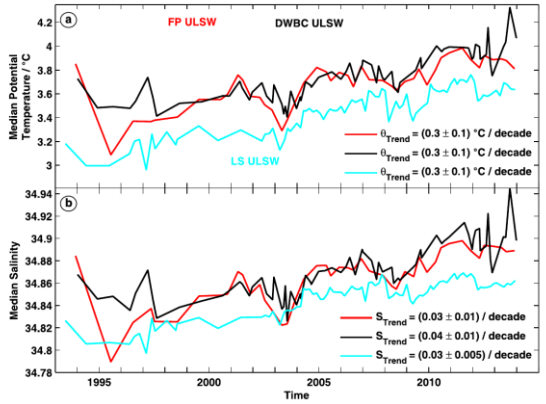

Figure 55: Time series of properties of ULSW (density range sq = [27.68,27.74] kg/m³) in Flemish Pass at 47°N (FP, red), in the DWBC east of Flemish Cap (black), and in the central Labrador Sea (LS, cyan) during 1993–2013. (a) Median potential temperature q (°C) and (b) median salinity, seasonal cycle was removed (Schneider et al., 2015).

Two recent studies deal with reconstructions of time series for the two LSW modes in the central Labrador Sea and in the two DWBC branches crossing 47°N (Schneider et al., 2015 and Kieke and Yashayev, 2015). Schneider et al. (2015) analysed data obtained from oceanographic surveys crossing Flemish Pass and the DWBC region at 47°N. Volume transports estimated for the first time with focus on LSW in Flemish Pass revealed a considerable southward transport of ULSW through Flemish Pass, the only LSW mode light and shallow enough to fully pass through this passage. Out of the total flow of ULSW crossing 47°N towards the south as part of the DWBC, between 2009 and 2013 a share of 15–27% (or -1.0 to -1.5

Sv) followed the Flemish Pass branch. About 98% of the denser DLSW were carried around Flemish Cap, as Flemish Pass is too shallow for considerable southward transport of this LSW mode.

Hydrographic time series reconstructed for the period 1993 to 2013 point to a significant warming of 0.3°C/decade and a salinification of 0.03/decade of the ULSW in Flemish Pass (Figure 55). These trends were almost identical for the evolution in the Labrador Sea and in the DWBC east of Flemish Cap. Consequently, long-term hydrographic variability of ULSW in Flemish Pass, as well as in the DWBC at 47°N, is dominated by changes imprinted upstream in the Labrador Sea, which are advected southward. Results from a numerical ocean model simulating hydrographic variability in Flemish Pass over fifty years suggest that these trends are part of a multi-decadal cycle (Schneider et al., 2015; Varotsou et al., 2015).

The warming observed over the years 1993-2013 fell into a period of generally weakening convection. While the early 1990s showed convective mixing down to 2000 m (e.g. Kieke and Yashayaev, 2015), the early 2000s revealed vertical mixed-layers ranging from less than 1000 m depth to less than 1500 m. After a relative increase of maximum convection depth in the winter of 2007/2008, convective mixing reached water depths of about 1200 m and less in at least four years. Probably one of the deepest mixing events happened recently in the strong winter of 2013–2014 resulting in mixed-layers exceeding 1700 m (Figure 56, Kieke and Yashayaev, 2015).

Temperature and salinity evolutions for the years 2002–2014 derived from autonomous profiling Argo floats and averaged over 500–1000 dbar and 1000–1500 dbar in the central Labrador Sea highlight those periods when convection was intensive enough to penetrate to depths of at least 1500 m. General tendencies towards an increasing warming of the interior Labrador Sea over this period were abruptly interrupted at times of convection extending to greater depths (2008, 2012, and 2014) and picked up again afterwards. The strong surface forcing of the winter season 2013/2014 thus led to a new fresh and cold LSW anomaly that is observed to already spread along the propagation pathways into the interior subpolar North Atlantic.

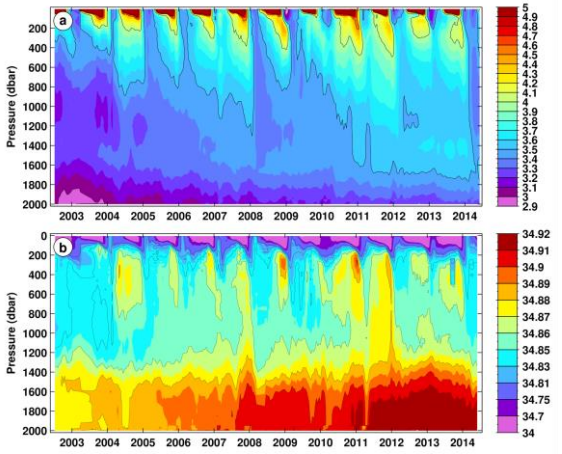

Figure 56: Time evolution of (a) potential temperature and (b) salinity in the western to central Labrador Sea derived from profiling *Argo* floats for the period 2002-2014 following *Kieke and Yashayaev* (2015). Periods of intensified water mass formation are characterized by a strong cooling and freshening of the water column extending from the surface to intermediate and deep water levels.

References

Kieke, D., and I. Yashayaev (2015), Studies of Labrador Sea Water formation and variability in the subpolar-North Atlantic in the light of international partnership and collaboration, Prog. Oceanogr., 132(3), 220-232, doi:10.1016/j.pocean.2014.12.010.

Mertens, C., M. Rhein, M. Walter, C. W. Böning, E. Behrens, D. Kieke, R. Steinfeldt, and U. Stöber (2014), Circulation and transports in the Newfoundland Basin, western subpolar North Atlantic, J. Geophys. Res., 119, 7772-7793, doi:10.1002/2014JC010019.

Schneider, L., D. Kieke, K. Jochumsen, E. Colbourne, I. Yashayaev, R. Steinfeldt, E. Varotsou, N. Serra, and M. Rhein (2015), Variability of Labrador Sea Water transported through Flemish Pass during 1993-2013, J. Geophys. Res., 120, 5514-5533, doi:10.1002/2015JC010939.

Varotsou, E., K. Jochumsen, N. Serra, D. Kieke, and L. Schneider (2015), Interannual transport variability of Upper Labrador Sea Water at Flemish Cap, J. Geophys. Res., 120, 5074-5089, doi: 10.1002/2015JC010705.

Salinity time-series in the North Atlantic

Ilaria Stendardo, Monika Rhein

Sea surface salinity (SSS) distribution in the ocean is influenced by evaporation and precipitation, modified by vertical and horizontal advection of water. Long-term changes in salinity during the last 5-6 decades are documented by several studies that show increase in salinity in regions where salinity is already high, and decrease in salinity in regions where salinity is already low. SSS changes, however, are not restricted to the surface but are transferred into the ocean's interior by vertical processes like subduction or convection, and then transported along the circulation pathways. Salinity could also vary by vertical migration of density surfaces caused either by wind-driven changes of ocean circulation or by thermodynamic processes, like poleward migration of isopycnals as a result of surface warming.

The study of salinity and freshwater distribution changes is constrained by the lack of temporal and spatial resolution of the observations especially before the starting of the Argo program in 1999, so that salinity anomalies could only be studied by averaging over several years. Thanks to the Argo program, the number of salinity profiles dramatically increased. The full Argo array was in place in the North Atlantic around 2005–2007. However, despite the Argo effort, the spatial and temporal coverage is not sufficient to identify salinity variations below the surface in detail, and the time period with the full Argo resolution (since 2005) is relatively short. These two issues motivated us to exploit the relation between the salinity profiles and dynamic height using the Gravest Empirical Mode (GEM) technique. This technique creates a transfer function between T/S profiles and dynamic height in order to parameterize temporal and spatial high-resolution salinity profiles (meaning daily projections onto a ¼° Cartesian grid) as a function of dynamic height from satellite altimetry available since 1993. In regions where the relation between salinity and dynamic topography is valid, the combined Argo and altimeter data allowed us to extend the high resolution time period from 1993 to 2012. The method was valid in the upper 700 m mainly at and near the pathways of the North Atlantic Current (NAC) where 7 regions were selected (Figure 57), but failed in regions with weak stratification or with ambiguities in the T/S relationships.

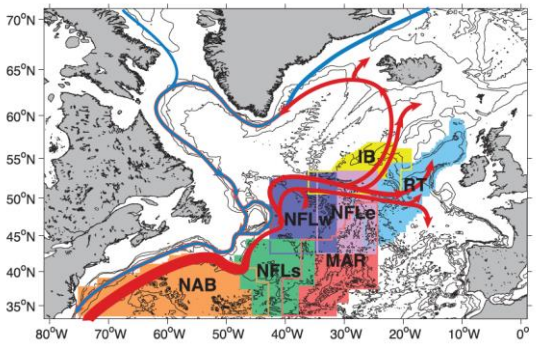

Figure 57: Map of the North Atlantic illustrating the regions selected: NAB (North American Basin) in orange, NFLs (southern Newfoundland basin) in green, MAR (Mid-Atlantic Ridge) in salmon, NFLw (western Newfoundland basin) in purple, NFLe (eastern Newfoundland basin) in pink, RT (Rockall Trough) in blue, and IB (Iceland Basin) in yellow. On top the schematic of the surface circulation represented by red (warm water of subtropical origin) and blue (cold water of subpolar origin) arrows.

Results from this analysis show multiannual large-scale salinity variability in the upper 700 m of the water column, albeit the amplitude in the eastern basins is weaker (Figure 59). Most of the changes are on interannual time-scale and coherent within all regions, with some exceptions. Moreover, the amplitudes are smaller in the north-eastern regions than in the regions further south and west. Salinity anomaly in the North American Basin (NAB) are correlated with the NAO (North Atlantic Oscillation) and can be followed by advection within the NAC from the NAB into the western subpolar North Atlantic. Despite the advection of saline water from the NAB, this signal is masked by the shifting of the location of the subpolar front that plays the major role in salinity variability in the central regions of the Newfoundland basin (NFLw and NFLe). The shifting of the subpolar front is also responding to the NAO. During

positive NAO, the subpolar front shifts south-eastward due to the intensification of the subpolar gyre. This factor counteracts the effect of the increased northward transport of saline water. In this case, the middle regions are subjected to a decrease in salinity due to the penetration of water of subpolar origin. The opposite happens during negative state of NAO. However, there are also years when the NAO is at a neutral state, during these time periods other atmospheric features might play a role. It has been discussed in several papers that the gyre response after 2001 seems not to be directly related to the NAO but rather follows other atmospheric forcing which are sometimes weakly correlated with the NAO. The north-eastern Atlantic also exhibits some inter-annual features, which are unrelated to the ones found along the pathway of the NAC, and presumably indicating eastern Atlantic pathways from the subtropical into the eastern subpolar gyre. Our analysis confirmed that the interannual variability is high and that it dominates the time series, obscuring potential trends from global warming in the 20-year time series. Only in the Rockall Trough a significant increase of 0.03 per decade has been found.

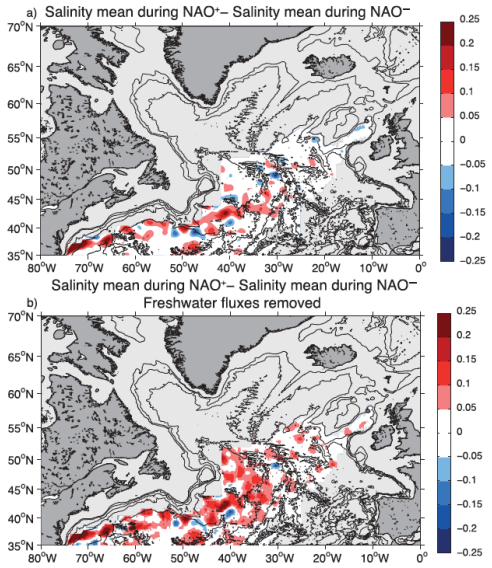

Figure 58: (a) Composite map of salinity showing the difference between NAO^+ and NAO^- in the upper 700 dbar of the water column. b) Composite map of salinity after removing the effect of the freshwater fluxes in the upper 700 dbar.

We also compared the salinity and surface freshwater fluxes (E-P) for the most extreme 5 positive NAO years and the 5 most negative NAO years with a composite analysis. During positive NAO, the freshwater fluxes show more precipitation over evaporation especially in the northern regions. In contrast, salinity is higher in the southern regions during NAO+, while in the north-eastern regions the differences between NAO+ and NAO– is negligible. This is especially highlighted in the salinity differences between the two composites (Figure 58), where higher salinities are found during NAO+ along the pathway of the NAC, but mostly restricted to the western basins. If the effect of freshwater fluxes is removed, salinity becomes even higher during NAO+, demonstrating that freshwater fluxes are damping the effect of the increased transport of salinity in the northern regions during positive NAO state (Figure 58).

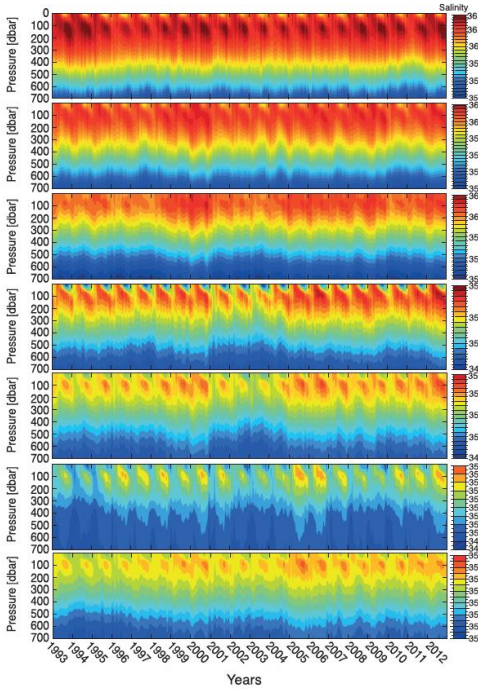

Figure 59: Hovmöller diagram showing the daily salinity distribution along pressure levels from the 1 January 1993 to the 31 December 2012 for each region. Contour every 0.05. Note that each subplot has a different colour scale

Reference:

Stendardo, I., M. Rhein, and R. Hollmann (2016), A high resolution salinity time series 1993-2012 in the North Atlantic from Argo and Altimeter data, J. Geophys. Res. Oceans, 121, doi:10.1002/2015JC011439.

Long-term observations of North Atlantic Current transport at the gateway between western and eastern Atlantic

Achim Roessler, Monika Rhein, Dagmar Kieke, and Christian Mertens

The upper branch of the Atlantic meridional overturning circulation (AMOC) is the northward transport of warm and saline water. Most of this flow passes through the narrow strait between Florida and the Bahamas (Florida Current). It continues along the continental slope of North America as the Gulf Stream that turns east at Cape Hatteras. Southeast of the Grand Banks of Newfoundland, a part of the Gulf Stream continues north into the North Atlantic Current (NAC) that transports the warm and saline water from the subtropics into the western subpolar North Atlantic. Subsequently, the NAC crosses the Mid-Atlantic Ridge (MAR) and enters the eastern subpolar North Atlantic, where part of it flows into the Nordic Seas and ultimately into the Arctic Ocean. Both AMOC and NAC are expected to weaken under global warming by about a third until the year 2100, and this will in turn reduce the projected temperature increase in western Europe.

In this paper we quantify the geostrophic NAC transports using an array of four bottom-mounted inverted echo sounders (PIES) deployed parallel to the Mid-Atlantic Ridge (2006-2010, Figure 60) in combination with shipboard and Argo CTD data, as well as satellite altimetry data. The PIES measure the acoustic round-trip travel time and the bottom pressure. The CTD data is used with the measured travel times to calculate transport time series of baroclinic (density dependent) transport variations employing the Gravest Empirical Mode technique. The barotropic (pressure dependent) component of the transport variations are inferred from the bottom pressure measurements.

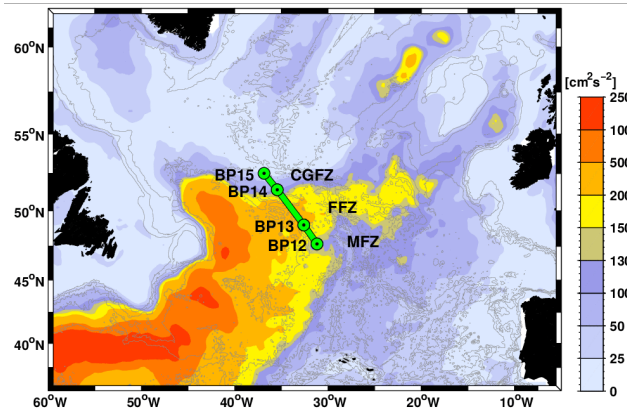

Figure 60: Map of the subpolar North Atlantic with the mean EKE from 1992 to 2013 from gridded geostrophic velocity provided by AVISO. The green dots show the array of four PIES. The main fracture zones are CGFZ: Charlie-Gibbs Fracture Zone, located in the northern segment of the PIES array, FFZ: Faraday Fracture Zone (central segment), and MFZ: Maxwell Fracture Zone (southern segment). Isobaths are given every 1000 m.

The PIES transport time series at the gateway between the western and eastern basin shows a deep reaching but surface intensified flow. The transport of warm, saline water of subtropical origin takes place in the upper 800 m and contributes 60% to the mean baroclinic transport of 29.4 Sv. The transports derived from the PIES travel time measurements (2006-2010) were found to be significantly correlated with the geostrophic velocity at the sea surface observed by satellite altimetry (Ssalto/DUACS, Aviso). This correlation was used to expand the 4 year transport time series to the full period of satellite observations from 1992 to 2013.

The mean baroclinic NAC transport between 1992 and 2013 is 27.5 ± 4.6 Sv (see Figure 61). The transport is always eastward. Extreme values range from about 14 Sv to 40 Sv. Assuming that the contribution of subtropical water to the

total flow does not change with time, the mean inflow of subtropical water into the eastern subpolar gyre results to 16.5 Sv, i.e., about half the strength of the Florida Current. There is no significant linear trend in the transport of the entire array, but the time series for individual segments show opposing trends. This suggests that the NAC was more focused to the central segment during the later years of the time series. The spectral analysis of the long transport time series spanning from 1992 to 2013 exhibits several significant peaks. The two most prominent peaks were found at 120 days, identified as the time scale of meanders and eddies, and at 4-9 years, most likely related to the North Atlantic Oscillation (NAO). By constructing transport composites of the 5 years of the most positive NAO and 5 years of the most negative NAO, this relation was investigated in more detail. The positive NAO years had a baroclinic transport that was 2.9 Sv higher, and the increase was found mainly in the southern segment. Both results fit with other observations and model studies of a zonally expanded and intensified subpolar gyre during years of high positive NAO. This direct response of the baroclinic NAC transport to the NAO explains about 30% of the measured baroclinic long-term transport variability of 8-9 Sv.

Reference:

Roessler, A., M. Rhein, D. Kieke, and C. Mertens (2015), Long-term observations of North Atlantic Current transport at the gateway between western and eastern Atlantic, J. Geophys. Res. Ocean., 120(6), 4003–4027, doi:10.1002/2014JC010662.

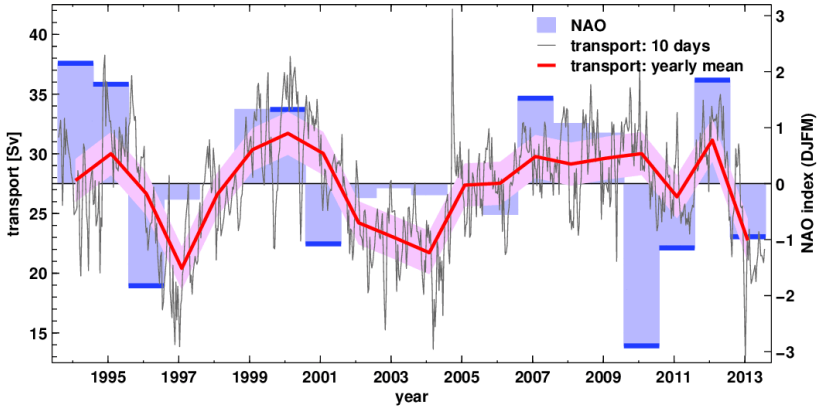

Figure 61: NAC transport time series based on the correlation between altimeter-derived surface velocities and PIES transports relative to 3400 dbar (gray line, 10 days). The uncertainty for 10 day values is 3.8 Sv. The thick red line represents yearly transport means, and the red shaded area is the corresponding uncertainty of 1.8 Sv. The annual means are centered on 31 January, which is taken as the center of the winter (DJFM) North Atlantic Oscillation index (blue bars (https://climatedataguide.ucar.edu/climate-data/hurrell-north-atlantic-oscillation-nao-index-station-based); using Ponta Delgada, Azores and Stykkisholmur/Reykjavik, Iceland). Years highlighted in dark blue are the five strongest positive and negative NAO years.

Routine work and emergency case support by the IUP radioactivity lab

Helmut W. Fischer, Bernd Hettwig

The laboratory

The Laboratory of Environmental Radioactivity at the Physics Department of Bremen University is operating since 1986, the year of the Chernobyl nuclear power plant accident, as official Bremen State Radiation Measurements Laboratory. In this function, it forms part of the nationwide IMIS network, operated by the Federal Office of Radiation Protection (BfS) on behalf of the Federal Ministry of the Environment (BMUB). The network provides routine monitoring data of radioisotope concentrations in all relevant environmental media and provides emergency support in case of necessity.

Routine program

The IUP Bremen laboratory contributes to this network by performing a continuous routine program, comprising a total of approx. 250 samples per year from a variety of media, ranging from waters and soil through plants and foodstuffs to residues and wastes. Data are obtained with high-sensitivity instruments and, if necessary, specialized wet chemistry techniques. Therefore, even very low levels of artificial and natural radionuclides can be detected, which are orders of magnitude below values of concern or official limits. As an example, many investigated milk samples still show residual values between 0.1 and 1 Becquerel per litre of the long-lived isotope cesium-137, originating, in approximately equal parts, from Chernobyl emissions transported through Europe in 1986 and from worldwide atmospheric nuclear weapons testing performed in the 1950s and 1960s. The current maximum permissible value in Europe for this isotope in milk is 370 Becquerel per litre.

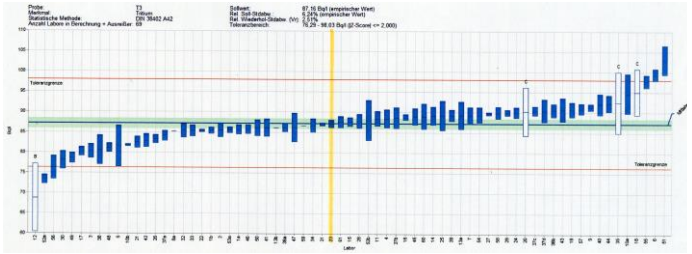

Figure 62: Results from an anonymous laboratory proficiency test for the radioisotope tritium in water. Each symbol represents a range of measured values from one participant. Data from different laboratories are sorted numerically along the x-axis. IUP results, exactly matching the true value (horizontal line), are marked.

Quality assurance

Measured concentration values might be decisive, so quality assurance is of high importance. The laboratory regularly participates in external proficiency tests, which consist of identifying radioisotopes and determining their activity concentrations in specially prepared samples. In the anonymous comparisons, the IUP lab usually performs extremely well, often being less than 2 % away from the “true” value, known initially only by the institution organizing the test. An example from a report is shown in Figure 62.

Imported goods

Imported goods are monitored routinely by state authorities. In the State of Bremen, with several large harbours, this is of high importance. Since 2011, special attention is paid to foodstuffs originating from Japan and the Pacific Ocean. No contamination with emissions from the nuclear power plants in Fukushima, damaged after the 2011 earthquake, could be detected in the approx. 25 samples, mainly sea fish, investigated during the years 2015 and 2016.

Local emergency case support

The IUP laboratory also provides local emergency support. Several times per year, local authorities ask for assistance

after positive response of radiation monitors during handling of transported goods, scrap metal or waste. The most spectacular case involved the discovery of five unlabelled 20 foot shipping containers at the Bremerhaven container terminal in 2015. Measurements performed on site

- confirmed the radiation level values registered by the Police using radiation dose rate meters (about 2.5 Microsievert per hour, 25 times the natural background level);
- confirmed that the radiation level was similar at all positions along the containers, excluding the existence of hidden small, strong radiation sources and the possibility of smuggling of radioactive material;
- identified natural radioisotopes from the uranium and thorium decay chains as main or only contributors to the radiation level and excluded the existence of significant amounts of artificial radioactivity in the containers, by in situ high resolution gamma spectroscopy;
- confirmed and quantified the above findings by investigating a sample taken from the cargo in the laboratory.

Together with the involved authorities, the material was identified as slag from tin production from tin ore in Southeast Asia. Currently, tin slag is becoming an attractive material for the electronics industry, due to its high content in tantalum and niobium. The measured activity concentrations (ca. 4 Becquerel per gram for member elements of the Uranium-238 decay chain, 14 Becquerel per gram for the Thorium-232 chain) were consistent with literature values and the measured radiation levels. Had the containers been labelled correctly, i.e. according to the corresponding category of natural radioactive material, shipping would have been performed following prescribed procedures (e.g. no road transport). On the other hand, the event could be regarded as a successful exercise for inter-institutional collaboration in a possible emergency case. This impression was confirmed in an internal workshop among eight involved institutions, organized by and at IUP.

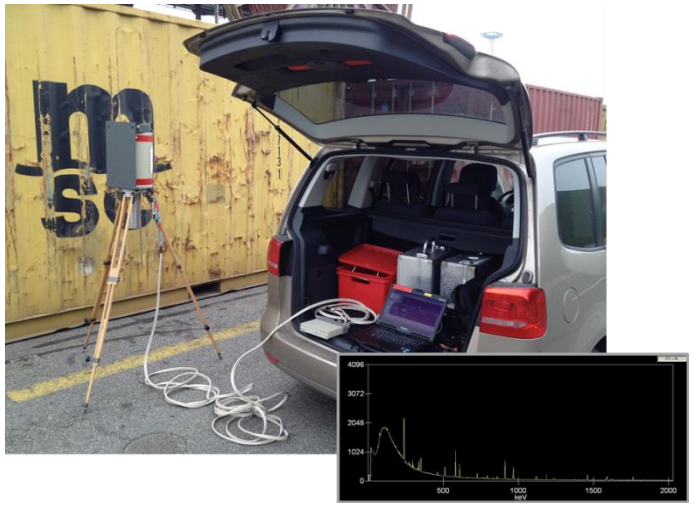

Figure 63: In situ gamma spectroscopy measurement at the containers emitting radiation at Bremerhaven container terminal. The insert displays the obtained gamma spectrum with peaks indicating natural radioisotopes.

Links

Yearly data collections are published on the laboratory website:
http://www.radioaktivitaet.uni-bremen.de/de/?Jahresberichte_Radioaktivitaet

Yearly overviews for whole Germany can be found at the website of BfS:
http://www.bfs.de/DE/mediathek/berichte/umweltradioaktivitaet/umweltradioaktivitaet_node.html

Transport of anthropogenic radionuclides between the Pacific and Indian Oceans

Daniela Pittauer and Helmut W. Fischer

Man-made radioisotopes are forms of radioactive elements present in the environment as a result of human activities. They originate from nuclear research and industry, including nuclear weaponry. This is also the case for plutonium isotopes. A nuclear material is created by nuclear fission or activation in a reactor core or a nuclear bomb explosion. Sometimes it is further processed industrially, for example in a weapons complex or spent fuel reprocessing plant. Even after being released into the environment, accidentally or deliberately, the substances keep a characteristic isotopic composition - a fingerprint of their origin.

Studying trace amounts of plutonium isotopes in ocean sediment cores in combination with natural radionuclides makes it possible to reconstruct sedimentation histories in individual study sites and quantify sedimentation and/or deposition rates. Additionally, plutonium isotopes provide information about transport of water masses and particles with the ocean currents between the identified source (e.g. nuclear test site or a damaged nuclear reactor) and the sampling location.

The sediment cores for this study were taken at deep sea stations in the West Pacific Ocean margin and the Indonesian Throughflow (ITF), which is a complex array of passages that provide a low latitude connection between Pacific and Indian Ocean (Figure 64). They were sampled during sea-

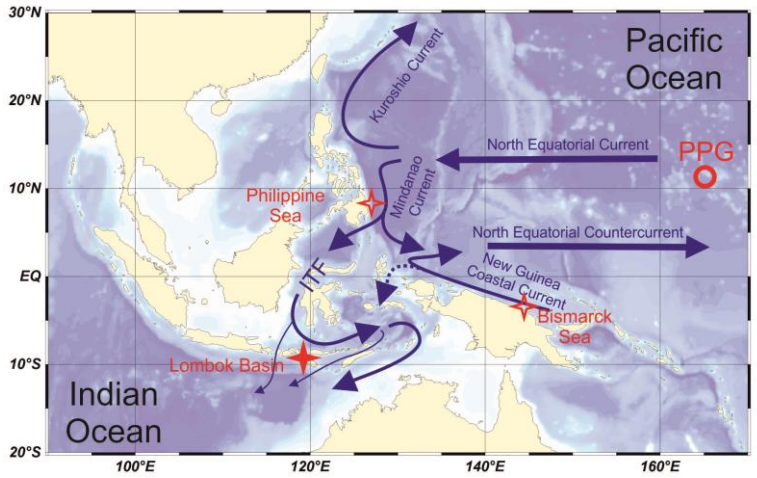

Figure 64: Locations of study sites in the Indonesian Throughflow (ITF) and west Pacific margin. Pacific Proving Grounds (PPG), where the U.S. performed 109 atmospheric tests during 1940's and 1950's, is marked with a circle.

going expeditions on the German research vessel "Sonne", organized by MARUM – Centre for Marine Environmental Sciences, University of Bremen, in 2005 and 2013. Samples taken from the upper sediment layers, covering approximately the last century of sedimentation, were studied by a combination of radiometric and mass spectrometry techniques, including gamma and alpha spectrometry at IUP and Alfred Wegener Institute in Bremerhaven, as well as accelerator mass spectrometry (AMS) at Department of Nuclear Physics, Australian National University in Canberra, and inductively coupled plasma mass spectrometry (ICP-MS) at Centre for Nuclear Technologies, Technical University of Denmark in Roskilde. Studying activities and ratios of plutonium isotopes revealed the deposition history and sources of plutonium in the region.

The United States conducted an extensive nuclear test programme at the Bikini and Enewetak Atolls in the Marshall Islands, known as the Pacific Proving Grounds (PPG), during 1940's and 1950's. The total estimated fission yield was 57.7 Mt, which is over 30% of 189 Mt globally. Moreover, PPG is an important local and regional source of anthropogenic radionuclides. Plutonium isotopes deposited from the local fallout are known to be distributed from the PPG by the North Equatorial Current and Kuroshio Current towards the Northwest Pacific Ocean marginal seas.

In the Lombok Basin, located more than 5000 km southwest of PPG, we could demonstrate that the transport of the transuranic radioisotopes is also significant in the southern direction, along the Mindanao Current and further through the ITF (Pittauer et al., submitted). Based on the end-member analysis of plutonium atom ratios, we inferred that the portion of PPG derived plutonium at this site was close to 100% during 1950's and 1960's. Starting in the 1970's, a portion of plutonium originating from the global stratospheric fallout is also present, yet PPG plutonium remains a significant source due to continuous remobilization until these days (Figure 65). Another transuranic isotope related to nuclear weapons testing, Americium-241, is also present in the sediments. This is not the case for a common fission product, Caesium-137, which is not well preserved in ocean sediments due to its higher solubility.

In our on-going research we focus in deep sea sediments at another two stations, in Philippines Sea east of Mindanao and Bismarck Sea east of Papua New Guinea. Here the plutonium deposition conditions at the entrance of North Pacific waters to the ITF are investigated, as well as possible exchange of anthropogenic radioisotopes between the North and South Pacific.

References

D. Pittauer, S.G. Tims, M.B. Froehlich, L.K. Fifield, A. Wallner, S.D. McNeil, H.W. Fischer: Continuous transport of Pacific-derived anthropogenic radionuclides towards the Indian Ocean, Scientific Reports, submitted.

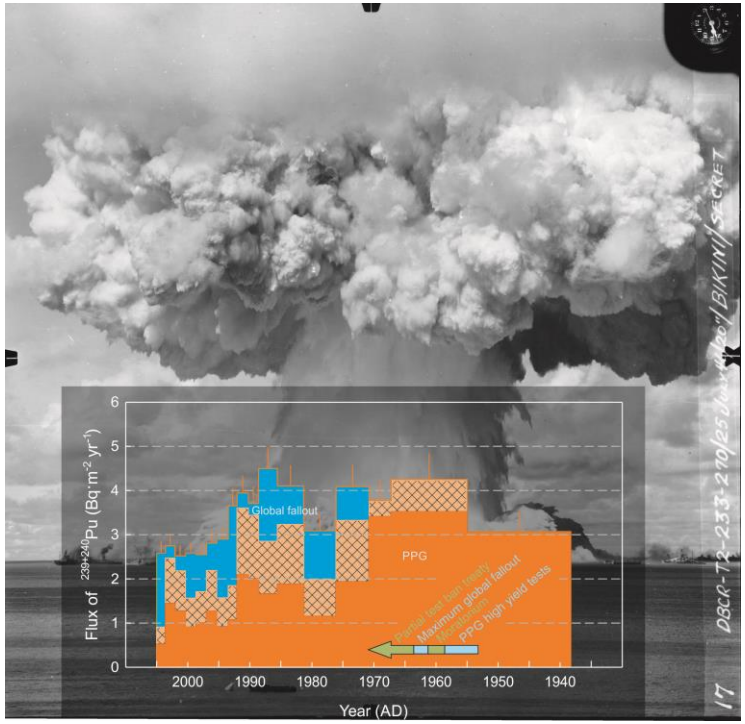

Figure 65: Mean yearly Plutonium isotopes fluxes to the sediment estimated based on the Lombok Basin core analysis, illustrating a continuous transport of the anthropogenic isotopes through the ITF. Different sources are distinguished by different colours: orange (and cross-hatched orange) stands for lower and upper estimate of PPG origin; the portion of global stratospheric fallout is marked in blue. Background photo: Bikini Nuclear Test 25 July 1946 (credit: Naval History and Heritage Command).

Radiometric dating of recent sediment cores

Daniela Pittauer, Manuel Pérez Mayo, Helmut W. Fischer

One of the Radioactivity measurements laboratory's major activities is to provide chronologies for sediment cores covering the most recent decades. During this time period, major changes to the environment, often caused by human activities, might have been recorded in the sedimentary record. Up to 100-150 years old sediments can be dated using the natural isotope ^{210}Pb, a member of the ^{238}U decay chain. This isotope has a suitable half-life of 22.3 years and its origin within the sediment is two-fold: Firstly, radioactive decay from its long-lived parent nuclide ^{226}Ra, being a common trace element in mineral grains in the sediment, is responsible for a part of ^{210}Pb, which is called "supported" ^{210}Pb. The second source is the deposition from the atmosphere, whereby ^{210}Pb originates from the gaseous intermediate decay chain member ^{222}Rn, which escapes from the soil. This additional ^{210}Pb contribution is called "excess" ^{210}Pb. With increasing depth (and age) within an undisturbed sediment, the "excess" ^{210}Pb decreases to a known proportion due to radioactive decay. This enables us to date the sediment layers and therefore construct an age model for the sediment core.

Both total and "supported" ^{210}Pb can be measured by a non-destructive technique, gamma-spectrometry. Additional radionuclide tracers detected within the same spectra can be used to verify the accuracy of the ^{210}Pb-based age models: anthropogenic radionuclides that are products of nuclear fission or activation in nuclear reactors or weapons, which can be detected in certain sediment horizons as markers of nuclear fallout periods. Examples of man-made isotopes with suitable half-lives are ^{137}Cs or ^{241}Am. Resulting chronologies provide high temporal resolution and are complementary to the radiocarbon technique, which is not suitable for the last Century, but in turn can date materials of organic origin up to several thousand years old.

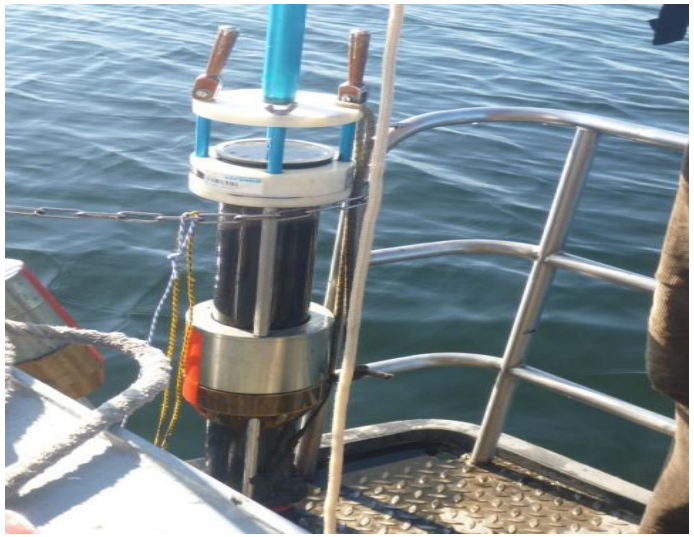

Figure 66: Sampling of a short sediment core at the lake Tegeler See near Berlin.

Lake and marine sediment cores contain information needed to improve our understanding of past environmental changes. Therefore, they serve as valuable archives of climate change, environmental pollution or changes in land use practices. We co-operate with other national or international institutions and provide sediment chronologies within paleoclimate or environmental studies:

- In the terrestrial environment, we have contributed to a study of phosphorous cycling in lake sediments

lead by the Leibniz-Institute of Freshwater Ecology and Inland Fisheries, Berlin (Rothe et al. 2015). This project described retention of phosphorous in the iron phosphate mineral vivianite during early sediment diagenesis in the lake Lower Havel.

- Recent layers from marine sediment cores taken in South Africa at the Namaqualand mudbelt, offshore the Olifants and Orange Rivers, were dated within a study of climate development and related vegetation shifts over the last 2 Millennia. This study (Hahn et al., 2016) of an international team of researchers, led by MARUM – Centre for Marine Environmental Sciences, shows a contrast in timing of wet periods in the catchment areas of both rivers, attributed to the shifts of climate zones, presumably in connection with Antarctic cooling and warming events.
- In another international cooperation led by Uruguay, we have provided a recent chronology for a Río de la Plata Estuary sediment core. This study shows that the studied sediments contain a distinct continental runoff record as a result of short-term climatic variability (Pacific Decadal Oscillation, Atlantic Multidecadal Oscillation and El Niño/La Niña Southern Oscillation) which influences the precipitation patterns over SE South America over the last Century.

In all cases, our contribution consisted in developing age models or calculating sedimentation rates, necessary for a consistent interpretation of other proxy data, and impossible to obtain from the core material without the radiometric methods offered at IUP.

References

A. Hahn, J.S. Compton, C. Meyer-Jacob, K.L. Kirsten, F. Lucasssen, M. Pérez Mayo, E. Schefuß, M. Zabel: Holocene paleoclimatic record from the South African Namaqualand mudbelt: A source to sink approach. Quaternary International, 404, Part B (2016), 121–135, doi:10.1016/j.quaint.2015.10.017

A. Marrero, A. Tudurí, L. Pérez, C. Cuña, P. Muniz, R.C. Lopes Figueira, M.M. de Mahiques, P.A. de Lima Ferreira, D. Pittauerová, T. Hanebuth, F. García-Rodríguez: Historical changes in terrigenous river supply from the Rio de la Plata basin to the inner shelf of Uruguay. Latin American Journal of Sedimentology and Basin Analysis, 21, 2, (2014) 165–179

M. Rothe, A. Kleeberg, B. Grüneberg, K. Friese, M. Pérez-Mayo, M. Hupfer: Sedimentary Sulphur:Iron Ratio Indicates Vivianite Occurrence: A Study from Two Contrasting Freshwater Systems. PLoS ONE 10(11), e0143737 (2015), doi:10.1371/journal.pone. 0143737

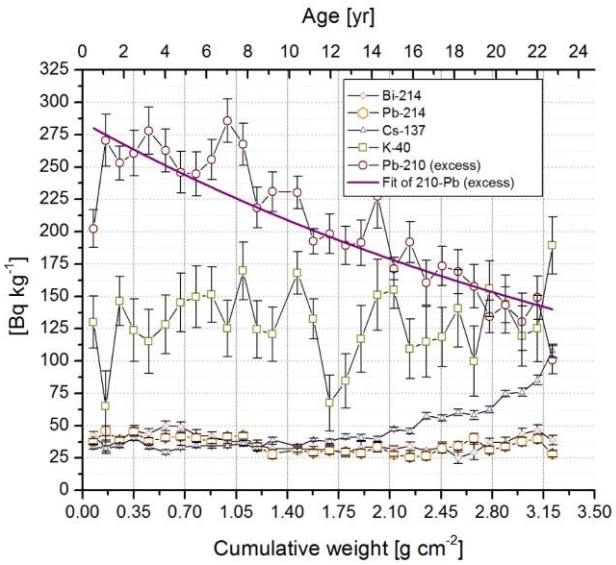

Figure 67: Radionuclide profiles used for interpretation of rates of recent sediment accumulation in Lower Havel Lake, Berlin, used in Rothe et al. (2015). The upper axis shows that, according to the developed age model, the sediment record covers the most recent 23 years. The values of anthropogenic ^{137}Cs are maximum at the depth of the core, and the maximum value related to Chernobyl nuclear reactor accident fallout is expected below the sampled interval. The cumulative weight is a quantity used for compaction corrected depth in sediment.

Teaching activities

Annette Ladstätter-Weißenmayer, Harry Küllmann, and Anja Gatzka

Today's graduate and postgraduate education in the field of Earth System and Environmental Science is a highly interdisciplinary and inter-institutional challenge. The existing research infrastructure at the University of Bremen (UB) and the Alfred Wegner Institute, Helmholtz Centre for Polar and Marine Research in Bremerhaven (AWI) offers a unique research environment in north-western Germany to study past, present and future of the Earth system. The education and qualification of Master and PhD students is carried out on an internationally competitive level.

In 2000, the international Master programme "Postgraduate Programme Environmental Physics" (PEP) accredited by the German Accreditation Council has been created at UB in collaboration with the AWI. Since its start, 94 students successfully finished this program with a Master degree, 13 with a Certificate. The foci of this programme are on the atmosphere, ocean, land and climate, as well as on remote sensing and dynamics.

From winter semester 2015/16 until winter semester 2016/17, 37 students started this study-programme at the University of Bremen. The students came from Bangladesh, Canada, China, Germany, Ghana, Greece, India, Iran, Ireland, Italy, Nigeria, Pakistan and Peru.

In 2006, a very successful collaboration between the University of Bremen and the Ocean University of Qingdao of China (OUC) started with the aim to offer Master double degrees in both universities. In this program, Chinese students start their studies in China, participate one year in the PEP programme in Bremen and then complete their studies at OUC. The German students start with one year of the PEP programme and then study one year at OUC in Qingdao.In addition to the regular PEP students, 2 ERASMUS students from Poland and a number of "Wahlfachstudenten" from the Physics Master programme at UB participate each year in the PEP programme.

In the last 16 years, around 83% of the graduates of our programme (Master + Certificate) started their PhD studies at the Institute of Environmental Physics (IUP) in Bremen, at the AWI in Bremerhaven or somewhere else, whereas the rest of around 17% applied directly for a job in industry or in climate or weather forecast related agencies.

As Bremen is one of the most important locations for aerospace in Germany, colleagues from the IUP and the AWI together with colleagues from the Electrical Engineering, Mathematics, and Production Engineering Departments of the University of Bremen have set up a curriculum for an international Master programme in Space Sciences and Technologies which will start in winter semester 2017/18. Students will get trained in experimental methods for space applications, numerical data analysis and interpretation using sophisticated models.

In 2006, in the context of the excellence initiative, the Bremen International Graduate School for Marine Sciences GLOMAR was launched and funded by the Deutsche Forschungsgemeinschaft (DFG). This Graduate School is a cooperation of the following partners: University of Bremen, DFG Research Centre Ocean Margin (RCOM), Centre for Marine Environmental Science (MARUM), Research Centre for Sus-

tainability Studies (ARTEC), AWI, German Maritime Museum (DMS), Max Planck Institute for Marine Microbiology,and Centre for Tropical Marine Ecology (ZMT). GLOMAR provides an optimal research environment for excellent PhD students and fosters excellence in education and research. In general, the Graduate School's educational concept allows PhD students to develop into excellent interdisciplinary researchers, with international contacts and a publication record in peer-reviewed international journals, skills in conducting research and in communication (on disciplinary and interdisciplinary levels to both experts and students as well as to the public), and in project management.

In 2009, the Helmholtz Graduate School POLMAR (Polar and Marine Research) started with the following partners: AWI (host institution), University of Bremen, Jacobs University Bremen, Max Planck Institute Bremen, University of Potsdam, Institute for Marine Resources (IMARE), and Hochschule Bremerhaven.

These programmes provide opportunities to PhD students coming from different disciplines to cooperate and exchange views on the common theme of linking 'data and modelling', leading to a better understanding of local processes within a global context. They provide a structured framework for education and qualification for excellent PhD students dealing with the challenging questions in Earth System Science and Polar and Marine Research. Developing all categories of skills needed for analysing complex climate and environmental systems and the development of integrated solutions in a supportive network of collaborating research institutions fosters outstanding career options. Structured training and supervision supported by a broad range of soft skill courses is indicative for the entire concept. Up to now more than 100 PhD students are within POLMAR.

The IUP Bremen regularly welcomes students from high schools in Bremen to carry out practical exercises. These events give the students the opportunity to work together with scientists in different research groups for a time period of 2 weeks to get a first impression of research work.

In addition the members of IUP are actively involved in the "Day of Physics" and "Saturday Morning Physics" giving the general public an overview of scientific work performed at IUP.

IUP Bremen Staff, June 2016

Visit us on http://www.iup.uni-bremen.de/index_e.html